U. S. DEPARTMENT OF THE INTERIOR

U. S. GEOLOGICAL SURVEY

ASSESSMENT OF THE EFFECTS OF LOCAL GEOLOGY USING LONG-PERIOD MICROTREMORS AND THE 1989 LOMA PRIETA EARTHQUAKE MOTIONS

by

Junpei Akamatsu, Masayuki Fujita and Hiroyuki Kameda
Disaster Prevention Research Institute
Kyoto University, Kyoto, Japan

Mehmet Çelebi and Roger D. Borcherdt
U.S. Geological Survey, 345 Middlefield Road
Menlo Park, California 94025–3591

OPEN–FILE REPORT 92–214

TABLE OF CONTENTS

Page No.

PREFACE

This report presents the results of cooperative work performed under collaboration of researchers from the United States Geological Survey (USGS) at Menlo Park, U.S.A. and those from the Urban Earthquake Hazard Research Center (UEHR), Disaster Prevention Research Institute, Kyoto University, Japan. The collaboration was motivated by the effects of the 1989 Loma Prieta earthquake on the San Francisco Bay area and its surrounding regions. In particular, the site effects on ground motion and earthquake damage caused thereby, thus demonstrate the importance of seismic mircrozonation.

As part of its comprehensive program of investigating the effects of the Loma Prieta earthquake regarding urban earthquake hazard, UEHR decided to pursue a possibility of studying the details of the site effects of the Loma Prieta earthquake for the purpose of development of appropriate methodology for microzonation. The main issue here was to verify a long-period microtremor technique that has been studied and developed at UEHR.

After several correspondences between the USGS group and the UEHR group including a visit of H. Kameda at Menlo Park in January 1990, discussion was made regarding the research subject and an appropriate form of collaboration. M. Çelebi and R. D. Borcherdt of USGS, and H. Kameda and J. Akamatsu of UEHR joined these arrangements. Through this, a joint research program which eventually led to this report was established.

The immediate goal of the joint research was to make direct comparison of long-period microtremor data with strong motion and aftershock recordings from the Loma Prieta earthquake with emphasis on specific site and geological effects on soil amplification of ground motions. The ultimate goal is to establish better and comprehensive understanding of ground motions on a scientific basis as well as to make it contribute to significant improvement of microzonation techniques for engineering purposes. It was thus agreed that a UEHR team would visit the Bay area and perform long-period microtremor measurements in cooperation with the USGS group. The location of these surveys were to be carefully selected so that their results can be compared with those from the Loma Prieta earthquake recordings to be provided by the USGS group.

The UEHR team performed the field activities for long-period microtremor measurements during the period of May 14–June 5, 1990. M. Fujita, a co-author of this report, joined the team and contributed also to the data analysis following it. N. Ichikawa took an essential role during the field activities as a technical staff.

Analysis of obtained data was performed, and discussion of the results as well as the development of joint reports continued. In the meantime, R. D. Borcherdt visited Kyoto, and H. Kameda and J. Akamatsu visited Menlo Park for these arrangements.

This report has been accomplished as an output of the joint works which took place as outlined above. A companion Open-File Report, identical except for some administrative parts, will be published by USGS. It is hoped that these reports will contribute to the development of the subject discussed herein as international cooperative efforts.

ACKNOWLEDGMENTS

This work was conducted under cooperation and assistance of many individuals and organizations from the U.S. and the Japanese sides. Microtremor measurements required installation of instruments at a fixed rock site reference point in each selected test field throughout the period of its measurement. The reference points for the three test fields, namely Peninsula cities, Santa Clara Valley and Santa Cruz were set, respectively, at the residence of Mr. S. Guilhamet (Station BIS), the residence of Professor A. S. Kiremidjian of Stanford University (Station KIR) and the Lick Observatory Electronics Lab. (Station LOE) at the University of California, Santa Cruz (USCS). Mr. T. P. Ricketts, Senior Development Engineer at USCS, provided much needed help. Generous understanding and cooperation of these individuals and organizations are gratefully acknowledged. Kind guidance by Mr. G. Sembera of USGS for site identification should also be acknowledged.

The microtremor measurements were conducted as a part of the UEHR/DPRI, Kyoto Univ. Team activities in the Bay region for a comprehensive study of the effects of the Loma Prieta earthquake. Assistance of the other Team members was very helpful. Especially, Mr. N. Ichikawa played a major role as a technical staff for field survey. The support of Professor M. Shinozuka of Princeton University (also Adjunct Professor at DPRI, Kyoto University) and Professor R. Minai of DPRI, Kyoto University, were essential in smooth execution of the project. Mr. H. Morikawa, Graduate Student at Kyoto University, assisted aftershock data processing, both in Menlo Park, California and in Kyoto, Japan.

1. INTRODUCTION

It has been widely recognized that local geology has significant effects on earthquake ground motions and consequently on the earthquake damage in urban areas. This has been experienced worldwide, including the United States and Japan. In the United States, it was typically observed in the San Francisco Bay regions during the 1906 earthquake (Borcherdt and Gibbs, 1976) and again during the 1989 Loma Prieta earthquake (Borcherdt and Glassmoyer, 1990; Kameda, 1990). In Japanese major earthquakes that have damaged urban regions including Tokyo (1923), Nagoya (1943), Niigata (1964), etc., the effects of local geology have been a pronounced common factor of hazards (Okamoto, 1984). This arises from complex geological conditions of these cities which are located on coastal soft alluvial plains near large river mouths like many other Japanese big cities.

This notion of the problem has led to the development of seismic microzonation techniques (Proceedings of 1982). Microzonation at present is a common tool for assessment of seismic risk of urban regions, and has been implemented in the development of earthquake preparedness by many local governments and municipal authorities both in the U.S. and Japan (Scawthorn *et al.*, 1984).

Despite the past tremendous developments, there are problem areas where further progress is required in the field of microzonation. The main subject dealt with in this work is related seismic microzonation in long-period ranges (1–10 s). This period range has not so far been a major issue in the microzonation techniques. However, recent urban developments require that these long-period ranges be incorporated in the microzonation technique. Specifically, high-rise buildings, flexible long-span bridges, sloshing of liquid fuels contained in storage tanks are involved in regard to this period range. In this period range, it is generally understood that surface waves are the main carrier of the seismic energy. It is recently suggested that P_L waves can also contribute significantly to the seismic motions in this period range.

Among various methodologies for microzonation, this study deals with application of long-period microtremor measurements. Microtremor technique has been proposed for use in microzonation for a long time (Kanai, 1961). Despite its simplicity in field survey activities, its physical verification is still under controversy. The question arises mainly regarding the ambiguities of source of excitation that causes microtremor, which makes it difficult to make physical understanding in terms of wave propagation theory. This prevents the technique from being used to establish a quantitative basis for evaluation of soil amplification of ground motions during earthquakes. These shortcomings are particularly pronounced in the range of period shorter than one second where the main excitation comes from widespread artificial sources including road and highway traffic, industrial activities, etc.

However, there is a higher possibility that the microtremor technique be a much more promising method if attention is focused on a long-period range (larger than one second), which, as indicated above, is of increasing engineering importance. It is known that the

long-period microtremor consists of microseisms that are regarded as the site response of the ground excited by natural sources including sea waves. This means that the site is subject to a uniform excitation which enables one to make physical interpretation of the measured microtremor. If simultaneous recordings are obtained on a soil site and on an outcrop of basement rock, it will be possible to evaluate the spectral amplification of the soil site on a quantitative basis. This idea has been proposed and practiced for application of long-period microtremors to seismic microzonation (Kagami *et al.*, 1982).

In attempts to apply the long-period microtremor technique to seismic microzoning, it is very important to make calibration between the microtremor recordings and actual earthquake recordings. Akamatsu (1991) made a comparative study in this direction, and demonstrated that soil amplification due to long-period microtremor agrees well with that from the surface-wave phase of earthquake recordings. This lays a seismological basis of long-period microtremor technique to be used for microzonation.

The primary objective of this study is an assessment of the effects of local geology using long-period microtremors and the 1989 Loma Prieta earthquake recordings. For this purpose, the joint works have been conducted by the researchers from the USGS and Kyoto University, whose research arrangements were described in detail in Preface. As indicated in Preface also, the ultimate goal of this study is to establish better and comprehensive understanding of earthquake ground motions on a scientific basis and to make it contribute to significant improvement of microzonation technique for engineering purposes.

In the following part of this report, field survey activities and major findings from the microtremor measurements in the areas affected by the Loma Prieta earthquake are described (2.). Then the strong motion recordings and the effects of local geology are demonstrated (3.). Similar results are presented by using the Loma Prieta aftershock records (4.). On this basis, comparative observations of the results from long-period microtremor and earthquake recordings, regarding frequency content, spectral site amplification, directivity of site amplification, etc. (5.). Then major conclusions of this study are summarized (6.).

While every phase of this study was performed in close cooperation among the authors, it will be a proper way to indicate the major contributor(s) of each section of this report as follows:

Preface	: H. Kameda
1. Introduction	: H. Kameda
2. Long-period microtremor measurements	: J. Akamatsu and M. Fujita
3. Strong motion recordings from the Loma Prieta earthquake	: R. D. Borcherdt
4. Loma Prieta aftershock records	: M. Çelebi
5. Comparative observations of the results from long-period micro-	: J. Akamatsu and M. Fujita

tremor and earthquake recordings

6. Conclusions : All Contributors
Appendix : J. Akamatsu and M. Fujita

REFERENCES

Akamatsu, J., M. Fujita, and K. Nishimura (1991). Vibrational characteristics of microseisms and their applicability to microzoning in a sedimentary basin, *J. Phys. Earth,* in press.

Borcherdt, R. D. and J. F. Gibbs (1976). Effects of local geological conditions in the San Francisco Bay region on ground motions and the intensities of the 1906 earthquake, *Bull. Seism. Soc. Am.,* **66**, 467–500.

Borcherdt, R. D. and G. Glassmoyer (1990). On the influence of local geologic deposits and crustal structure on ground motions generated by the Loma Prieta earthquake in the San Francisco Bay region, California, *Bull. Seism. Soc. Am.,* submitted.

Kagami, H., C. M. Duke, G. C. Liang, and Y. Ohta (1982). Observation of 1- to 5-second microtremors and their application to earthquake engineering, Part II. Evaluation of site effect upon seismic wave amplification due to extremely deep soil deposits, *Bull. Seism. Soc. Am.,* **72**, 987–998.

Kameda, H. (editor) (1990). Loma Prieta Earthquake of October 17, 1989, Reconnaissance Report, Natural Disasters Report No. B–1–3, Japanese Group for the Study of Natural Disaster Science.

Kanai, K. (1961). Measurement of microtremors, *Bull. Eq. Res. Inst.*, **39**.

Okamoto, S. (1984). Introduction to earthquake engineering, second edition, *University of Tokyo Press.*

Proceedings of the Third International Earthquake Microzonation Conference, Seattle, USA (1982).

Scawthorn, C., C. Arnold, and R. E. Scholl (editors) (1984). Proceedings of the U.S.–Japan Workshop on Urban Earthquake Hazards Reduction, Stanford.

2. LONG-PERIOD MICROTREMOR MEASUREMENTS

2.1 Observation and Analysis

Long-period microtremors (>1 s), or microseisms, are considered to be mainly generated by sea-waves; their frequency contents at a site vary with time according to sea-wave and weather conditions. Therefore, an estimation of ground effects on microseisms should be based on simultaneous observations at ground sites and rock sites. Amplification factors for microseisms were evaluated with spectral ratios of ground sites to rock sites taken as reference sites.

Observation systems are 3-component velocity seismograms with 14-bit digital recorders. Natural periods of the seismometers are 10 s (PELS–76, 190 v/m/s) for ground sites and 1 s (PK–101, 260 v/m/s) for reference sites. To suppress artificial (mainly traffic) high-frequency noises, a set of low-pass filters with cut-off frequencies of 1, 3 and 10 Hz were used according to noise condition. Sensitivity and reliability of the two systems were checked through simultaneous recordings at the reference sites (see Figs. A.1, A.15, and A.21). At ground sites, seismometers were set on the pavement of the sidewalk, covered with carton boxes and sand bags to prevent local winds.

All recordings were made for 11 min. with 50 Hz sampling; however, only 164 s intervals with good artificial noise conditions were analyzed. Analyzing procedures are as follows:

(1) selection of analyzing intervals,

(2) instrumental correction to obtain velocity seismograms of 0.1–3 Hz band,

(3) rotation of horizontal components to get proper direction of motions,

(4) calculation of amplitude spectra with F.F.T. and their ratio.

Instrumental corrections were achieved with Z-transform in the time domain (Morii and Nishimura, 1986). The horizontal components were rotated to the direction parallel and normal to the major structural line, such as the long axis of the bay, to examine the directional characteristics in soil amplifications depending on the configuration of bedrock. Spectra were obtained with a 10% cosine taper and triangular smoothing weight of 25 points.

2.2 Site Locations

Peninsula cities—In the bay area, the general trend of geological division is parallel to the long axis of the bay. We set the measuring line perpendicular to the trend, from a hillside in San Mateo to the bay coast in Foster City with 14 sites, including 4 strong-motion sites. Figure 2.1 shows the site locations, 3 sites on the Franciscan assemblage (KJf), 3 sites on Quaternary alluvium (Qal) and 8 sites on artificial fill overlying bay mud (Qm). **BIS** on unit KJf was used for the reference site. Table 2.1 lists the site locations, surface geology and observational information.

Santa Clara Valley—Observations were carried out at 6 sites across the Santa Clara Valley from Los Altos Hills to Alum Rock, the eastern part of San Jose, as shown in Figure 2.2. Table 2.2 lists the site locations, geology and observational information. Three sites, **SNV**, **AGN** and **SJI**, on thick soil deposits (Qal) were set near the strong motion sites. **PAH** is on Tertiary and Quaternary sedimentary rocks (QTs). **ARP** is located on the bedrock (TMzs), on the opposite side of the valley. **KIR** was used for the reference site. In analysis the data at **ARP** was also used for comparison.

Santa Cruz—Figure 2.3 shows the site locations and surface geology in the city of Santa Cruz. The measuring line of 5 km long, consisting of 18 sites, covers the typical geological setting: marine terrace deposits (Qm) and alluvium (Qal), across the heavily damaged San Lorenzo river side area. 15 sites were located at the same places as the aftershock observation sites (King *et al.*, 1990). The reference site is **LOE** on quartz diorite of the metasedimentary rocks unit (sch). Table 2.3 lists the site specifications.

2.3 Results of Spectral Analyses

Peninsula cities—Figures A1–14 show velocity seismograms, amplitude spectra and their ratios. The horizontal components are rotated to the direction parallel and normal to the long axis of the bay, that is, N40°W and N50°E, respectively. Figure A1 shows the difference between the system responses observed at the same place, **BIS**. It is ascertained that the differences between the systems in the given frequency bands (Table 4) are within 5%. The characteristics of spectral ratios are as follows:

BIS, AP6 and MTR on unit KJf (Figs. A2–3):
AP6 and MTR show nearly the same spectra as those at the reference site, **BIS**, in the wide frequency range of 0.1–3 Hz.

SYL, CHE and OT2 on unit Qal (Figs. A4–6):
Amplitude spectra are nearly the same as those at the reference site in the frequency range lower than 1 Hz. They increase with frequency above 1 Hz, showing the combined effects of increase of traffic noises and changes of ground responses. As the spectral contents of traffic noise are considered to increase monotonically with frequency in the same manner between the vertical and horizontal components, the spectral peaks around 1.8 Hz in the horizontal components at **SYL** are attributable to the soft alluvial deposits.

OTA, FOX, AP2, ARG, CHA, MAL, LON, and RWS on Qm (Figs. A7–14):

Spectral contents at the bay mud sites are quite different from those at the reference site. The differences become larger from west to east: the frequency at which amplification takes place becomes lower and the amplification becomes larger. These characteristics are more remarkable in

the horizontal components than vertical ones at all sites, showing the low rigidity of the bay mud and artificial fill. Although the characteristics are not so typical at **OTA** and **FOX**, which are located near the boundary between units **Qal** and **Qm**, the horizontal amplifications are larger than vertical ones in the range of 0.8–2 Hz. The horizontal spectra at **RWS** have two peaks around 0.5 Hz and 1.3 Hz, which might be considered as the fundamental and higher resonances at the site.

Figure 2.4 shows the general trend of spectral change with site locations, where f_{peak} denotes peak frequency and f_{rise}, the frequency at which amplification occurs in the horizontal components. Systematic decreases of f_{peak} and f_{rise} are remarkable. Although f_{peak} can be variable according to the spectral contents of incident microseisms, observed f_{peak} seems to reflect the characteristic frequency of ground at the site, because the spectral ratio also peaks at the same frequency.

Table 2.4 and Figure 2.5 show the mean spectral ratios in several frequency bands. Frequency-dependent large amplifications at bay mud sites and their systematic change with site locations are very remarkable. In addition to this, it is obvious that there are directional differences in amplifications: in the horizontal components, amplifications in the direction parallel to the geological divisions (N40°W) are generally larger than those in normal direction (N50°E), except higher frequency bands at **MAL** and **LON**.

Santa Clara Valley—Figures A15–20 show the velocity seismograms, their spectra and ratios. The horizontal components are rotated to N40°W and N50°E, parallel and normal to the axis of the valley. All the ground sites are compared with **ARP** as well as **KIR**, because the amplitudes at the reference site, **KIR**, are considerably larger than those at **ARP** (Fig. A20).

Figure A15 shows the reliability of the systems. The differences in the given bands are less than 5%. Tables 2.5.1–2.5.3 and Figures 2.6.1 and 2.6.2 show the mean spectral ratios in the given frequency bands. The amplitude ratios are calculated to **KIR**, **ARP** and assumed regular wave fields. The regular wave field is obtained with assumptions of (1) line source of microseisms along the coastal region of the Pacific, (2) propagation of microseisms as plane surface waves in the direction of N50°E, and (3) attenuation of waves in a functional form of $e^{-\alpha r}$, where α is the attenuation coefficient in km^{-1} and r is distance in km. Each e in the band is estimated from the simultaneous observations at **KIR** and **ARM** and listed in Table 2.5.3. Amplification characteristics at sites are as follows:

KIR and **PAH** on **QTs** (Figure A16):
Spectral contents of these sites are nearly the same in the whole frequency range of 0.1–3 Hz. However, they are much larger than those of corresponding components at the rock site, **ARP**, even in the frequency range lower than 1 Hz. It is suggested that there are some amplifications at the rock sites on unit QTs compared to unit TMzs, even if we take account of wave attenuation, as discussed in section 2.4.

SNV, AGN and SJI on thick deposits of unit Qal (Figures A17–19):
In the frequency range lower than about 0.8 Hz, the ratios to **KIR** show complicated variations around 1.

Comparing **ARP**, large amplification occurs at all these sites in the different manner between the vertical and horizontal components. Horizontal $f_{\rm rise}$s are about 0.2 Hz at **SNV** and **AGN**, and 0.15 Hz at **SJI**, which are much lower than $f_{\rm rise}$ at the bay mud sites in Peninsula cities. The amplifications occur in a wide frequency range without sharp peaks below 1 Hz, except 0.4 Hz peak in the N50°E component at **SNV**. Systematic directional differences in the horizontal components are not obvious.

Santa Cruz—Figures A21–38 show seismograms, spectra and their ratios. Seismograms are high-passed at 0.25 Hz to remove the following unfavorable long-period noises. During the observations in Santa Cruz, the local winds were relatively strong (up to 7 m/s) and made gust effects on the reference site, which was located in a redwood forest. Figure 2.7 shows the amplitudes of 3 components at **LOE** and their variation with time. The amplitudes of 3 components at **LOE** during the observations at **WAL, BLA, BAS, SBR, EFF, CEW, PGM,** and **FNT** differs remarkably from one another. In particular, the EW component shows the unfavorable condition of the seismometer setting.

Table 2.6 and Figure 2.8 show the mean spectral ratios in which the vertical components at **LOE** were used as references for all 3 components, since it can be safely assumed that in the ordinary condition the spectral amplitudes of microseisms at the rock site are considered nearly the same between the vertical and horizontal components. The errors due to this are estimated as $(11 \pm 11\%)$ for the 0.25–0.5 Hz band and $(2 \pm 14\%)$ for the 0.5–1.0 Hz band, respectively.

Generally, the soil amplifications occur in the frequency range higher than about 0.6 Hz, reflecting the small dimension of geological structures in Santa Cruz. Long-period amplifications are smaller than those in Peninsula cities and the Santa Clara Valley. On average amplifications at the alluvial sites (Qal) are larger than those at the marine terrace deposits (Qt). The amplification characteristics at the sites are as follows:

BAR on marble (m) (Figure A22):
Spectral contents at **BAR** are the same as those at **LOE** in the frequency range of 0.25–3 Hz.

KAL, SHE, TRE, SBR, and **EFF** on unit Qt (Figures A23–27):
Spectral contents at **KAL**, located on the boundary between unit Qt and metamorphic rocks (m), are the same as those at **LOE**. For other 4 sites, $f_{\rm rise}$s are at 0.6–1.0 Hz and $f_{\rm peak}$s, 1.0–1.7 Hz in the horizontal components.

11 sites on Qal (Figures A28–38):
At **WAL** and **BLA**, which are located on and near the boundary between units Qt and Qal, their $f_{\rm rise}$s and $f_{\rm peak}$s are about 0.8 Hz and 1.5–2.0 Hz,

respectively. For the other sites on unit Qal, f_{rise} ranges from 0.6 Hz to 0.8 Hz, and f_{peak} from 1.0 Hz to 1.2 Hz, except **WAL** and **BLA**. These values are slightly lower than those for sites on unit Qt. There are large amplifications in the vertical component at **CED** due to unknown factors.

2.4 Discussion

Significant site-specific amplifications due to surface geology and bedrock structures were obtained through field surveys in the three areas. We discuss the results in comparison with the geological structures.

Peninsula cities—Figure 2.9 is a reproduction of a vertical cross section showing late Quarternary sediments based on borehole data (Atwater *et al.*, 1977). The section shows a few km north to our profile. In general, frequency characteristics of amplifications and their variations with site locations (Figures 2.4 and 2.5) appear very consistent to the depth to bedrock and/or the thickness of the artificial fill on bay mud (Qm).

It is interesting to note the typical cases: In Foster City the depth to bedrock is 50 ft. near the middle point between **OTA** and **FOX**, and 270 ft. near **LON**. In Redwood Shores, these are 285 ft. at **AP2** and 650 ft. near **RWS**, which are much deeper than in Foster City (Bishop and Williams, 1974). The largest amplifications in the lower frequency at **RWS** must reflect the largest thickness of sediments, including fill. Despite nearly the same depth to bedrock at **LON** and **AP2**, **LON** has much larger amplifications than **AP2**, the differences of which might be attributed not only to the effect of the soft surface layer (Qm) but also to the difference in distance from the vertical edge of bedrock (TMzs). The latter factor is possibly connected to the effect of configuration of bedrock on propagating surface waves (Drake, 1980), which is also suggested from the observation of directional characteristics in the horizontal amplifications, that is, larger amplification in the direction parallel to the edge of bedrock (N40°W).

It seems necessary to take into account that in the marginal part there is a larger variation of physical properties in the direction normal to the margin; namely, the elastic constants and the bedrock depth change within a wavelength. This seems to bring the directional difference in the effective physical properties, which could cause the observed difference in amplifications. In the central part of the Santa Clara Valley, the differences in horizontal amplifications are not systematic (Figures 2.6.1 and 2.6.2). The same features are observed in the Kyoto basin, Japan, where the directed amplifications are more remarkable in the marginal area of the basin (Akamatsu *et al.*, 1991). In this connection, it is interesting that the larger excitations of radial components than the transverse ones were observed in the long-period range during the Loma Prieta earthquake at ground sites as discussed in section 3.

Comparison of amplification factor with soil profile type—Hensolt and Brabb (1990) zoned San Mateo County on the basis of depth to bedrock and soil properties mainly of

shear-wave velocity for design of engineered structures. From definition of their soil profile type, our observation sites in Peninsula cities are specified as follows:

S1: BIS, AP6, MTR, SYL, CHE, OT2, FOX
S2: OTA
S3: AP2
S4: ARG, CHA, MAL, LON, RWS

CHE, OT2, FOX and **OTA** are located near the boundary between S1 and S2. **AP2** is near the boundary between S2 and S3. **ARG** is on the boundary between S3 and S4. Amplification at **OTA** (S2) is slightly larger than those at **CHE, OT2** and **FOX** in the frequency range of 0.5–1.0 Hz. Amplification of **AP2** (S3) is much larger than that at **OTA** (S2) sites in the higher frequency range of 0.5–1.0 Hz, although not so large in the lower frequency range of 0.35–0.7 Hz. Amplifications at S4 sites and their frequency characteristics are remarkable with variation from site to site. This would imply that the soil profile type can oversimplify the soil condition. Therefore, there is a strong prospect that the microtremor measurement will be a useful tool for assessment of site condition based on frequency characteristics. It will also provide useful information at sites where the soil properties are not known in sufficient detail to determine the soil profile type.

Santa Clara Valley—There are large differences in amplitudes between **KIR** and **ARP**, west and east of the valley in the frequency range higher than 0.2 Hz. It seems reasonable to consider the attenuation during propagation of microseism as surface waves. In the Los Angeles Basin, the attenuation coefficients were estimated at 0.016 for $T = 6$ sec and 0.032 for $T = 3$ sec. In the Santa Clara Valley, we obtained 0.014 for 0.125–0.25 Hz, nearly the same as that for the Los Angeles basin, and 0.062 for 0.25–0.5 Hz, which is much larger than for the Los Angeles basin. This may suggest that there are some differences in amplification between the two rock sites; larger amplification at Tertiary and Quaternary sedimentary rocks than Mesozoic and Tertiary sedimentary rocks.

The depth to bedrock in the central parts of the valley is not well known. The depths of the layer with shear wave velocity larger than 2500 ft/s are about 700 ft. at **SNV** and **AGN**, and 500 ft. at **SJI**. Amplifications at alluvial sites (Figure 2.6) extend to the frequency range lower than those in Peninsula cities (Figure 2.5). This must reflect the thickness of alluvial sediments and may also depend on the locations, that is, the central part far from the edge of bedrock.

Amplifications in the higher frequency range of 0.5–1.0 Hz (Figure 6.2) are lower than those for Peninsula cities (Figure 5), which may reflect the differences in soil conditions on the uppermost layer such as shear wave velocities and consequently Poisson's ratio between alluvial sediments (Qal) and fill on bay mud (Qm).

The differences in amplifications between the two horizontal components are not systematic in the alluvial sites, which might be connected to the fact that these sites are located far from the margin of the valley as discussed already.

Santa Cruz—Amplifications of microseisms (Figure 2.8) appear mainly in the frequency range higher than about 0.6 Hz, reflecting the small scale of the geological structures. However, mean spectral ratios seem generally to relate to the thickness of alluvial deposits as follows:

From the preliminary report for the seismic refraction experiments (King *et al.*, 1990), the depth to a velocity layer with $V_p > 3.0$ km/s is around 5 m on the upper terrace and about 10 m on the lower terrace. It is also suggested that the thickness of alluvial deposits is more than 70 m at sites on unit Qal. Amplifications in the range of 0.5–1.0 Hz are nearly 1 at KAL on the upper terrace of the west side of the San Lorenzo River. They increase from the upper terrace to the lower terrace, and to the alluvial deposits around the river. This general trend is considered to reflect the velocity structures.

2.5 SUMMARY

From observations in the Bay Area and Santa Cruz, amplifications of miroseisms due to soil deposits are summarized as follows:

(1) Site-specific amplifications can be discussed with spectral ratios of ground sites to rock sites.

(2) Frequency characteristics of amplifications are related to the depth to bedrock and physical properties of soil deposits.

(3) Amplifications of horizontal components are larger than those of vertical ones, reflecting low rigidity of deposits.

(4) In the marginal parts of the basin, there is a difference in amplifications between the horizontal components, parallel and normal to the long axis of the bay, suggesting the effect of configuration of bedrock on propagating surface waves.

(5) It is suggested that amplification at Tertiary and Quaternary sedimentary rocks is larger than that at Mesozoic and Tertiary sedimentary rocks.

(6) Microtremor measurement will provide useful knowledge for evaluation of the site factor needed to determine the design of structure.

REFERENCES

Akamatsu, J., M. Fujita, and K. Nishimura (1991). Vibrational characteristics of microseisms and their applicability to microzoning in a sedimentary basin, *J. Phys. Earth,* in press.

Atwater, B. F., C. W. Hedel, and E. J. Helley (1977). Late Quaternary depositional history, Holocene sea-level changes, and vertical crustal movement, southern San Francisco Bay, California, *U.S. Geol. Surv. Prof. Pap.* **1014**.

Bishop, C. C. and J. W. Williams (1974). Thickness of alluvium, Santa Clara County, California, State of California, The Resources Agency, Dept. of Conservation, *Special Report* **97**.

Drake, L. A. (1980). Love and Rayleigh waves in an irregular soil layer, *Bull. Seism. Soc. Am.*, **70**, 571–582.

Hensolt, W. H. and E. E. Brabb (1990). Maps showing elevation of bedrock and implications for design of engineered structures to withstand earthquake shaking in San Mateo County, California, *U.S. Geol. Surv. Open-File Rep.* **90–496**.

King, K., D. Carver, R. Williams, D. Worley, E. Cranswick, and M. Meremonte (1990). Santa Cruz seismic investigations following the October 17, 1989 Loma Prieta earthquake, *U.S. Geol. Surv. Open-File Rep.* **90–307**.

Morii, W. and K. Nishimura (1986). Introduction of library program (71)—filtering of equispaced data, *Bull. Data Processing Center*, Kyoto University, **19**, 312–318 (in Japanese).

Table 2.1. Site geology and records of observations in Peninsula Cities.

			Observation for ground site						Observation for reference site					
	Site		File	ID	Date	Time		L.P.F.	File	ID	Time		L.P.F.	
No.	Code	Geology	Name	No.	M D	H M	Amp(x)	(Hz)	Name	No.	H M	Amp(x)	(Hz)	Comments
1					5 23				BIS01.SP	1	15:53	100	10	p.u. step response
2					5 23				BIS02.SP	1	16:10	20000	10	
3	BIS	KJf	BIS2.LP	1	5 23	17:00	10000	10	BIS03.SP	1	17:00	20000	10	for systems check
4	FOX	Qm	FOX.LP	1	5 24	10:00	5000	1	BIS04.SP	1	10:00	20000	10	
5	AP2*	Qm	AP2.LP	1	5 24	11:15	5000	3	BIS04.SP	2	11:15	20000	10	
6	RWS*	Qm	RWS.LP	1	5 24	12:30	2500	3	BIS04.SP	3	12:30	20000	10	
7	RWS*	Qm	RWS2.LP	1	5 24	12:35	2500	1						
8	ARG	Qm	ARG.LP	1	5 24	15:00	2500	1	BIS05.SP	1	15:00	20000	10	
9	CHA	Qm	CHA.LP	1	5 24	16:01	5000	1	BIS05.SP	2	16:00	20000	10	
10	LON	Qm	LON.LP	1	5 24	17:00	5000	1	BIS05.SP	3	17:00	20000	10	
11	LON	Qm	LON2.LP	1	5 24	17:23	5000	1						
12	MAL*	Qm	MAL.LP	1	5 24	18:20	5000	1	BIS06.SP	1	18:20	20000	10	
13					5 25				BIS07.SP	1	9:00	20000	10	
14	MTR	KJf	MTR.LP	1	5 25	10:30	10000	10	BIS07.SP	2	10:30	20000	10	
15	SYL	Qal	SYL.LP	1	5 25	12:00	5000	3	BIS07.SP	3	12:00	20000	10	
16	CHE	Qal	CHE.LP	1	5 25	14:00	10000	3	BIS08.SP	1	14:00	10000	10	
17	OT2	Qal	OT2.LP	1	5 25	15:00	10000	3	BIS08.SP	2	15:00	10000	10	
18	OTA	Qm	OTA.LP	1	5 25	16:00	5000	3	BIS08.SP	3	16:00	10000	10	
19	AP6*	TMzs	AP6.LP	1	5 25	17:30	25000	10	BIS09.SP	1	17:30	20000	10	

* : Strong motion seismograph site

Geology : Qm=fill on bay mud, Qal=Alluvium, KJf=Franciscan Formation, TMzs=Tertiary and Mesozoic sedimentary rocks.

Table 2.2. Site geology and records of observations in Santa Clara Valley.

			Observation for ground site							Observation for reference site					
	Site		File	ID	Date		Time		L.P.F.	File	ID	Time		L.P.F.	
No.	Code	Geology	Name	No.	M	D	H	M	Amp(x) (Hz)	Name	No.	H	M	Amp(x) (Hz)	Comments
1	KIR	QTs	KIR.LP	1	5	31	17:30		5000 10	KIR01.SP	1	17:30		5000 10	for systems check
2										KIR02.SP	1	9:00		2000 10	
3										KIR02.SP	2	10:00		2000 10	
4	ARP	TMzs	ARP.LP	1	6	1	11:00		10000 10	KIR02.SP	3	11:00		2000 10	
5										KIR02.SP	4	12:00		2000 10	
6	SJ1*	Qal	SJ1.LP	1	6	1	13:00		2500 1	KIR02.SP	5	13:00		2000 10	
7										KIR02.SP	6	14:00		2000 10	
8	AGN*	Qal	AGN.LP	1	6	1	15:30		5000 1	KIR03.SP	1	15:30		2000 10	
9	SNV*	Qal	SNV.LP	1	6	1	17:00		5000 1	KIR03.SP	2	17:00		2000 10	
10	PAH*	QTs	PAH.LP	1	6	1	18:30		5000 10	KIR03.SP	3	18:30		2000 10	
11										KIR04.SP	1	19:15		2000 10	for temporal variation
12										KIR04.SP	2	20:15		2000 10	for temporal variation
13										KIR04.SP	3	21:15		2000 10	for temporal variation
14										KIR04.SP	4	22:15		2000 10	for temporal variation
15										KIR04.SP	5	23:15		2000 10	for temporal variation
16					6	2				KIR04.SP	6	0:15		2000 10	for temporal variation
17										KIR04.SP	7	1:15		2000 10	for temporal variation
18										KIR04.SP	8	2:15		2000 10	for temporal variation
19										KIR04.SP	9	3:15		2000 10	for temporal variation
20										KIR04.SP	10	4:15		2000 10	for temporal variation
21										KIR04.SP	11	5:15		2000 10	for temporal variation
22										KIR04.SP	12	6:15		2000 10	for temporal variation
23										KIR04.SP	13	7:15		2000 10	for temporal variation
24										KIR04.SP	14	8:15		2000 10	for temporal variation
25										KIR04.SP	15	9:15		2000 10	for temporal variation

* : Strong motion seismograph site

Geology : Qal=Alluvium, QTs=Quaternary and Tertiary sedimentary rocks, TMzs=Tertiary and Mesozoic sedimentary rocks.

Table 2.3. Site geology and records of observations in Santa Cruz City.

			Observation for ground site							Observation for reference site				
	Site		File	ID	Date	Time		L.P.F.		File	ID	Time		L.P.F.	
No.	Code	Geology	Name	No.	M D	H M	Amp(x)	(Hz)		Name	No.	H M	Amp(x)	(Hz)	Comments
1	LOE*	sch	LOE.LP	1	5 17	11:45	1000	10		LOE01.SP	1	11:45	10000	10	LP without pre-amp(SA-55)
2										LOE02.SP	1	14:00	10000	10	too windy at BAR
3	CONF	Qal	CNFINN.LP	1	5 17	16:50	10000	1							system check for LP
4	BAR*	m	BAR.LP	1	5 18	8:30	10000	3		LOE03.SP	1	8:30	10000	10	
5	KAL*	Qt	KAL.LP	1	5 18	9:30	25000	10		LOE04.SP	1	9:30	10000	10	
6	SHE*	Qt	SHE.LP	1	5 18	10:30	10000	3		LOE05.SP	1	10:30	10000	10	
7	TRE*	Qt	TRE.LP	1	5 18	11:30	5000	3		LOE06.SP	1	11:30	10000	10	
8	TRE*	Qt	TRE2.LP	1	5 18	13:00	5000	3		LOE07.SP	1	13:00	10000	10	LP CH.3 down
9										LOE07.SP	2	14:00	10000	10	
10	WAL*	Qal	WAL.LP	1	5 18	15:00	2500	1		LOE08.SP	1	15:00	10000	10	
11	BLA*	Qal	BLA.LP	1	5 18	16:00	5000	1		LOE09.SP	1	16:00	10000	10	
12	WAS*	Qal	WAS.LP	1	5 18	17:01	10000	1		LOE10.SP	1	17:00	10000	10	
13	CED*	Qal	CED.LP	1	5 18	18:00	10000	1		LOE11.SP	1	18:00	10000	10	LP CH.3 down
14	LAU*	Qal	LAU.LP	1	5 18	19:00	10000	1		LOE12.SP	1	19:00	10000	10	
15	LAV*	Qal	LAV.LP	1	5 18	20:00	10000	1		LOE13.SP	1	20:00	10000	10	
16	CE2*	Qal	CE2.LP	1	5 19	9:00	10000	1		LOE14.SP	1	9:00	10000	10	
17	BAS*	Qal	BAS.LP	1	5 19	10:00	10000	1		LOE15.SP	1	10:00	10000	10	
18	SBR*	Qt	SBR.LP	1	5 19	11:00	10000	3		LOE16.SP	1	11:00	10000	10	
19	EFF*	Qt	EFF.LP	1	5 19	12:10	10000	3		LOE17.SP	1	12:10	10000	10	
20	CEW	Qal	CEW.LP	1	5 19	15:00	10000	1		LOE18.SP	1	15:00	10000	10	
21	CEW	Qal	CEW2.LP	1	5 19	15:11	1000	10		LOE19.SP	1	15:11	10000	10	for short-period tremor
22	PGM	Qal	PGM.LP	1	5 19	16:00	10000	1		LOE20.SP	1	16:00	10000	10	
23	PGM	Qal	PGM2.LP	1	5 19	16:12	1000	10		LOE21.SP	1	16:11	10000	10	for short-period tremor
24	FNT	Qal	FNT.LP	1	5 19	17:00	10000	1		LOE22.SP	1	17:00	10000	10	
25	FNT	Qal	FNT2.LP	1	5 19	17:11	1000	10		LOE23.SP	1	17:11	10000	10	for short-period tremor
26	LOE*	sch	LOE2.LP	1	5 19	18:15	25000	3		LOE24.SP	1	18:15	10000	10	for systems check
27										LOE25.SP	1	18:30	100	10	p.u. step response
28	LOE*	sch	NOISE.LP	1	5 19	18:34	25000	10							system noise
29										LOE26.SP	1	18:45	10000	10	system noise

* : Ahtershock observation site (King et al., 1990)

Geology : sch=Metasedimentary rocks, m=Marble, Qt=Marine terrace deposits, Qal=Alluvium.

Table 2.4. MEAN SPECTRAL RATIO OF MICROSEISMS IN PENINSULA CITIES

BAND	0.20 - 0.667 HZ			0.125 - 0.25 HZ			0.175 - 0.35 HZ			0.25 - 0.50 HZ			0.35 - 0.70 HZ			0.50 - 1.00 HZ		
	UD	N40W	N50E	UD	N40W	N50E	UD	N40W	N50E	UD	N40W	N50E	UD	N40W	N50E	UD	N40W	N50E
KJf and TMzs																		
AP6	0.97	1.43	0.94	1.22	1.06	1.17	1.15	1.16	1.09	1.03	1.35	0.89	0.88	1.67	0.89	0.90	1.89	1.09
MTR	0.90	0.82	0.90	1.03	0.79	0.89	1.02	0.79	0.94	0.96	0.84	0.94	0.84	0.83	0.88	0.93	0.83	0.76
MEAN	0.94	1.12	0.92	1.13	0.92	1.03	1.09	0.98	1.02	0.99	1.10	0.91	0.86	1.25	0.88	0.92	1.36	0.93
DEV	0.04	0.31	0.02	0.09	0.13	0.14	0.06	0.18	0.08	0.03	0.25	0.02	0.02	0.42	0.00	0.02	0.53	0.16
Qal																		
SYL	0.79	1.01	0.89	0.72	1.07	0.99	0.75	1.08	0.93	0.86	0.97	0.87	0.78	0.97	0.87	0.75	1.14	1.12
CHE	0.88	0.91	0.80	0.91	0.65	0.69	0.87	0.84	0.76	0.91	0.83	0.77	0.87	0.93	0.83	0.97	1.18	1.01
OT2	0.74	0.77	0.80	0.86	0.63	0.93	0.88	0.65	0.89	0.84	0.73	0.76	0.66	0.82	0.78	1.03	1.08	1.02
MEAN	0.80	0.90	0.83	0.83	0.78	0.87	0.83	0.86	0.86	0.87	0.84	0.80	0.77	0.91	0.83	0.92	1.13	1.11
DEV	0.06	0.10	0.04	0.08	0.21	0.13	0.06	0.18	0.07	0.03	0.10	0.05	0.08	0.07	0.04	0.12	0.04	0.08
Qw																		
OTA	0.87	1.08	0.90	0.73	1.27	1.02	0.80	1.12	0.91	0.91	1.04	0.86	0.89	1.10	0.89	0.87	1.50	1.45
FOX	0.74	0.95	0.74	0.92	1.33	1.16	0.99	1.09	0.99	0.84	0.85	0.77	0.60	0.92	0.66	0.61	1.53	1.04
AP2	0.81	1.18	0.88	1.45	1.40	1.07	1.23	1.12	0.89	0.89	0.99	0.79	0.60	1.31	0.89	0.83	4.52	3.42
ARG	0.73	2.18	1.45	1.16	1.36	0.96	0.97	1.25	0.90	0.78	1.32	1.09	0.64	3.10	1.95	1.98	12.92	13.28
CHA	1.06	3.75	2.94	1.39	2.12	1.51	1.45	1.85	1.32	1.03	1.70	1.37	0.94	5.13	4.23	3.53	11.08	9.23
MAL	1.28	4.43	3.55	1.41	2.14	1.84	1.30	1.95	1.61	0.98	2.24	1.86	1.47	5.92	4.82	4.60	10.87	12.75
LON	1.00	3.63	3.13	1.57	3.61	1.97	1.35	2.95	1.56	1.07	2.42	1.54	0.88	4.18	4.32	5.25	11.28	14.01
RWS	1.66	5.71	4.20	1.45	1.55	1.41	1.47	1.41	1.70	1.31	4.98	3.57	1.76	7.60	5.49	6.57	17.30	13.09
MEAN	1.02	2.86	2.22	1.26	1.85	1.37	1.20	1.59	1.24	0.98	1.94	1.48	0.97	3.66	2.91	3.03	8.88	8.53
DEV	0.30	1.66	1.29	0.28	0.74	0.36	0.23	0.60	0.33	0.16	1.27	0.87	0.40	2.32	1.88	2.14	5.35	5.29

Table 2.5.1. MEAN SPECTRAL RATIO OF MICROSEISMS IN SANTA CLARA VALLEY (TO KIR)

BAND	0.143 - 0.5 HZ			0.20 - 0.667 HZ			0.125 - 0.25 HZ			0.175 - 0.35 HZ			0.25 - 0.50 HZ			0.35 - 0.70 HZ			0.50 - 1.00 HZ		
	UD	N40W	N50E	UD	N40W	N50E	UD	N40W	N50E	UD	N40W	N50E	UD	N40W	N50E	UD	N40W	N50E	UD	N40W	N50E
QTs																					
KIR	1.00	1.00	1.00	1.00	1.00	1.00	1.00	1.00	1.00	1.00	1.00	1.00	1.00	1.00	1.00	1.00	1.00	1.00	1.00	1.00	1.00
QTs																					
PAH	0.71	0.84	1.09	0.76	1.11	1.03	0.78	0.79	0.87	0.70	0.71	0.94	0.69	0.87	1.19	0.82	1.29	1.10	0.83	1.38	1.16
Qal																					
SNV	0.74	1.14	2.27	0.74	1.27	1.93	0.80	0.78	0.76	0.74	1.17	1.31	0.75	1.29	2.91	0.71	1.30	2.14	0.87	1.44	1.35
AGN	0.50	1.09	1.31	0.48	0.99	1.23	0.70	0.87	0.90	0.52	1.08	1.13	0.44	1.16	1.48	0.49	0.90	1.33	1.01	1.66	1.69
SJI	0.88	1.08	1.17	0.67	0.87	0.97	1.02	1.43	1.38	1.06	1.16	1.44	0.82	0.96	1.08	0.47	0.72	0.78	0.60	1.02	1.39
MEAN	0.71	1.10	1.58	0.63	1.04	1.38	0.84	1.03	1.01	0.77	1.14	1.29	0.67	1.13	1.82	0.56	0.97	1.41	0.83	1.37	1.47
DEV	0.16	0.03	0.49	0.11	0.17	0.41	0.14	0.29	0.27	0.22	0.04	0.13	0.17	0.14	0.79	0.11	0.24	0.56	0.17	0.27	0.15
TMzs																					
ARP	0.57	0.32	0.38	0.38	0.21	0.24	0.88	0.64	0.79	0.72	0.37	0.44	0.44	0.21	0.22	0.21	0.14	0.19	0.17	0.16	0.17

Table 2.5.3. MEAN SPECTRAL RATIO OF MICROSEISMS IN THE SANTA CLARA VALLEY (TO KIR-ARP INTERPOLATION)

BAND	0.143 - 0.5 HZ			0.20 - 0.667 HZ			0.125 - 0.25 HZ			0.175 - 0.35 HZ			0.25 - 0.50 HZ			0.35 - 0.70 HZ			0.50 - 1.00 HZ		
	UD	N40W	N50E	UD	N40W	N50E	UD	N40W	N50E	UD	N40W	N50E	UD	N40W	N50E	UD	N40W	N50E	UD	N40W	N50E
QTs																					
KIR	1.00	1.00	1.00	1.00	1.00	1.00	1.00	1.00	1.00	1.00	1.00	1.00	1.00	1.00	1.00	1.00	1.00	1.00	1.00	1.00	1.00
QTs																					
PAH	0.75	0.95	1.22	0.83	1.20	1.10	0.79	0.83	0.90	0.72	0.80	1.03	0.75	1.04	1.41	1.98	1.60	1.33	1.01	1.70	1.41
Qal																					
SNV	0.92	1.78	3.33	1.13	2.45	3.50	0.84	0.94	0.83	0.85	1.73	1.82	1.03	2.42	5.34	1.32	2.81	4.17	1.76	3.02	2.70
AGN	0.70	2.13	2.33	0.89	2.60	2.95	0.75	1.14	1.04	0.63	1.95	1.83	0.71	2.98	3.68	1.24	2.85	3.62	2.88	5.04	4.80
SJI	1.31	2.42	2.36	1.37	2.75	2.78	1.12	1.98	1.64	1.34	2.38	2.60	1.47	2.99	3.25	1.45	2.89	2.62	2.14	3.91	4.90
MEAN	0.98	2.11	2.67	1.13	2.60	3.08	0.91	1.35	1.17	0.94	2.02	2.09	1.07	2.80	4.09	1.34	2.85	3.47	2.26	3.99	4.13
DEV	0.25	0.26	0.47	0.20	0.12	0.31	0.16	0.45	0.34	0.30	0.27	0.37	0.31	0.26	0.90	0.09	0.04	0.64	0.46	0.83	1.01
TMzs																					
ARP	1.00	1.00	1.00	1.00	1.00	1.00	1.00	1.00	1.00	1.00	1.00	1.00	1.00	1.00	1.00	1.00	1.00	1.00	1.00	1.00	1.00
ALPHA (X0.01/km)	2.22	4.49	3.86	3.62	6.14	5.60	0.52	1.78	0.97	1.31	3.95	3.26	3.23	6.30	6.08	6.24	7.71	6.89	7.00	7.41	6.96

Table 2.5.2. MEAN SPECTRAL RATIO OF MICROSEISMS IN THE SANTA CLARA VALLEY (TO ARP : NORMALIZED BY ARP/KIR)

BAND	0.143 - 0.5 HZ			0.20 - 0.667 HZ			0.125 - 0.25 HZ			0.175 - 0.35 HZ			0.25 - 0.50 HZ			0.35 - 0.70 HZ			0.50 - 1.00 HZ		
	UD	N40W	N50E	UD	N40W	N50E	UD	N40W	N50E	UD	N40W	N50E	UD	N40W	N50E	UD	N40W	N50E	UD	N40W	N50E
QTs																					
KIR	1.75	3.09	2.63	4.05	6.20	4.99	1.14	1.56	1.28	1.39	2.70	2.27	2.25	4.86	4.60	4.78	6.92	5.37	5.80	6.43	5.74
PAH	1.23	2.59	2.88	3.25	6.61	4.88	0.89	1.23	1.11	0.97	1.92	2.14	1.55	4.24	5.46	3.92	8.91	5.89	4.83	8.87	6.68
MEAN	1.49	2.84	2.76	3.60	6.41	4.94	1.02	1.40	1.20	1.18	2.31	2.21	1.90	4.55	5.03	4.35	7.92	5.63	5.32	7.65	5.74
DEV	0.26	0.25	0.13	0.40	0.21	0.06	0.13	0.17	0.09	0.21	0.39	0.07	0.35	0.31	0.43	0.43	1.00	0.26	0.49	1.22	0.47
Qal																					
SNV	1.29	3.51	5.97	3.04	6.85	9.54	0.91	1.22	0.96	1.03	3.15	2.98	1.68	6.28	13.39	3.39	8.99	11.45	5.07	9.26	7.72
AGN	0.88	3.36	3.44	2.03	5.17	5.76	0.79	1.36	1.14	0.72	2.90	2.55	0.99	5.63	6.79	2.33	6.20	7.11	5.84	10.66	9.69
SJI	1.53	3.32	3.09	2.10	3.96	4.09	1.17	2.24	1.76	1.47	3.13	3.27	1.85	4.65	4.98	2.24	4.96	4.18	3.49	6.56	7.97
MEAN	1.23	3.40	4.17	2.39	5.33	6.46	0.96	1.61	1.29	1.07	3.06	2.93	1.51	5.52	8.39	2.65	6.71	7.58	4.80	8.83	8.46
DEV	0.27	0.08	1.28	0.46	1.19	2.28	0.16	0.45	0.34	0.31	0.11	0.30	0.38	0.67	3.61	0.52	1.68	2.99	0.98	1.70	0.88
TMzs																					
ARP	1.00	1.00	1.00	1.00	1.00	1.00	1.00	1.00	1.00	1.00	1.00	1.00	1.00	1.00	1.00	1.00	1.00	1.00	1.00	1.00	1.00

Table 2.6. MEAN SPECTRAL RATIO OF MICROSEISMS IN SANTA CRUZ CITY

BAND	0.20 - 1.00 HZ			0.25 - 0.50 HZ			0.35 - 0.70 HZ			0.50 - 1.00 HZ		
	UD	NS	EW	UD	NS	EW	UD	NS	EW	UD	NS	EW
■												
BAR	0.79	0.83	0.87	0.81	0.89	0.88	0.82	0.80	0.89	0.79	0.79	0.88
Qt												
KAL	0.96	0.87	0.98	0.95	0.74	0.91	0.86	0.72	0.79	0.93	0.90	0.98
SHE	0.90	1.51	1.21	0.96	1.12	0.96	0.81	1.10	0.93	0.86	1.71	1.37
TRE	1.14	3.11	3.49	0.83	1.00	1.16	0.87	1.28	1.41	1.28	4.36	4.91
SBR	0.87	2.09	1.75	0.82	0.95	1.06	0.76	1.09	1.17	0.89	2.79	2.20
EFF	1.07	1.65	1.27	0.87	0.87	0.95	1.12	1.35	1.25	1.19	2.11	1.50
MEAN	0.99	1.85	1.74	0.89	0.94	1.01	0.88	1.11	1.11	1.03	2.37	2.19
DEV	0.10	0.75	0.91	0.06	0.13	0.09	0.12	0.22	0.22	0.17	1.17	1.42
QaL												
WAL	1.63	3.08	3.69	0.82	1.19	1.66	1.00	1.59	2.00	2.09	4.21	4.97
BLA	1.18	2.48	3.09	0.72	0.79	1.08	1.01	1.29	1.54	1.46	3.47	4.28
WAS	1.12	2.30	2.31	1.05	1.10	1.09	0.96	1.49	1.33	1.17	3.06	3.06
CED	3.09	2.10	2.42	2.67	1.18	1.41	3.12	1.44	1.59	3.46	2.67	3.00
CE2	0.97	3.36	2.93	0.77	1.06	1.07	0.75	1.38	1.25	1.07	4.79	4.07
CEW	0.95	1.63	1.55	0.91	1.04	0.86	0.92	1.23	0.95	1.00	2.05	2.01
PGM	0.96	1.85	1.71	0.76	0.68	0.78	0.84	0.91	0.91	1.11	2.59	2.28
FNT	1.65	1.84	1.58	0.99	0.80	0.86	1.06	0.97	1.02	2.06	2.50	2.04
LAU	1.01	3.85	3.90	0.89	1.11	1.22	0.78	1.41	1.34	1.07	5.49	5.53
LAV	0.98	1.91	2.49	1.00	0.99	1.24	0.77	1.43	1.50	0.96	2.49	3.27
BAS	1.47	1.66	1.64	1.06	1.05	1.06	1.09	1.03	1.15	1.70	1.95	2.02
MEAN	1.36	2.37	2.48	1.06	1.00	1.12	1.12	1.29	1.33	1.56	3.20	3.32
DEV	0.60	0.71	0.80	0.52	0.16	0.25	0.65	0.22	0.31	0.72	1.10	1.18

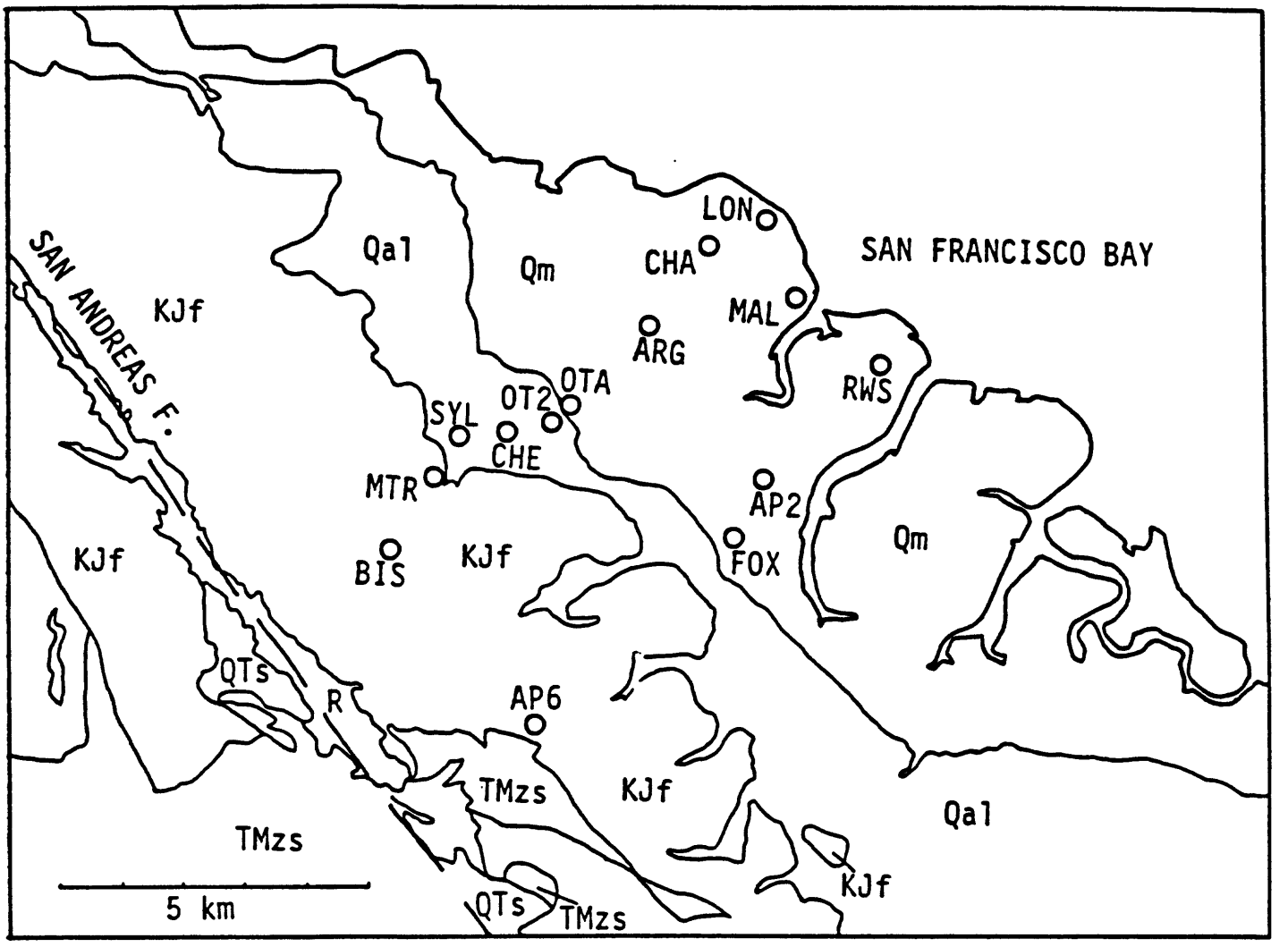

Fig. 2.1. Locations of sites and surface geology in Peninsula cities.
BIS: reference site.
AP6, AP2, RWS and MAL: strong motion seismograph sites.

Geology Qm : Holocene estuarine mud.
Qal : Quarternary alluvium.
KJf : Franciscan Formation, Mostly well-indurated sandstone and shell.
TMzs: Tertiary and Mesozoic sedimentary rocks.

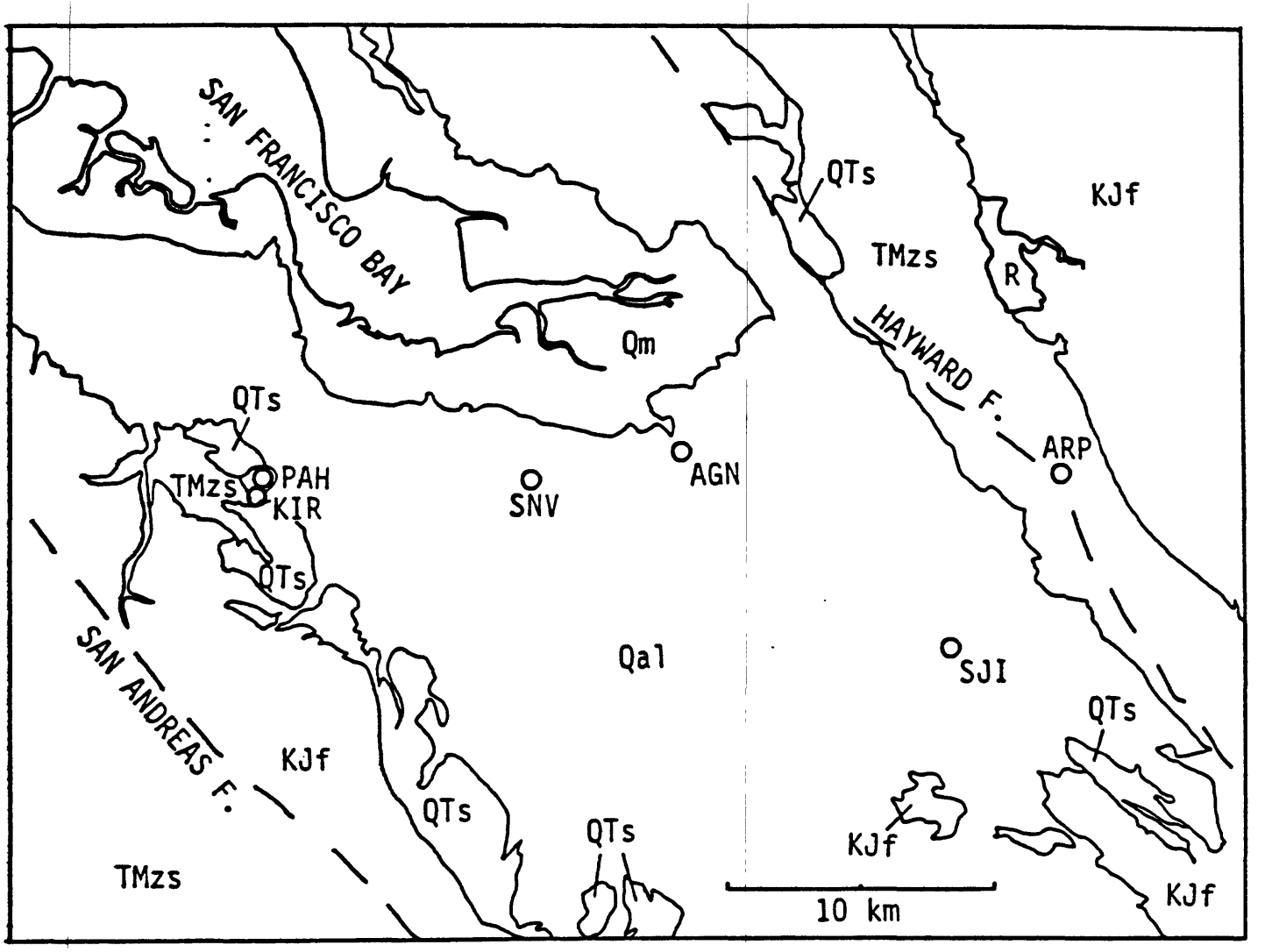

Fig. 2.2. Locations of sites and surface geology in Santa Clara Valley.
KIR: reference site.
SNV, AGN and SJI: strong motion seismograph sites.

Geology Qm : Holocene estuarine mud.
Qal : Quarternary alluvium.
KJf : Franciscan Formation, Mostly well-indurated sandstone and shell.
TMzs: Tertiary and Mesozoic sedimentary rocks.

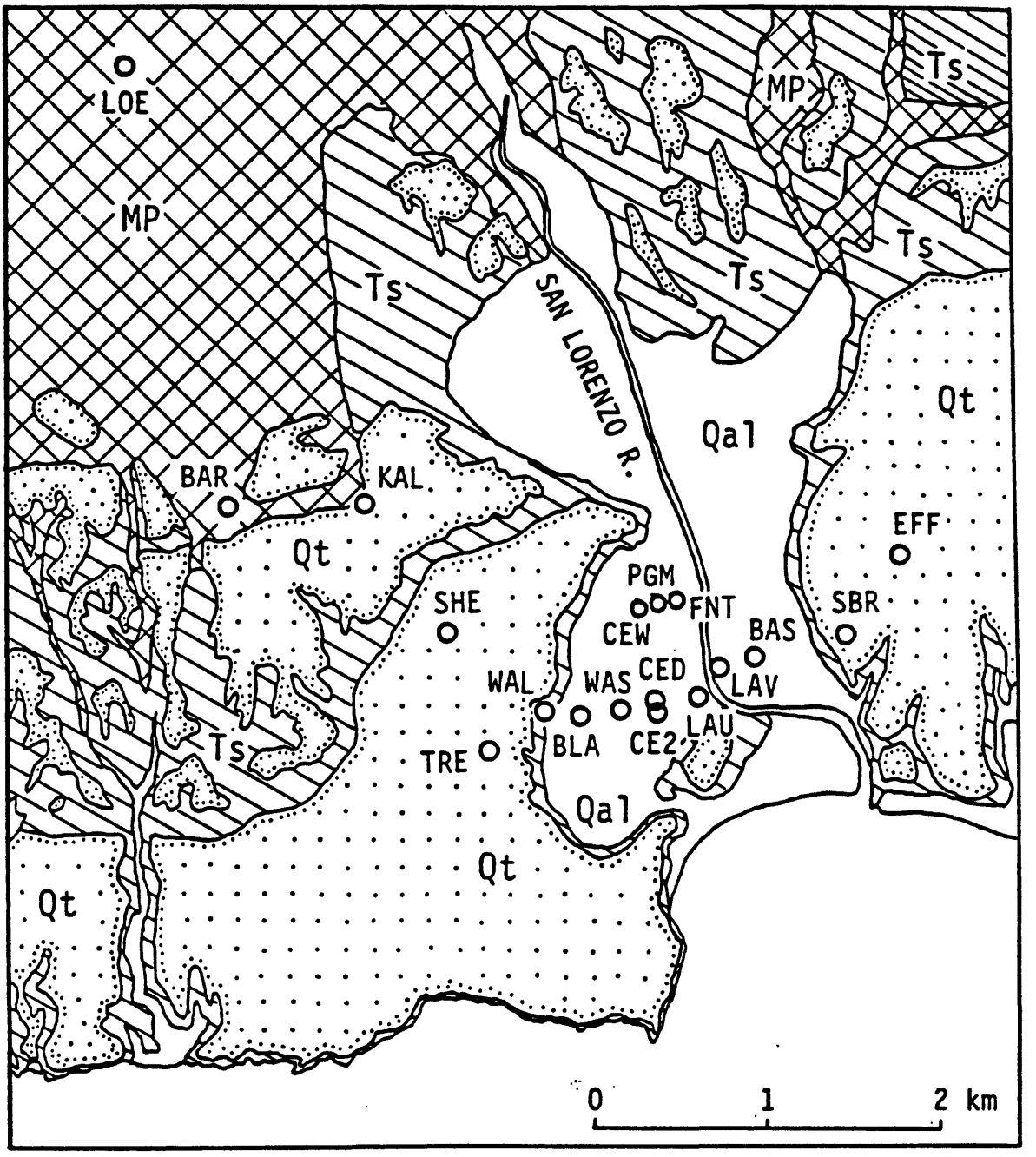

Fig. 2.3. Locations of sites and surface geology in Santa Cruz. All the sites except **CEW**, **PGM** and **FNT** are the same as the aftershock observation sites (King et al., 1990).
LOE: reference sites.

Geology **MP** : Metasedimentary rocks and Marble.
Qt : Marine terrace deposits.
Qal : Alluvium.

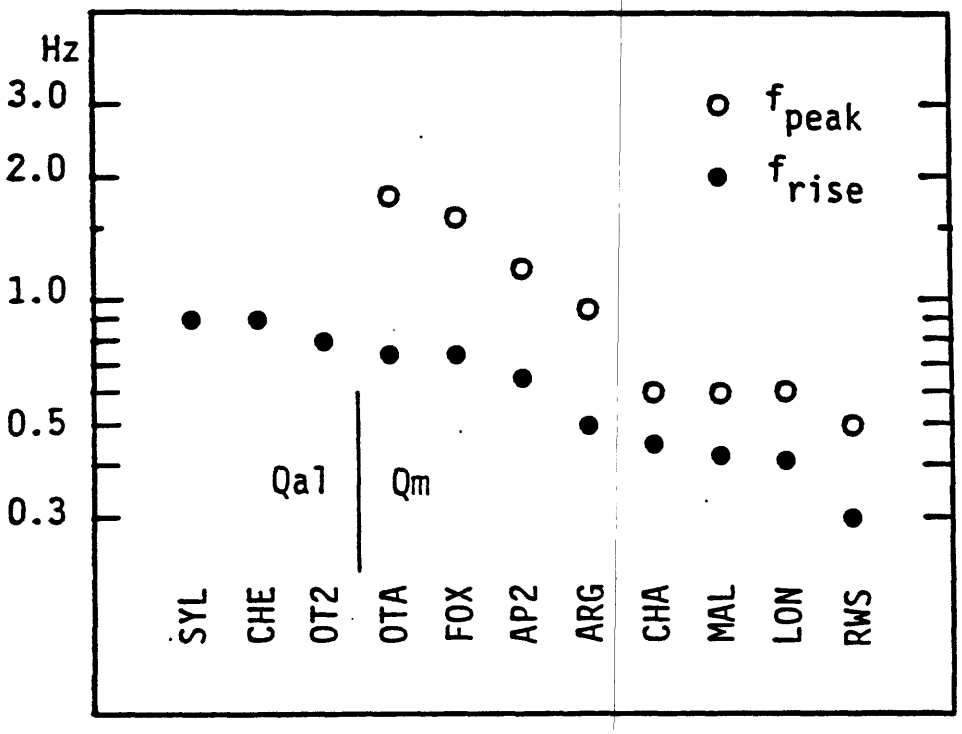

Fig. 2.4. Peak frequency (f_{peak}) and frequency at which amplification occurs (f_{rise}) in the horizontal components in Peninsula Cities.

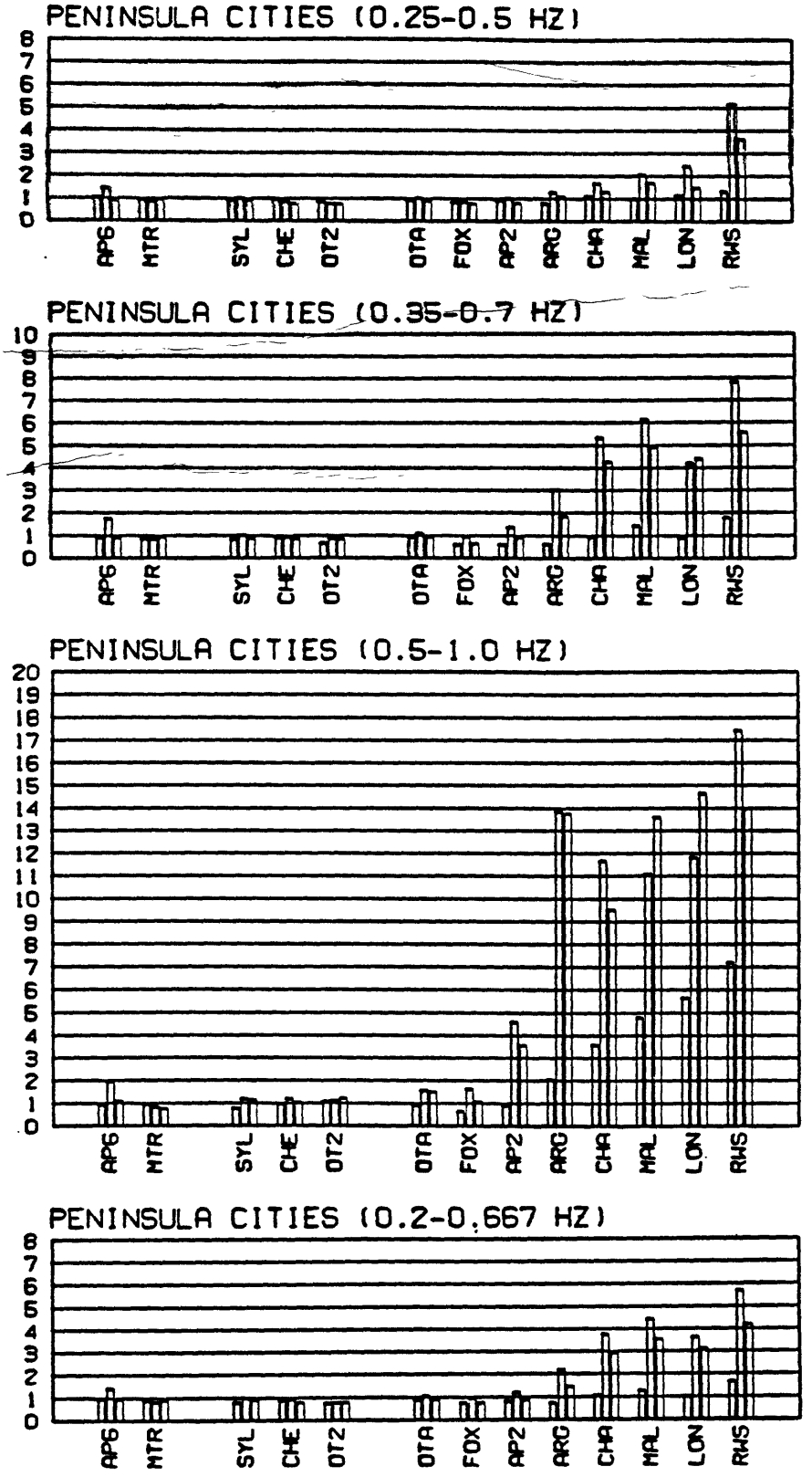

Fig. 2.5. Mean spectral ratios in the given frequency bands in Peninsula Cities. Left bar = vertical component, middle = parallel (N40 W) and right = normal (N50 E) to the general trend of geological division in the peninsula area, respectively.

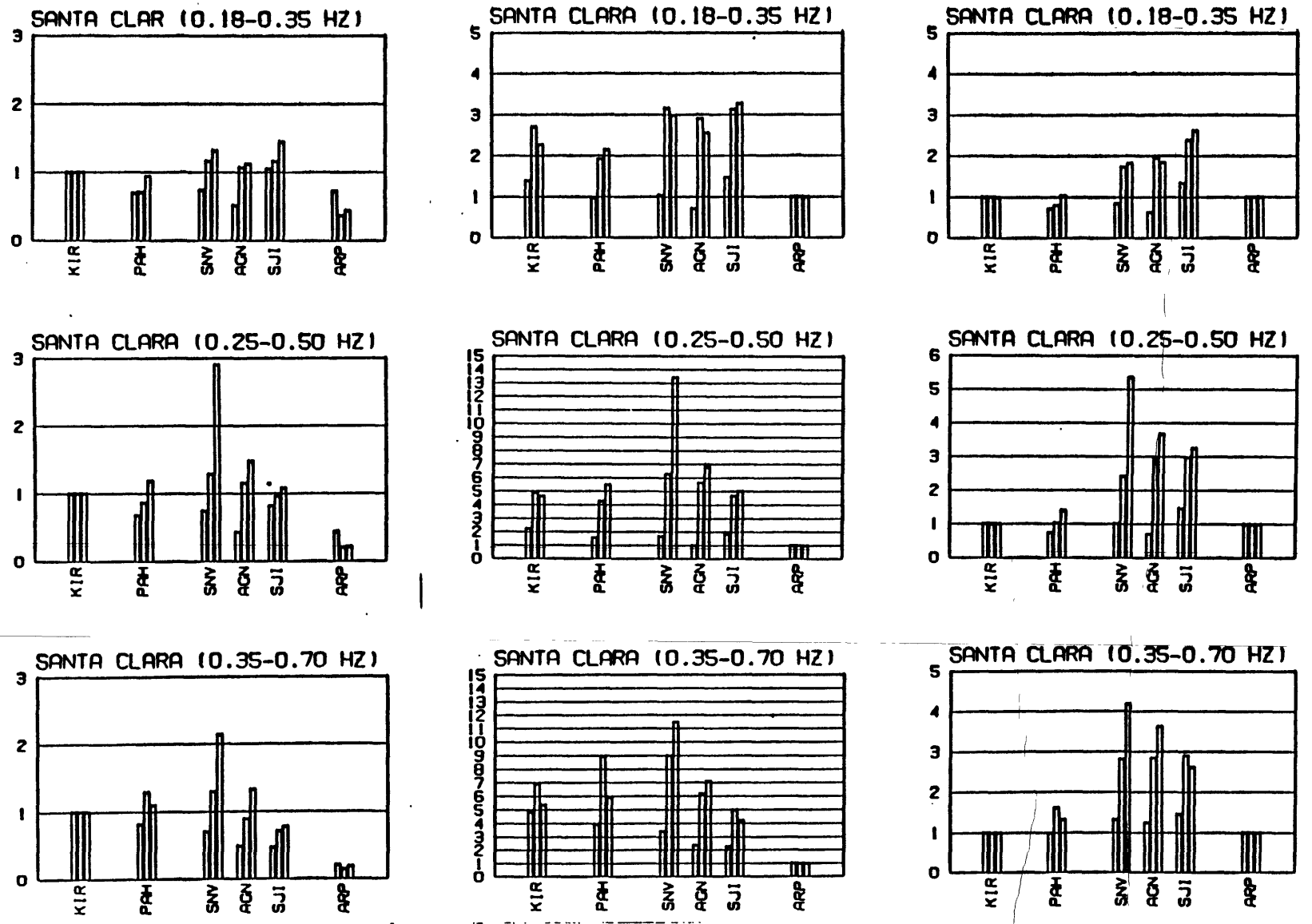

Fig. 2.6.1. Mean spectral ratios in the given frequency bands in Santa Clara Valley. Left bar = vertical, middle = parallel (N40 W), right = normal (N50 E) to the long axis of the valley, respectively. Reference is KIR (left figures), ARP (center figures) and regular wave field interpolated between KIR and ARP (right figures).

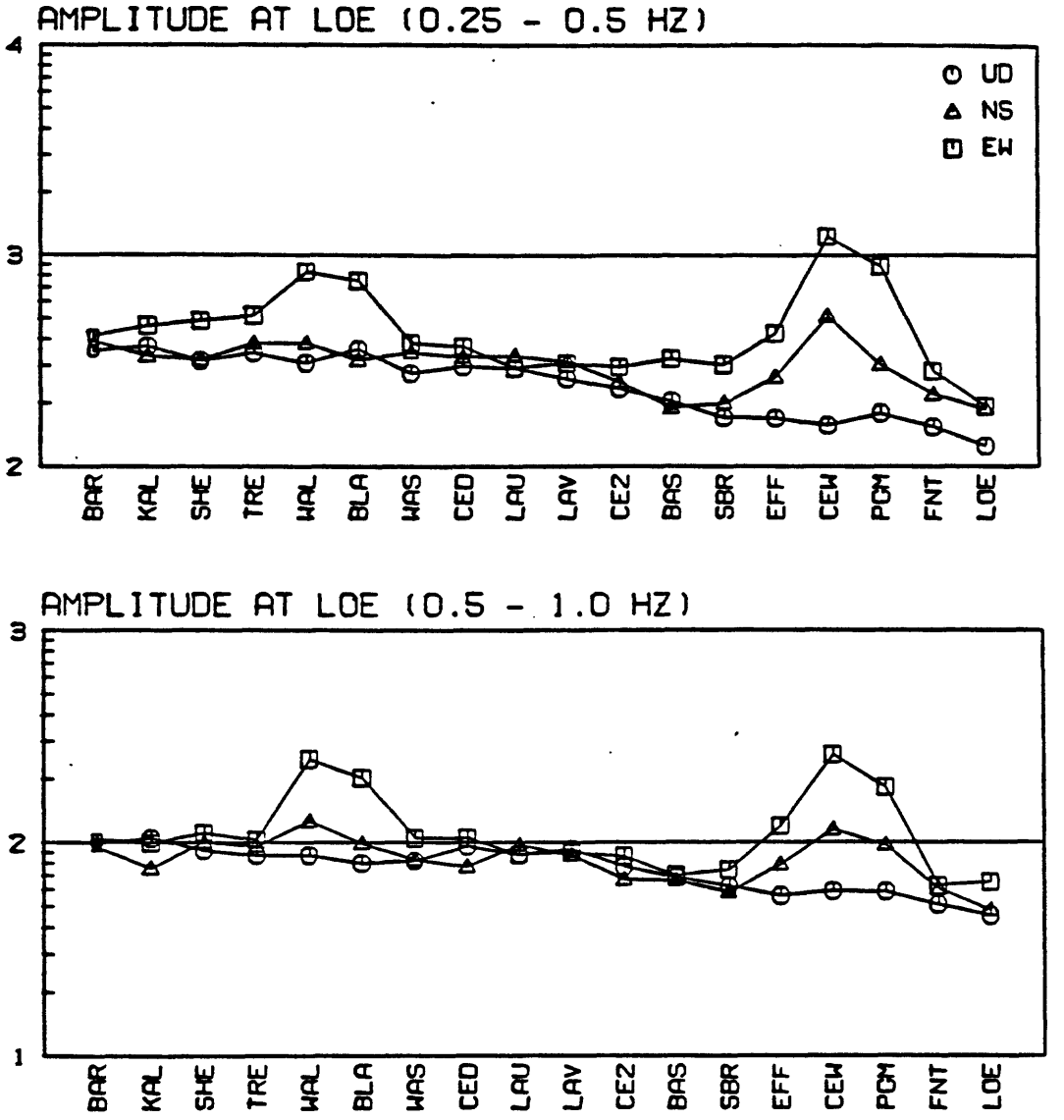

Fig. 2.7. Variations of amplitudes at LOE with time, at which ground site observations were carried out. : UD, : NS and : EW.

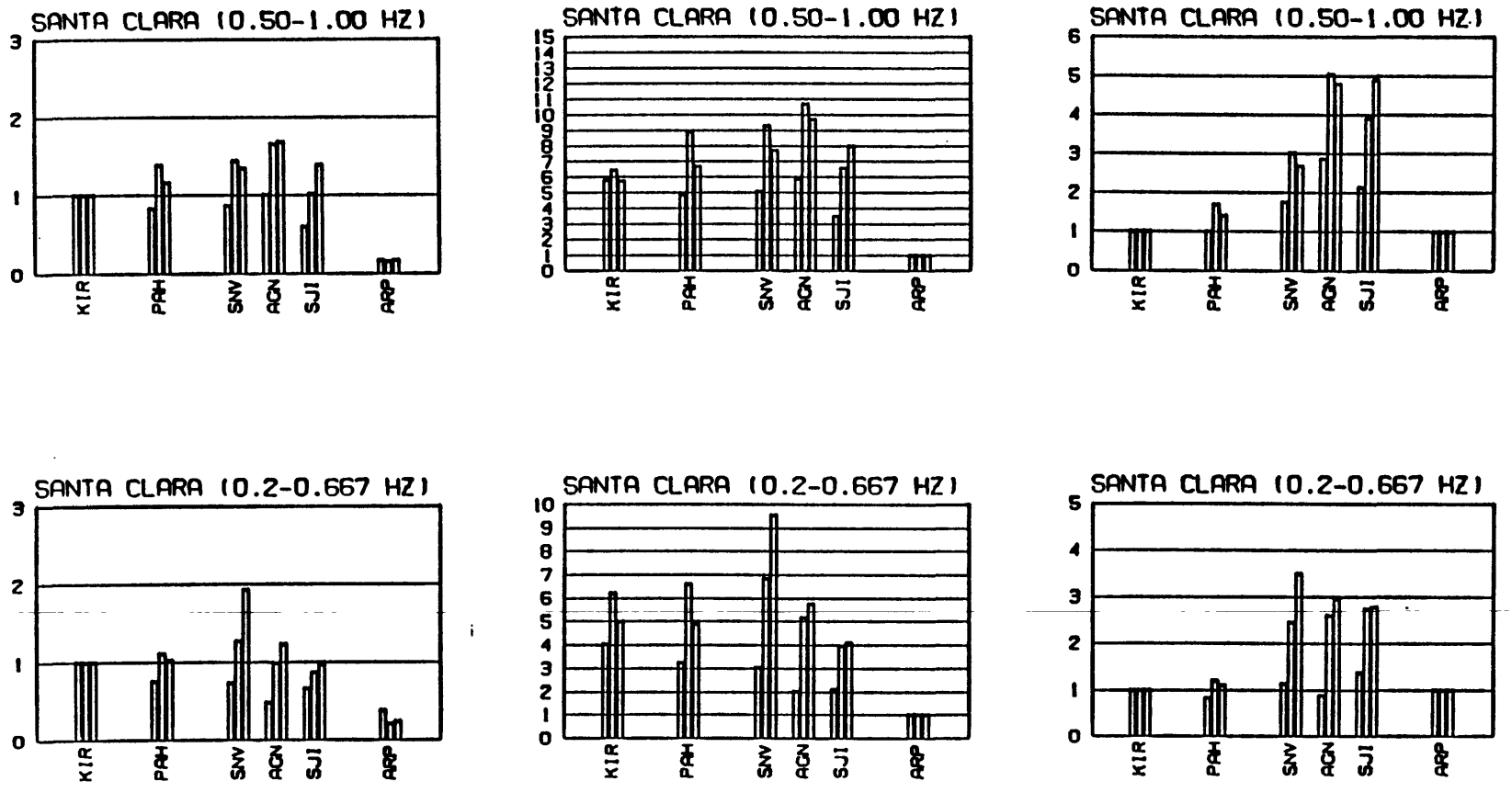

Fig. 2.6.2. Mean spectral ratios in the given frequency bands in Santa Clara Valley. Left bar = vertical, middle = parallel (N40 W), right = normal (N50 E) to the long axis of the valley, respectively. Reference is KIR (left figures), ARP (center figures) and regular wave field interpolated between KIR and ARP (right figures).

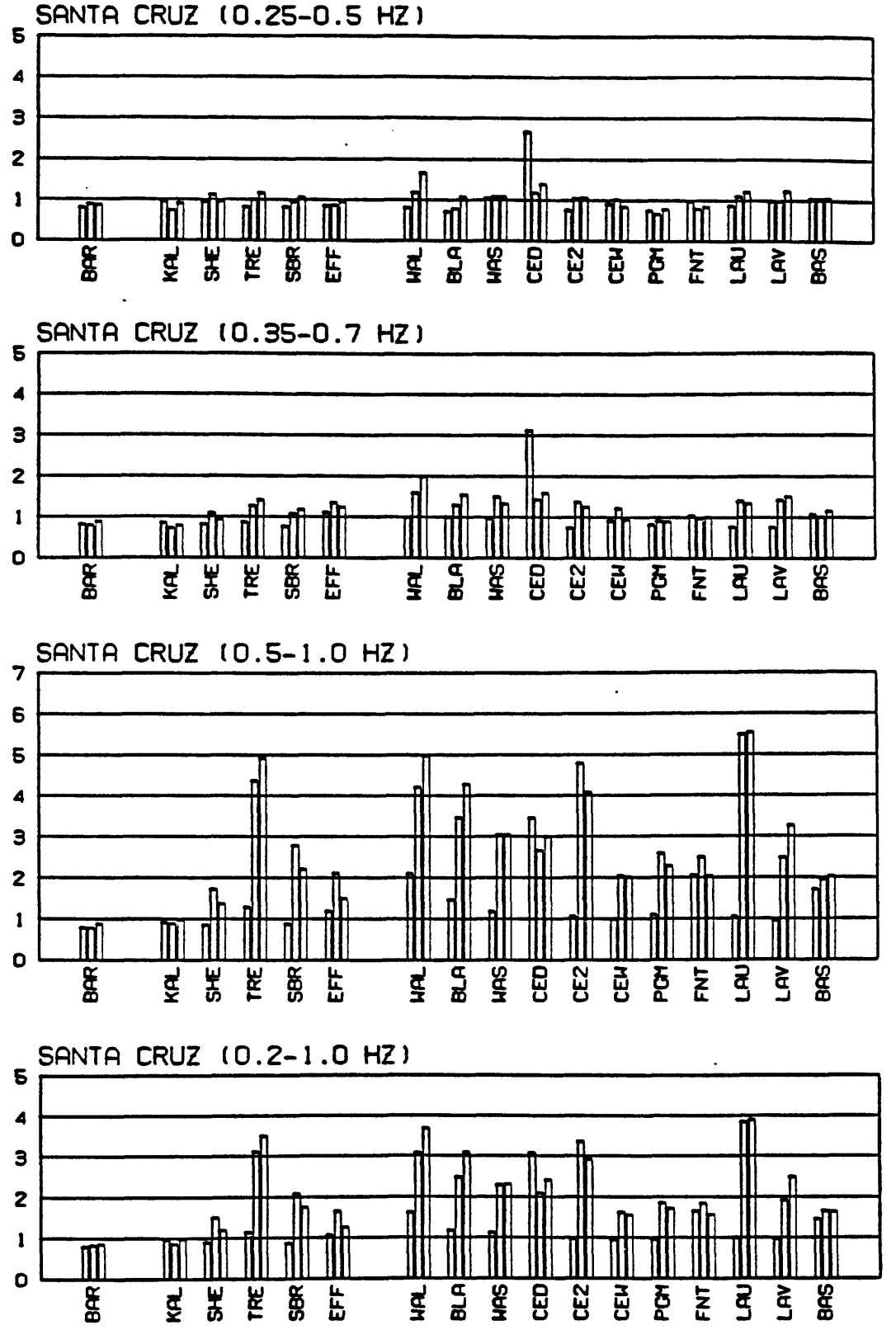

Fig. 2.8. Mean spectral ratios in the given frequency bands in Santa Cruz City. Left bar = UD, middle = NS, right = EW.

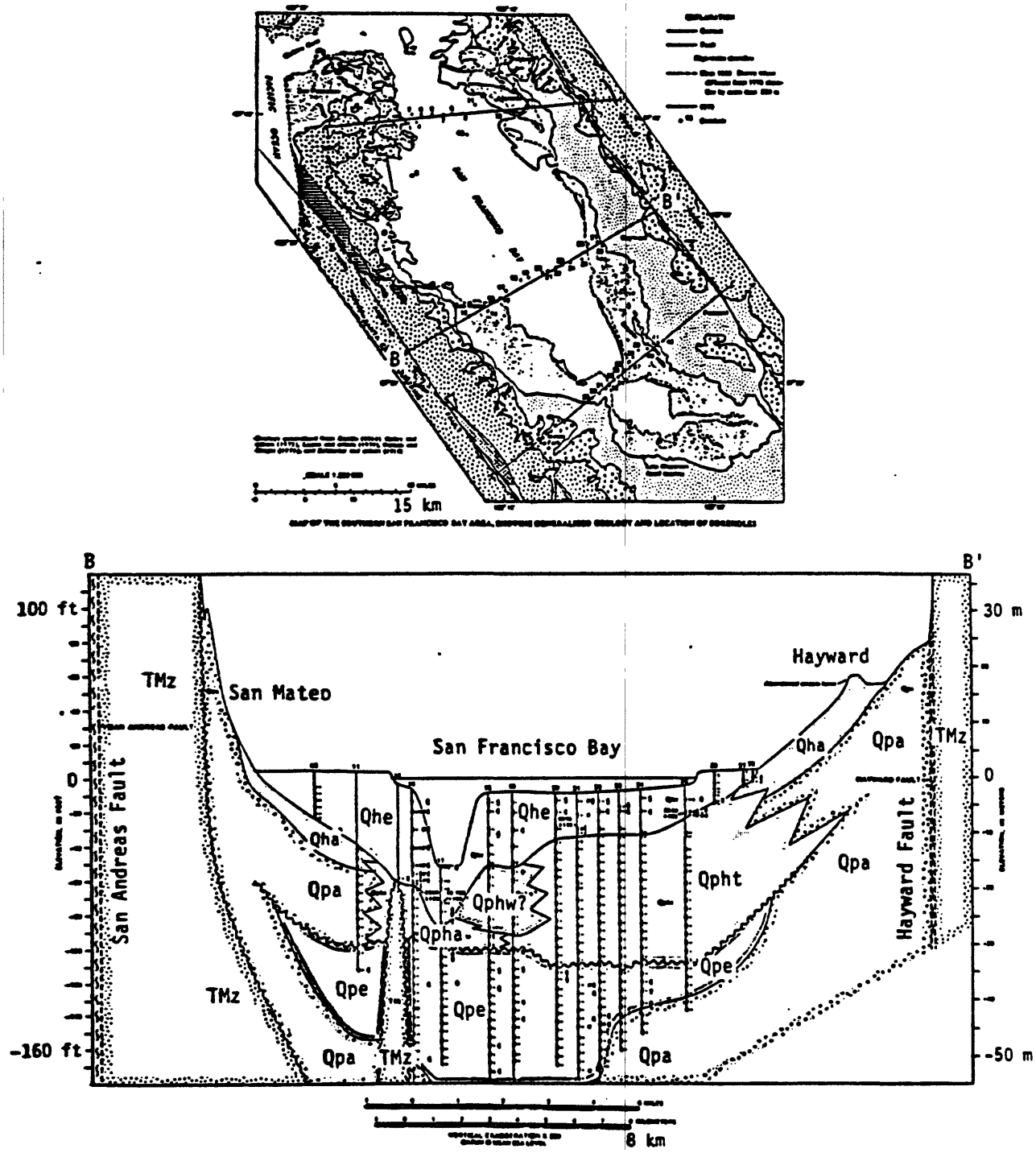

Fig. 2.9. Vertical cross section based on borehole data near Peninsula Cities sites (after Atwater et al., 1977).

Qhe : Estuarine deposits (Holocene).
Qha : Alluvial deposits (Holocene).
Qpha: Alluvial deposits (late Pleistocene and Holocene).
Qphw: Eolian deposits (late Pleistocene and Holocene).
Qpht: Terreatrial deposits, undivided (Pleistocene and Holocene).
Qpe : Estuarine deposits (late pleistocene).
Qpa : Alluvial deposits (late Pleistocene).
TMz : Bedrock (Mesozoic and Tertiary).

3. STRONG-MOTION RECORDINGS FROM THE LOMA PRIETA EARTHQUAKE

3.1 General Remarks

The Loma Prieta earthquake provided one of the largest strong-motion data sets yet obtained for a damaging earthquake in a region underlain by a variety of geologic deposits in close proximity (Shakal *et al.*, 1989; Maley *et al.*, 1989). This new data set provides an important opportunity to compare the response of various geologic deposits to potentially damaging levels of motion with those observed using microtremors and comparative low-strain observations from distant man-made sources.

Analyses of the strong-motion data at various stages of data availability have been presented previously (Borcherdt, 1990; Borcherdt and Glassmoyer, 1990; Borcherdt and Glassmoyer, in press). Data compilations and analyses pertinent to comparing the various methodologies for ground response determinations are reproduced here to facilitate comparisons. Locations for the combined set of 34 free-field stations analyzed in the San Francisco Bay region are shown in Figure 3.1. Geologic deposits in the San Francisco Bay region are generalized into 6 units (Figure 3.1). These six units include: Cretaceous granitic rocks (Kg), Jurassic and Cretaceous rocks of the Franciscan assemblage (KJf), Mesozoic and Tertiary sedimentary rocks (TMzs), Tertiary and Quaternary sediments (QTs), Quaternary alluvium (Qal), and Quaternary (Holocene) bay mud (Qhbm). A detailed description of the units is provided by Lajoie (Borcherdt *et al.*, 1975).

To develop a uniform data set to quantify the influence of various geologic deposits on recorded strong motions, the horizontal recordings at each site were resolved into radial and transverse components. These components are parallel and perpendicular, respectively, to the direction from source to receiver. Peak amplitudes inferred for the vertical, radial, and transverse components of acceleration, velocity and displacement are summarized, together with site identifications, shear velocity (Fumal, 1990), and distances in Table 3.1.

To quantify the influence of local geologic deposits on recorded motions, ratios of peak amplitude for each measure of motion were first computed with respect to "local" rock sites (RIN, PIE, CSH, AP7, WOD) and normalized by the ratios of corresponding hypocentral distance. Sites in San Francisco and rock sites used as normalization sites were further normalized to the corresponding near value for Franciscan sites. These ratios together with statistics for each geologic sample are summarized in Table 3.2. Corresponding charts are provided in Borcherdt and Glassmoyer (1990).

3.2 Amplification Ratios Calculated from Strong Motions

These ratios of peak amplitude show that in general ratios of peak horizontal motion exceed those for peak vertical motion. They show that for horizontal motion ratios of peak acceleration, velocity and displacement increase with decreasing firmness or shear velocity at the site. They show that on the average the largest amplifications of horizontal motion occur for the radial component of motion for sites on fill, bay mud. They show that in

general maximum amplifications for peak accelerations on "soil" (Qal, Qhbm) are often comparable to and in some cases exceed those for velocity and displacement.

To further quantify the response of the various deposits, spectral ratios were computed for each site with respect to local "rock" sites, **RIN, PIE, CSH, AP7, WOD** and normalized by corresponding ratios of hypocentral distance (Table 3.3). The ratios are computed as the ratio of the modulus of the discrete Fourier transforms from time series 40.96 seconds in length. A leakage correction corresponding to 10 percent cosine taper and triangular smoothing windows of 7 and 15 points have been applied, respectively, to the numerator and denominator. To facilitate comparisons with microtremor data, geometric averages of the spectral ratios were computed for the period bands (0.1–0.5, 0.5–1.5, 1.5–5.0, 0.1–5.0 and 0.4–2.0 seconds; Table 3.3). Values for the short-, intermediate-, and long-period bands are charted (Figures 3.2, 3.3, and 3.4).

The charted average ratios show that, in general, for vertical motion the larger amplifications often occur in the short-period band consistent with the observation that ratios of peak vertical acceleration often exceed corresponding ratios of peak vertical velocity and displacement. For horizontal motion they show that the larger amplifications frequently occur for the intermediate- and long-period bands for radial motion at fill, bay mud sites. Greater response for horizontal motion in the intermediate- and long-period bands is consistent with observations of larger ratios of peak velocity and displacement for corresponding components of motion.

Average spectral ratios for the period band 0.4–2.0 sec provide a useful parameter to summarize variations in ground response of interest for earthquake engineering. Mean values computed for averages over this period band for each geologic unit (Table 3.3) indicate that average amplification levels, in general, increase with decreasing mean shear velocity for the units. The "soil" site amplifications implied for the radial direction consistently exceed those in the transverse direction for sites in each area, with the exception of those in the west bay near Foster City normalized by AP7. For sites in this area, the larger amplifications in the transverse direction are thought to be more indicative of the response characteristics of the normalization site than of directional amplification characteristics of the "soil" sites.

3.3 Comparison with Past Low-Strain Motions

Previous measurements of ground response in the San Francisco Bay region at 99 sites using low-strain motions generated by distant man-made explosions permit a comparison of average response estimates determined at low-strain levels with those determined at significantly higher strain levels associated with the Loma Prieta earthquake.

Mean vlaues computed for each geologic unit are shown for the low-strain and strong-motion data sets in Figures 3.5 and 3.6. (Those shown for horizontal motion represent the average of the east–west and north–south components for the low-strain data set and the average of the radial and transverse components for the strong-motion data set.) Testing

the null hypothesis that the means for the data sets corresponding to each geologic sample are equal shows that the null hypothesis can be rejected at the 5% level of significance only for the horizontal responses determined for the fill, bay mud sample. This difference for the fill, bay mud sample is due in part to the nonlinear response associated with liquefaction at the Treasure Island site and possibly the AP2 site. Another factor contributing to smaller values for the smaller Loma Prieta sample is due to the need to normalize the sites in the Foster City–Redwood Shores area to site AP7, thought to have a somewhat higher response than the mean value for sites on the Franciscan assemblage used to normalize the low-strain data. Comparison of the mean values determined from the two data sets with those derived from microtremors are provided in a subsequent chapter.

REFERENCES

Borcherdt, R. D. (1970). Effects of local geology on ground motion near San Francisco Bay, *Bull. Seism. Soc. Am.*, **60**, 29–61.

Borcherdt, R. D. (1990). Influence of local geology in the San Francisco Bay region, California on ground motions generated by the Loma Prieta earthquake of October 17, 1989, *Proc. Int'l. Symposium on Safety of Urban Life and Facilities*, Tokyo Inst. Tech., Tokyo, Japan.

Borcherdt, R. D. and J. F. Gibbs (1976). Effects of local geological conditions in the San Francisco Bay region on ground motions and the intensities of the 1906 earthquake, *Bull. Seism. Soc. Am.*, **66**, 467–500.

Borcherdt, R. D. and G. Glassmoyer (1990). Local geology and its influence on strong ground motion generated by the Loma Prieta earthquake of October 17, 1989, *Proc. Nat'l. Conf. The Loma Prieta Earthquake One Year Later*, Assoc. Bay Area Gov'ts., Oakland, CA.

Borcherdt, R. D., J. F. Gibbs, and K. R. Lajoie (1975). Prediction of maximum earthquake intensity in the San Francisco Bay region, California, for large earthquakes on the San Andreas and Hayward faults, *U.S. Geol. Survey Misc. Field Studies Map MF-709*, scale 1:125,000, 11 pp.

Fumal, T. E. (1990). Shear-wave velocity estimates and site geology for strong-motion recording sites of the Loma Prieta earthquake of October 17, 1989, *U.S. Geol. Surv. Open-File Rep.* in press.

Maley, R., A. Acosta, F. Ellis, E. Etheridge, L. Foote, D. Johnson, R. Porcella, M. Salsman, and J. Switzer (1989). U.S. Geological Survey records from the northern California (Loma Prieta) earthquake of October 17, 1989, *U.S. Geol. Surv. Open-File Rep.* **89–568**, 85 pp.

Shakal, A., M. Huang, M. Reichle, C. Ventura, T. Cao, R. Sherburne, M. Savage, R. Darrah, and C. Petersen (1989). CSMIP strong-motion records from the Santa Cruz Mountains (Loma Prieta), California earthquake of 17 October 1989, *California Strong Motion Instrumentation Program Report No.* **OSMS 89–06**, 195 pp.

Table 3.1 - Site description and peak acceleration, velocity, and displacement for the vertical, radial, and transverse components of motion.

Station Description	Name	H.Dist. km	E.Dist. km	R.Dist. km	Acc-Z cm/s/s	Vel-Z cm/s	Disp-Z cm	Acc-R cm/s/s	Vel-R cm/s	Disp-R cm	Acc-T cm/s/s	Vel-T cm/s	Disp-T cm	Geologic Unit	Avg.S. Vel.m/s 1-15-91	Std. Dev.
Saratoga---CSMIP	SAR	33	27	12	353	26.3	15.50	450	39	9.62	297	54.3	31.80	QTs	440	55
Agnews State Hosp.---CSMIP	ASH	44	40	27	82.3	9.68	4.92	159	29.3	17.50	169	17.4	12.90	Qhaf	240	25
Sunnyvale---USGS	SVL	40	42	26	78.6	7.36	2.93	206	25	10.00	223	30.1	15.70	Qhaf/Qpa	240	25
SLAC---USGS	SLA	54	51	35	89.6	9.15	2.93	214	19.9	4.00	242	45.9	10.70	QTs	420	*
Mission San Jose---CSMIP	MSJ	57	55	42	81.3	6.39	4.54	121	10.4	4.14	103	7.03	4.47	Qpa/QTs	265	10
Woodside Fire Station---CSMIP	WOD	57	55	39	46.9	6.84	2.08	40.9	8.46	3.47	104	16.7	7.45	QTs	440	55
Fremont---USGS	FRE	58	55	42	87.6	4.64	1.28	143	10.2	2.17	161	10.4	2.59	Qpa	265	10
APEEL 9 (Crys.Spr. Res.)---USGS	AP9	64	63	40	50.4	6.62	2.04	116	30.9	5.65	97	16.9	10.90	QTs	450	
APEEL 10 (Skyline Blvd.)---CSMIP	AP10	05	63	47	36.4	7.76	2.50	67.7	11.2	5.46	107	20	7.19	TMzs	405	
APEEL 7 (Pulgas Temple)---CSMIP	AP7	05	63	47	59.7	6.01	2.30	122	13.5	4.25	114	17.3	6.33	TMzs	435	
APEEL 2---USGS	AP2	66	04	47	61.0	7.7	1.05	194	30.9	4.71	266	54.7	10.90	Qal/Qhbm/Qpa	130	
Redwood Shores (F. City)---CSMIP	RSH	67	05	47	101	8.39	3.55	266	33.7	9.27	264	43.1	13.80	Qal/Qhbm	115	
Maley Residence (F. City)---USGS	MAL	66	66	50	73.5	3.6	0.76	103	14	4.27	89.5	18.4	5.91	Qal/Qhbm	150	
CSUH Stadium Grounds---CSMIP	CSH	73	70	56	44.4	4.61	2.29	44.4	4.74	3.15	76.6	7.22	2.55	TMzs	525	
Muir School (APEEL 2E)---CSMIP	MUR	73	71		90.5	3.82	2.14	90.5	15.7	4.16	125	12.6	3.40	Qpa	260	
Hayward BART Station---CSMIP	HWB	74	72	58	81	4.71	1.74	81	11.1	2.79	187	11.3	3.70	Qpa	365	95
San Francisco Airport---CSMIP	SF1	01	79	63	63.3	5.27	1.77	223	19.6	3.12	378	34.5	5.36	Qal/Qhbm	180	*
South San Francisco---CSMIP	SSF	65	84	76	31.2	4.4	1.35	31.2	6.37	1.29	105	8.84	2.90	KJfss	910	40
Oakland Office Bldg.---CSMIP	OOF	93	92	76	141	6.19	1.30	165	21.8	4.73	241	34.1	6.25	Qpa/Qpa	305	*
Diamond Heights---CSMIP	DIA	94	92	76	42.4	6.68	1.36	90.3	7.32	0.82	95.7	14.7	5.14	KJfsh	745	140
Piedmont Jr. High---CSMIP	PIE	94	92	77	25.4	2.89	0.99	46.6	4.94	1.68	97.5	12.3	3.80	KJfss	745	140
Oakland Harbor Wharf---CSMIP	OHW	96	94	79	85.1	10.5	1.83	261	25.9	5.29	322	40	12.90	Qal/Qhbm/Qpa	230	*
Rincon Hill---CSMIP	RIN	98	94	79	26.4	3.98	1.05	88.4	4.09	1.37	97.6	13.2	5.48	KJfsh	745	140
Yerba Buena Island---CSMIP	YBI	97	96	80	26.9	4.22	1.13	39.5	4.41	1.40	67.9	14.3	4.32	KJfsh	745	140
Pacific Heights---CSMIP	PAC	96	96	81	30.5	5.93	2.25	36.1	4.63	0.70	68.7	17.2	5.47	KJfsh	745	140
Emeryville ---USGS	EMT	96	97	81	57.3	4.88	0.73	230	26.9	4.03	237	36.3	7.85	Qal/Qhbm	240	
Treasure Island---CSMIP	TRI	99	96	82	15.9	1.16	1.15	121	12.3	5.66	137	33.1	12.90	Qal/Qhbm	130	*
Presidio---CSMIP	PRE	99	96	82	56.2	11.3	3.05	117	12.8	2.12	163	32.1	7.52	sp	515	5
Berkeley (Lawrence Lab.)---CSMIP	BKL	100	99	83	36	4.35	1.48	38	8.78	2.27	113	21	3.50	TMzs	610	*
Cliff House---CSMIP	CLI	101	99	83	60.6	7.51	1.58	80	11.7	2.10	89.9	22	7.20	KJfsh	745	140
Golden Gate Bridge---USGS	GGB	101	100	83	54.8	11.6	2.62	134	19.2	3.85	204	32.3	6.32	Qal/sp	515	5
Bonita Point---CSMIP	BON	105	104	88	34.1	7.28	2.17	34.1	9.3	2.04	60.5	12.1	4.26	KJfss	745	140
Richmond City Hall---CSMIP	RCH	109	108	92	30.5	4.55	1.09	30.5	11.6	1.73	139	17.5	3.03	QTs	440	55

Table 3.2 -- Ratios of peak acceleration, velocity, and displacement with respect to local rock station (RIN,AP7,CSH,PIE,YBI, or WOD) or mean value for sites on unit KJf (normalized by hypocentral distances).

Station	H.Dist. km	Avg. S 30m	norm.sta.	Acc-Z	Vel-Z	Disp-Z	Acc-R	Vel-R	Disp-R	Acc-T	Vel-T	Disp-T
South San Francisco—CSMIP	85	910	SSF/KJf	0.92	0.88	0.82	0.53	1.10	0.97	1.08	0.59	0.80
Rincon Hill—CSMIP	96	710	RIN/KJf	0.94	0.89	1.27	1.31	0.80	1.16	1.13	1.00	1.26
Yerba Buena—CSMIP	97	710	YBI/KJf	0.90	0.95	0.78	0.76	0.86	1.20	0.79	1.09	1.00
Pacific Heights—CSMIP	96	710	PAC/KJf	1.03	1.36	1.57	0.74	0.92	0.60	0.81	1.32	1.28
Diamond Heights—CSMIP	94	710	DIA/KJf	1.38	1.46	0.91	1.79	1.39	0.68	1.08	1.09	1.16
Piedmont Jr. High—CSMIP	94	710	PIE/KJf	0.82	0.46	0.66	0.87	0.94	1.39	1.10	0.91	0.69
MEAN (KJf)		743		1.00	1.00	1.00	1.00	1.00	1.00	1.00	1.00	1.00
STANDARD DEVIATION		82		0.20	0.36	0.34	0.47	0.22	0.31	0.15	0.24	0.29
CSUH Stadium Grounds—CSMIP	73	525	CSH/KJf	1.11	0.78	1.18	0.64	0.69	2.01	0.67	0.41	0.44
Woodside Fire Station—CSMIP	57	440	WOD/KJf	0.97	0.92	0.85	0.56	0.98	1.75	0.72	0.64	1.02
APEEL 7 (Pulgas Temple)—CSMIP	65	435	AP7/KJf	1.34	0.91	1.06	1.57	1.77	2.43	0.89	0.88	0.98
MEAN (norm. sta.-- south)		467		1.14	0.87	1.03	0.92	1.15	2.07	0.76	0.71	0.82
STANDARD DEVIATION		51		0.19	0.08	0.17	0.56	0.56	0.34	0.12	0.26	0.32
Cliff House—CSMIP	101	710	CLI/KJf	2.11	1.76	1.13	1.72	2.38	1.86	1.09	1.74	1.74
Bonita Point—CSMIP	105	710	BON/KJf	1.24	1.78	1.62	0.71	1.97	1.88	0.76	1.00	1.07
MEAN		710		1.67	1.77	1.37	1.21	2.17	1.87	0.93	1.37	1.40
Presidio—CSMIP	99	515	PRE/KJf	1.93	2.62	2.15	2.31	2.57	1.86	1.95	2.51	1.79
Golden Gate Bridge—USGS	101	515	GGB/KJf	1.92	2.74	1.89	2.69	3.93	3.44	2.49	2.57	1.53
MEAN (ep)		515		1.92	2.68	2.02	2.50	3.25	2.65	2.22	2.54	1.66
Berkeley (Lawrence Lab.)—CSMIP	100	610	BKL/PIE	1.59	2.21	1.58	0.86	1.89	1.44	1.23	1.81	1.21
APEEL 10 (Skyline Blvd.)—CSMIP	65	405	AP10/AP7	0.61	1.29	1.09	0.55	0.83	1.29	0.94	1.15	1.13
MEAN (TMzs)		508		1.10	1.75	1.33	0.71	1.36	1.36	1.08	1.48	1.17
APEEL 9 (Crys.Spr. Res.)—USGS	64	450	AP9/AP7	0.83	1.09	0.87	0.94	2.26	1.31	0.84	0.96	1.70
Richmond City Hall—CSMIP	109	440	RCH/PIE	1.39	2.52	1.27	0.75	2.72	1.19	1.65	1.65	1.14
Saratoga—CSMIP	33	440	SAR/WOD	4.12	2.19	4.25	5.35	2.62	1.58	1.63	1.68	2.44
SLAC—USGS	54	420	SLA/WOD	1.72	1.26	1.32	4.11	2.21	1.08	2.19	2.31	1.35
MEAN (QTs)		438		2.02	1.76	1.93	2.79	2.45	1.29	1.58	1.64	1.66
STANDARD DEVIATION		13		1.45	0.70	1.56	2.30	0.26	0.21	0.56	0.55	0.57
MEAN ("ROCK")		596		1.41	1.48	1.38	1.51	1.73	1.53	1.21	1.34	1.24
STANDARD DEVIATION		160		0.78	0.69	0.80	1.31	0.89	0.65	0.52	0.62	0.46
Hayward BART Station—CSMIP	74	365	HWB/CSH	1.87	1.05	0.78	1.87	2.40	0.91	2.50	1.61	1.49
Oakland Office Bldg.—CSMIP	93	305	OOF/PIE	5.51	2.94	1.30	3.50	4.34	2.80	2.45	2.75	2.66
Fremont—USGS	58	285	FRE/CSH	1.22	0.80	0.45	2.57	1.72	0.55	1.89	1.15	0.81
Mission San Jose—CSMIP	57	285	MSJ/CSH	1.45	1.44	1.57	2.15	1.73	1.04	1.06	0.86	1.39
Muir School (APEEL 2E)—CSMIP	73	280	MUR/CSH	2.05	0.83	0.94	2.05	3.33	1.33	1.64	1.76	1.36
MEAN (Qpa)		304		2.42	1.41	1.01	2.43	2.71	1.32	1.91	1.62	1.54
STANDARD DEVIATION		35		1.76	0.89	0.44	0.65	1.13	0.87	0.60	0.73	0.68
Sunnyvale—USGS	46	240	SVL/WOD	1.28	0.86	1.12	3.38	2.35	2.30	1.71	1.62	1.68
Agnew State Hosp.—CSMIP	44	240	ASH/WOD	1.29	1.08	1.81	2.49	2.64	3.86	1.24	0.71	1.32
MEAN (Qhaf)		240		1.28	0.97	1.47	2.92	2.50	3.08	1.48	1.17	1.50
MEAN (Qal)		286		2.10	1.29	1.14	2.57	2.65	1.83	1.79	1.49	1.53
STANDARD DEVIATION		43		1.54	0.76	0.47	0.64	0.93	1.20	0.55	0.69	0.56
Emeryville Towers—USGS	96	240	EMT/PIE	2.35	2.44	0.77	5.13	6.11	2.50	2.54	3.08	2.66
Oakland Harbor Wharf—CSMIP	96	230	OHW/PIE	2.62	5.13	1.88	5.69	5.35	3.21	3.37	3.98	4.27
San Francisco Airport—CSMIP	81	180	SF1/KJf	1.77	1.00	1.02	3.59	3.21	2.23	3.69	2.20	1.04
Maley Residence (F. City)—USGS	68	150	MAL/AP7	1.29	0.63	0.35	0.88	1.09	1.05	0.82	1.11	0.98
APEEL 2—USGS	66	130	AP2/AP7	1.39	1.30	0.46	1.61	2.32	1.12	2.37	3.21	1.75
Treasure Island—CSMIP	99	130	TRI/YBI	0.80	0.28	1.04	3.13	2.85	4.12	2.06	2.36	2.83
Redwood Shores (F. City)—CSMI	67	115	RSH/AP7	1.74	1.44	1.59	2.36	2.57	2.25	2.57	2.57	2.24
MEAN (Qaf/Qhbm)		168		1.68	1.74	1.02	3.20	3.36	2.36	2.49	2.64	2.25
STANDARD DEVIATION		50		0.68	1.64	0.56	1.76	1.76	1.09	0.93	0.91	1.15
MEAN ("SOIL")		156		1.89	1.52	1.08	2.89	3.00	2.09	2.14	2.07	1.89
STANDARD DEVIATION		76		1.16	1.25	0.50	1.31	1.40	1.13	0.82	0.98	0.95

Table 3.3a -- Average spectral ratios for specified period bands for "rock" sites as normalized by local rock station (RIN,AP7,CSH,PIE,YBI, or WOD) or mean value for sites on unit KJf and hypocentral distance.

Station	H.Dist km	S vel. m/s	Vertical period bands (secs)					Radial period bands (secs)					Transverse period bands (secs)				
			0.1-0.5	.5-1.5	.5-5.0	.1-5.0	.4-2.0	0.1-0.5	0.5-1.5	1.5-5.0	0.1-5.0	0.4-2.0	0.1-0.5	.5-1.5	.5-5.0	.1-5.0	.4-2.0
South San Francisco---CSMIP	85	910	1.07	1.00	0.69	1.04	0.96	1.06	1.02	1.31	1.07	1.07	1.18	0.82	0.53	1.12	0.85
Rincon Hill---CSMIP	96	745	1.13	1.00	1.15	1.11	1.11	1.17	1.12	0.93	1.15	1.04	0.95	1.09	1.21	0.98	0.92
Yerba Buena---CSMIP	97	710	0.78	0.98	0.60	0.81	0.90	0.69	0.61	0.97	0.69	0.58	0.75	0.85	0.98	0.77	0.91
Pacific Heights---CSMIP	98	710	0.72	0.99	1.67	0.81	1.07	0.62	0.99	0.88	0.69	0.93	0.56	1.01	1.44	0.66	0.98
Diamond Heights---CSMIP	94	710	1.36	1.44	1.20	1.38	1.39	1.62	1.26	0.94	1.53	1.36	1.57	1.30	1.14	1.53	1.42
Piedmont Jr. High---CSMIP	94	710	0.92	0.61	0.48	0.85	0.56	0.84	1.01	0.96	0.88	1.02	0.97	0.92	0.69	0.95	0.92
MEAN (KJf)		749	1.00	1.00	1.00	1.00	1.00	1.00	1.00	1.00	1.00	1.00	1.00	1.00	1.00	1.00	1.00
STANDARD DEVIATION		80	0.25	0.27	0.43	0.23	0.27	0.37	0.22	0.15	0.32	0.25	0.35	0.18	0.34	0.30	0.21
CSUH Stadium Grounds---CSM	73	525	1.42	1.10	0.52	1.34	1.06	1.49	0.86	1.02	1.39	0.78	1.38	0.88	0.55	1.28	0.77
Woodside Fire Station---CSMIP	57	440	0.82	0.79	0.87	0.82	0.77	0.60	0.91	1.28	0.68	0.82	0.72	0.99	1.10	0.76	0.91
APEEL 7 (Pulgas Temple)---CS	65	435	1.78	1.00	0.92	1.63	0.97	1.19	1.65	1.57	1.28	1.60	1.48	1.29	1.18	1.45	1.22
MEAN (norm.sta. south)		467	1.34	0.97	0.77	1.26	0.94	1.09	1.14	1.29	1.12	1.06	1.19	1.05	0.94	1.16	0.96
STANDARD DEVIATION		51	0.48	0.16	0.22	0.41	0.15	0.46	0.44	0.28	0.38	0.47	0.42	0.22	0.34	0.36	0.23
Cliff House---CSMIP	101	710	1.05	1.91	1.61	1.21	2.06	0.78	2.24	1.71	1.04	1.90	0.81	1.42	1.88	0.92	1.34
Bonita Point---CSMIP	105	710	0.79	1.28	1.72	0.91	1.28	0.89	1.94	2.62	1.12	1.90	0.86	0.77	1.98	0.88	0.96
MEAN		710	0.92	1.60	1.66	1.06	1.67	0.83	2.09	2.16	1.08	1.90	0.83	1.09	1.93	0.90	1.15
Presidio---CSMIP	99	515	2.06	2.01	2.46	2.07	2.10	1.65	2.43	1.55	1.75	2.23	1.52	2.20	2.18	1.62	1.99
Golden Gate Bridge---USGS	101	515	1.56	1.82	2.88	1.66	2.03	1.70	4.34	3.64	2.18	4.05	1.18	3.13	2.90	1.48	2.66
MEAN (sp)		515	1.81	1.92	2.67	1.87	2.06	1.68	3.39	2.60	1.96	3.14	1.35	2.67	2.54	1.55	2.33
Berkeley (Lawrence Lab.)---CS	100	610	0.90	2.90	1.80	1.20	2.60	0.65	1.96	2.28	1.06	1.78	0.68	2.34	1.87	0.96	2.18
APEEL 10 (Skyline Blvd.)---CS	65	405	0.46	0.97	1.05	0.56	0.99	0.68	0.88	1.86	0.76	0.82	0.44	1.50	1.64	0.63	1.54
MEAN (TMzs)		508	0.68	1.94	1.43	0.88	1.80	0.77	1.42	2.07	0.91	1.30	0.56	1.92	1.76	0.80	1.86
APEEL 9 (Crys.Spr. Res.)---US	64	450	0.73	1.37	1.46	0.85	1.31	1.06	0.93	2.94	1.15	0.94	0.97	1.06	1.18	0.99	1.01
Saratoga---CSMIP	33	440	4.15	2.44	1.86	3.81	2.28	5.01	2.00	2.31	4.48	1.92	3.57	1.13	1.44	3.14	1.30
Richmond City Hall---CSMIP	109	440	2.00	2.60	2.30	2.10	2.50	2.07	3.53	1.54	2.25	2.70	1.61	3.46	1.59	1.87	2.72
SLAC---USGS	54	420	4.28	2.42	1.74	3.91	2.46	3.98	2.96	1.69	3.73	2.94	3.11	2.64	1.67	2.99	2.41
MEAN (QTe)		438	2.79	2.21	1.84	2.67	2.14	3.04	2.36	2.12	2.90	2.13	2.32	2.07	1.47	2.25	1.86
STANDARD DEVIATION		13	1.73	0.56	0.35	1.47	0.56	1.78	1.14	0.64	1.49	0.90	1.23	1.18	0.22	1.01	0.83
MEAN ("ROCK")		596	1.47	1.51	1.43	1.48	1.50	1.47	1.72	1.68	1.52	1.60	1.28	1.52	1.43	1.31	1.42
STANDARD DEVIATION		160	1.06	0.69	0.67	0.94	0.66	1.16	1.02	0.77	1.02	0.90	0.81	0.82	0.59	0.71	0.65

Table 3.3b -- Average spectral ratios for specified period bands for "soil" sites as normalized by local rock station (RIN,AP7, CSH,PIE,YBI, or WOD) or mean value for sites on unit KJf and hypocentral distance.

Station	H.Dist.	S vel.	Vertical					Radial					Transverse				
	km	m/s	period bands (secs)					period bands (secs)					period bands (secs)				
			0.1-0.5	0.5-1.5	1.5-5.0	0.1-5.0	0.4-2.0	0.1-0.5	0.5-1.5	1.5-5.0	0.1-5.0	0.4-2.0	0.1-0.5	.5-1.5	.5-5.0	.1-5.0	.4-2.0
Hayward BART Station---CSMIP	74	365	3.01	1.00	0.74	2.64	1.38	2.09	2.44	1.04	2.09	2.30	2.23	1.78	0.84	2.11	1.88
Oakland Office Bldg.----CSMIP	93	305	5.20	3.20	2.40	4.80	3.40	3.02	3.87	8.81	3.29	3.99	1.81	3.75	4.01	2.17	3.87
Fremont---USGS	58	285	1.58	1.04	1.82	1.52	1.14	1.58	2.33	1.89	1.69	2.40	1.45	1.52	1.54	1.46	1.87
Mission San Jose---CSMIP	57	285	2.08	1.03	1.31	1.91	1.27	1.39	2.23	2.07	1.54	2.16	1.47	1.12	1.24	1.42	1.20
Muir School (APEEL 2E)---CSMIP	73	280	2.76	1.06	1.11	2.45	1.06	1.85	3.40	3.05	2.11	3.43	1.82	1.65	1.86	1.80	1.78
MEAN (Qps)		304	2.93	1.47	1.48	2.66	1.85	1.99	2.85	2.93	2.14	2.86	1.76	1.96	1.80	1.79	2.04
STANDARD DEVIATION		35	1.39	0.97	0.85	1.27	0.99	0.64	0.74	2.18	0.69	0.81	0.32	1.03	1.24	0.35	0.95
Sunnyvale---USGS	46	240	2.60	1.10	2.05	2.37	1.23	3.04	2.16	3.43	2.94	2.07	2.40	1.14	1.99	2.21	1.17
Agnew State Hosp.---CSMIP	44	240	2.33	1.22	1.47	2.14	1.31	2.78	1.63	1.81	2.58	1.50	2.17	0.88	1.32	1.96	0.91
MEAN (Qhaf)		240	2.47	1.16	1.76	2.26	1.27	2.91	1.90	2.62	2.76	1.79	2.29	1.01	1.66	2.09	1.04
MEAN (Qal)		286	2.79	1.38	1.56	2.55	1.54	2.25	2.58	2.64	2.32	2.55	1.91	1.69	1.83	1.88	1.75
STANDARD DEVIATION		43	1.16	0.81	0.57	1.06	0.83	0.69	0.78	1.84	0.64	0.86	0.37	0.96	1.04	0.33	0.92
Emeryville Towers---USGS	98	240	3.40	2.50	2.50	3.30	2.60	1.88	5.75	9.06	2.72	5.79	1.92	4.31	8.17	2.53	4.81
Oakland Harbor Wharf---CSMIP	96	230	4.10	3.40	5.30	4.00	4.00	3.38	7.02	8.30	4.11	6.62	2.48	6.34	7.23	3.23	5.81
San Francisco Airport---CSMIP	81	180	1.78	1.51	0.88	1.70	1.63	2.92	4.01	3.11	3.07	3.71	2.79	3.43	1.42	2.82	3.57
Maloy Residence (F. City)---USGS	88	150	1.25	1.11	1.00	1.22	1.10	0.84	1.32	2.42	0.98	1.23	0.51	1.57	1.75	0.71	1.40
APEEL 2---USGS	66	130	1.75	1.28	0.78	1.85	1.50	0.67	2.62	1.67	0.97	2.22	0.49	3.35	2.13	0.94	2.81
Treasure Island---CSMIP	99	130	0.83	0.31	0.44	0.74	0.45	1.58	4.53	2.52	2.03	3.79	1.44	2.72	4.63	1.76	2.46
Redwood Shores (F. City)---CSMIP	67	115	1.99	1.58	0.99	1.69	1.58	2.93	3.18	4.32	3.02	2.91	2.12	3.26	3.29	2.32	3.21
MEAN (Qaf/Qhbm)		168	2.16	1.67	1.70	2.07	1.84	2.03	4.06	4.49	2.41	3.75	1.66	3.57	4.09	2.04	3.38
STANDARD DEVIATION		50	1.17	1.00	1.72	1.16	1.15	1.07	1.92	2.96	1.16	1.91	0.91	1.46	2.70	0.95	1.39
MEAN ("SOIL")		227	2.48	1.52	1.63	2.31	1.69	2.14	3.32	3.66	2.37	3.15	1.79	2.63	2.96	1.96	2.57
STANDARD DEVIATION		76	1.17	0.69	1.23	1.10	0.97	0.88	1.61	2.53	0.90	1.55	0.88	1.54	2.29	0.69	1.41

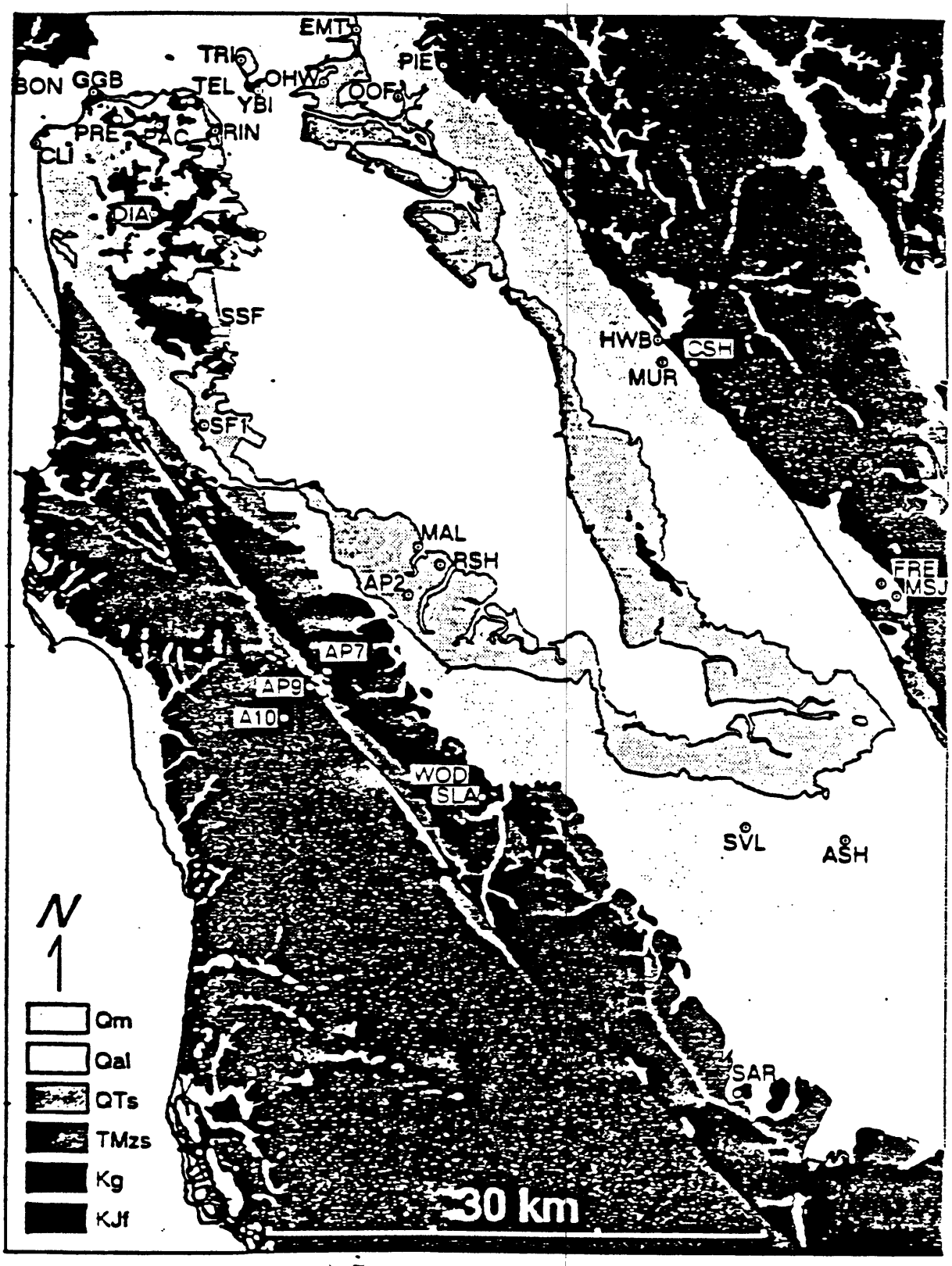

Figure 1. Location map for free-field stations in the San Francisco Bay region, California, which recorded the Loma Prieta earthquake of October 17, 1989.

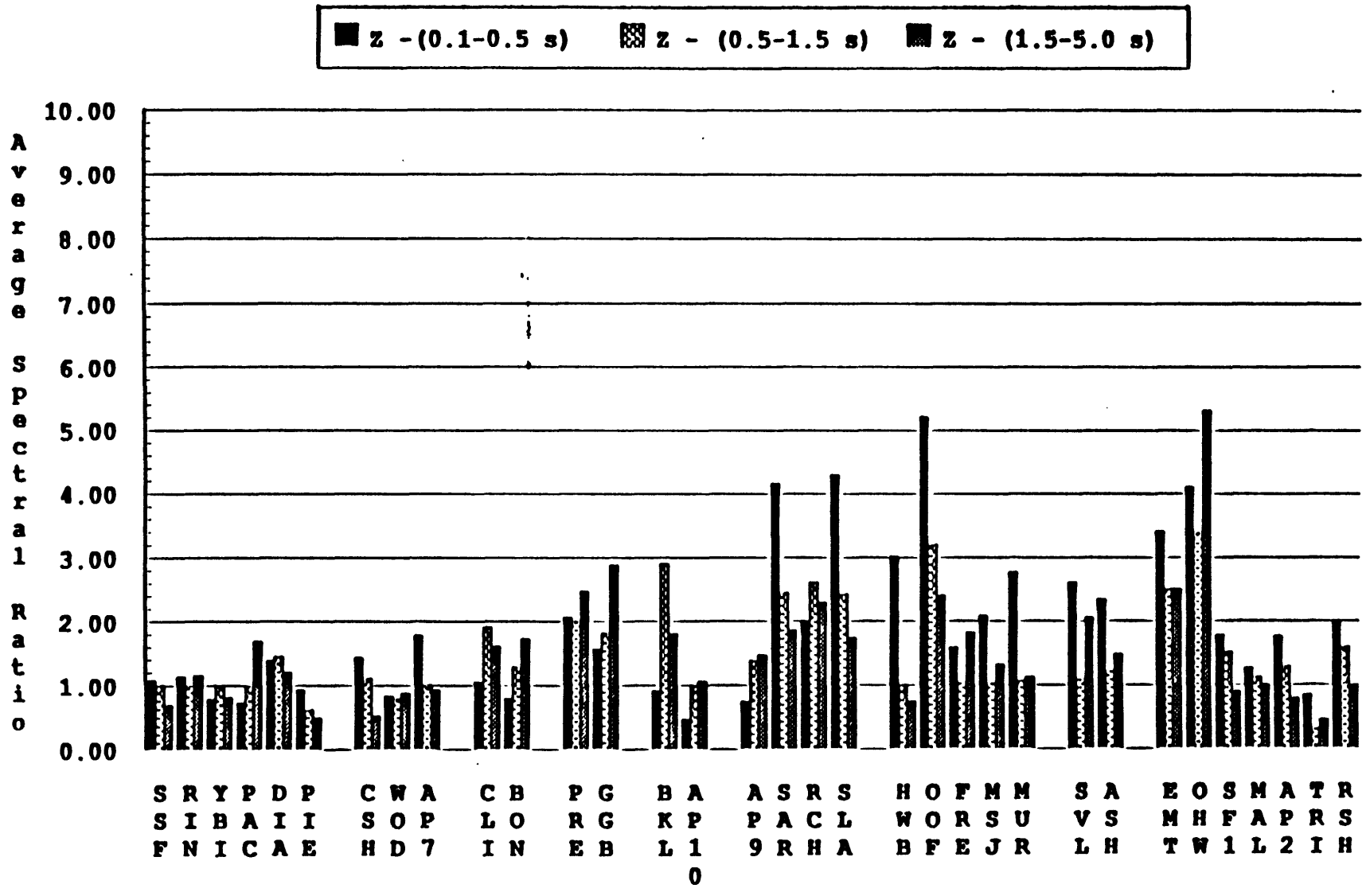

Figure 3.2 — Average spectral ratios for short-, intermediate-, and long-period bands for vertical motion.

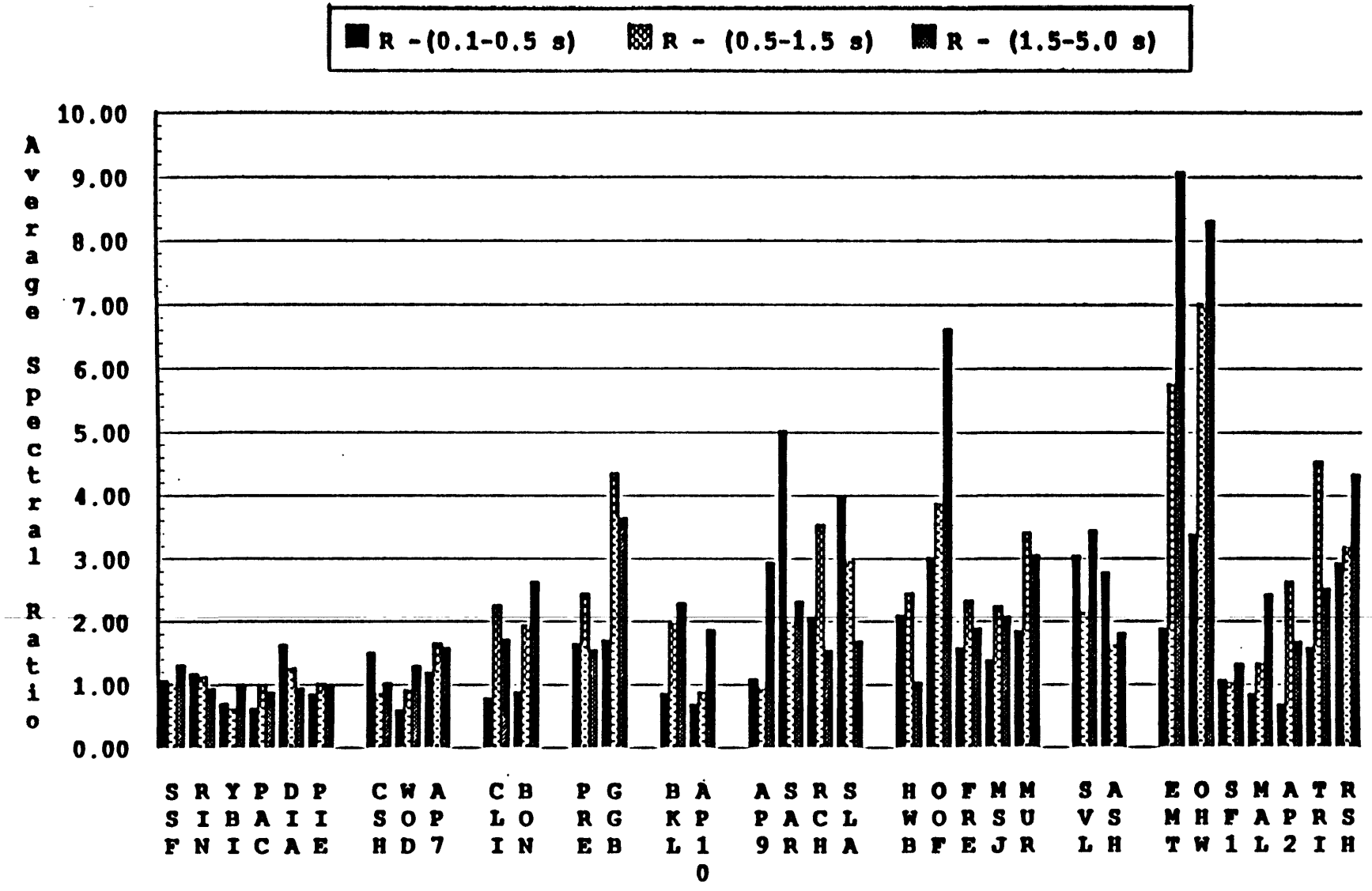

Figure 3.3 — Average spectral ratios for short-, intermediate-, and long-period bands for radial motion.

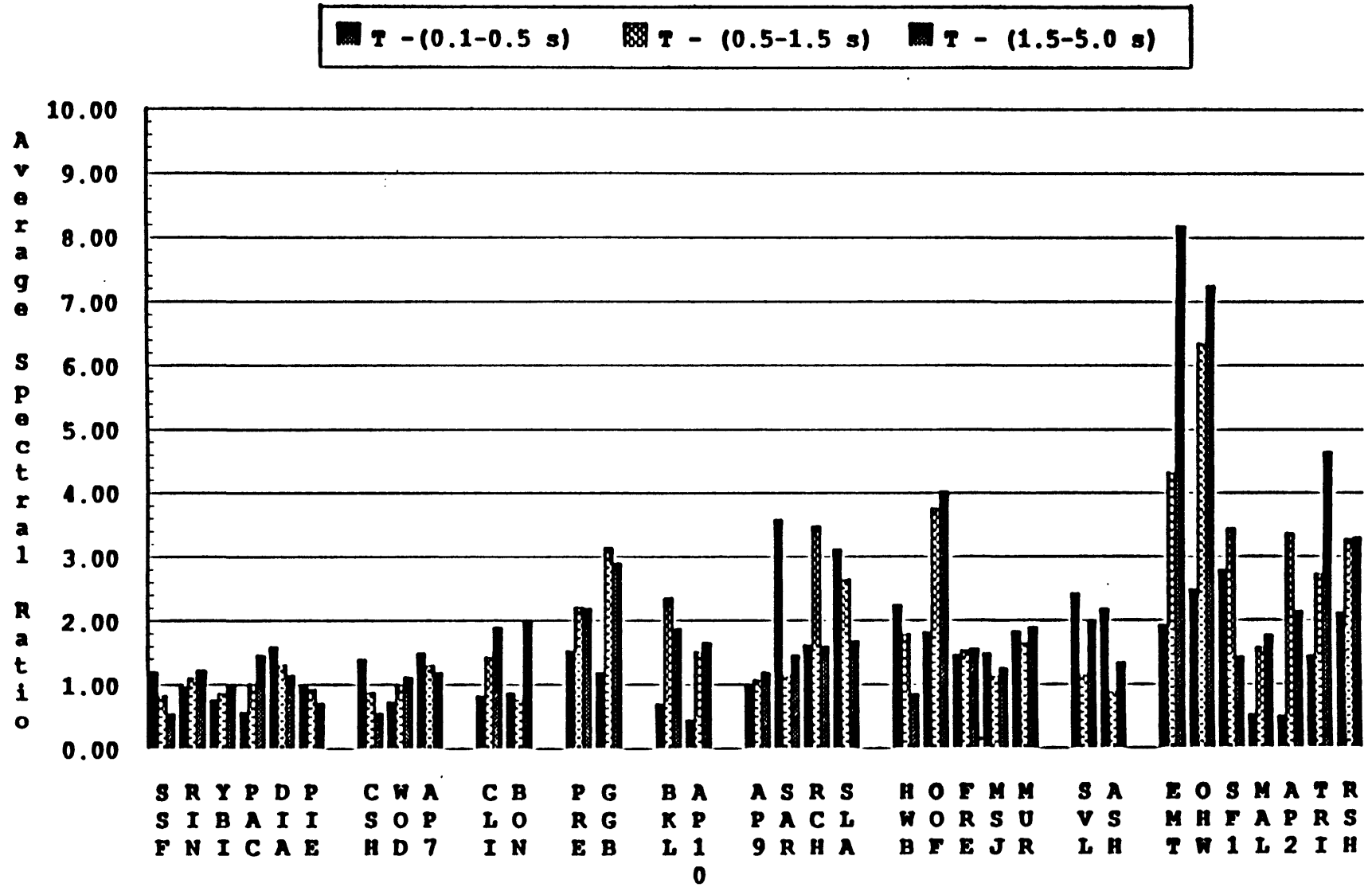

Figure 3.4 – Average spectral ratios for short-, intermediate-, and long-period bands for transverse motion.

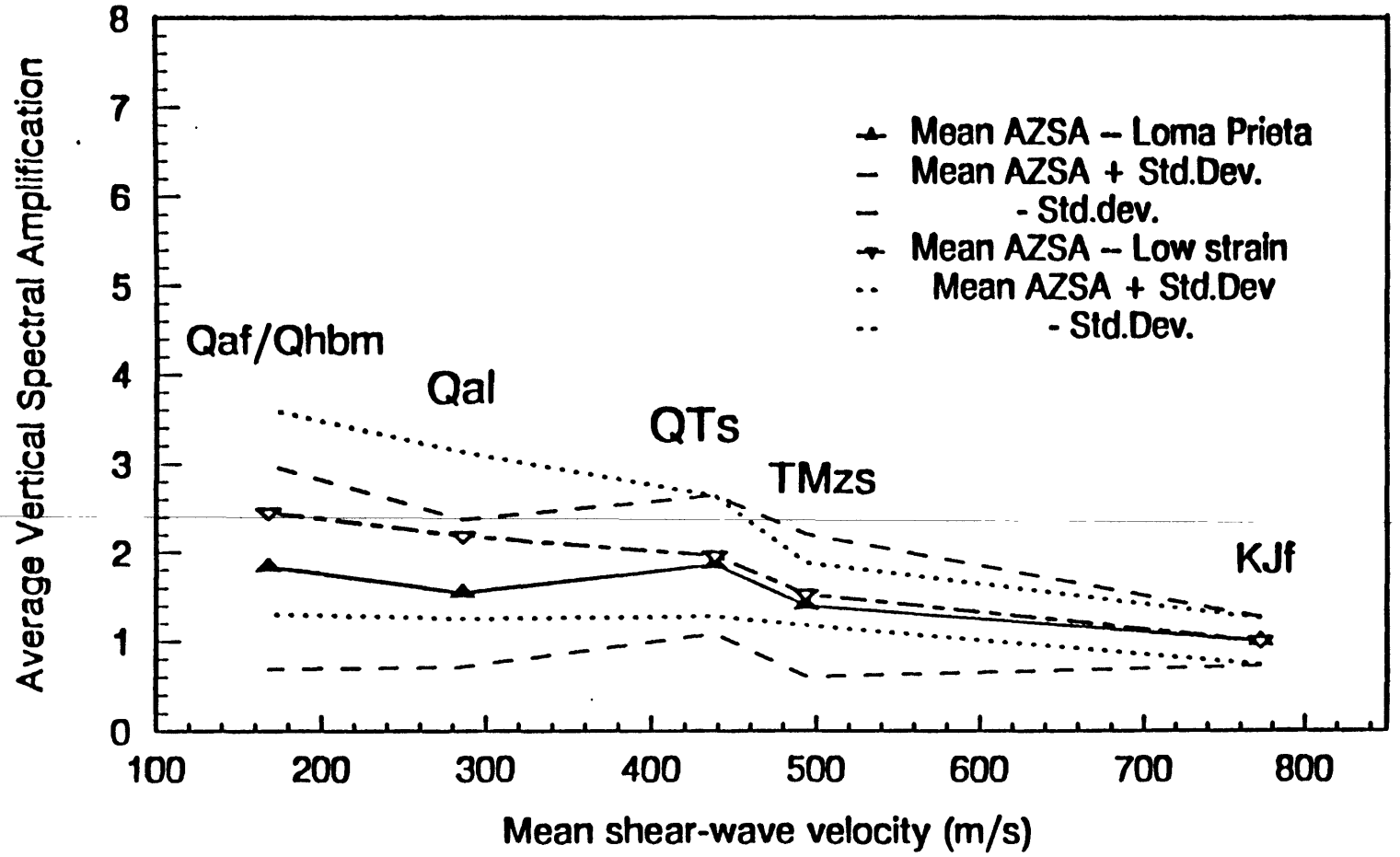

Figure 3.5 Statistics for mean amplifications computed from low-strain and strong-motion recordings of vertical ground motion obtained on generalized geologic units.

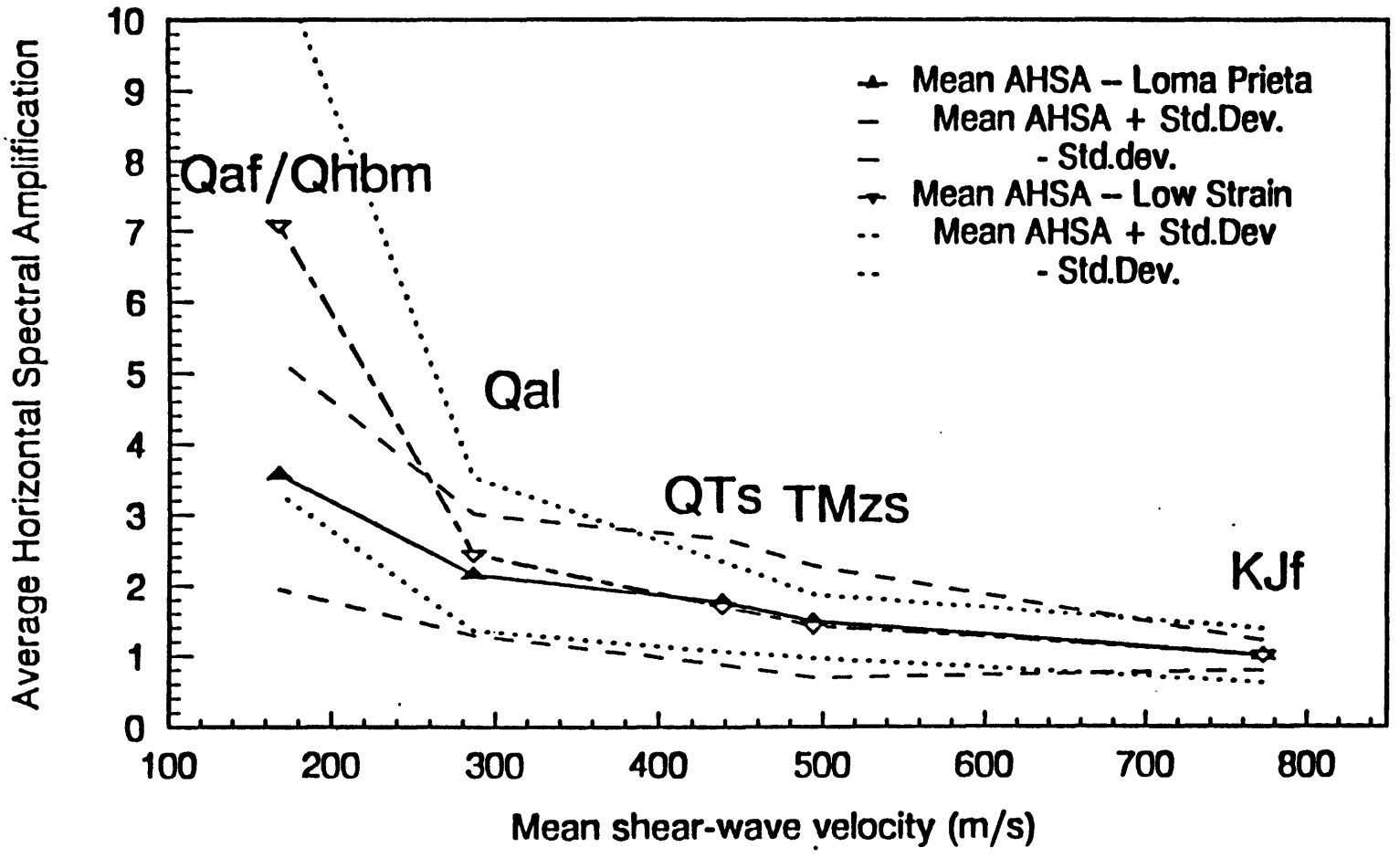

Figure 3.6 Statistics for mean amplifications computed from low-strain and strong-motion recordings of average horizontal motion obtained on generalized geologic units.

4. LOMA PRIETA AFTERSHOCK RECORDS

4.1 General Remarks

Following the main shock of the 17 October 1989 Loma Prieta earthquake [$M_s = 7.1$], several organizations attempted and successfully recorded many aftershocks at temporary stations with deployments of a variety of portable instruments. Some of these temporary deployments were co-located with permanent strong-motion stations of both the United States Geological Survey (USGS) and the California Division of Mines and Geology (CDMG) of the State of California.

The major organizations that deployed temporary aftershock recording instruments were:

(1) United States Geological Survey (USGS),

(2) Lamont–Doherty Geological Observatory (LDGO), Columbia University, New York,

(3) Lawrence Livermore National Laboratory (LLNL), Livermore, CA.

These organizations coordinated with each other to prevent duplication and complemented the various deployment schemes. However, each organization used a different type of recording system; thus providing an opportunity to compare their performances.

The purpose of this section is to describe the general objectives of aftershock recordings and the general deployment schemes. The reasoning behind inclusion of this section in this report is to provide the background information of the aftershock recording efforts that form the basis for comparison with the microtremor recording results.

4.2 Description of Deployments

The deployments by key organizations are summarized in Table 4.1.

Table 4.1 Summary of Deployments

Organization	No. of Stations	No. of Records	References
USGS			
Menlo Park	94	15621	10
Golden, CO	101	8216	4
LDGO	22	144	7
LLNL	7	1455	8

USGS Deployments—The aftershock recording deployments executed by USGS were carried out in several stages by different groups. However, in general, the efforts will be categorized into two:

(1) San Francisco Peninsula and South Bay Deployment (Menlo Park Office),

(2) Santa Cruz and Vicinity Deployment (Golden, CO, office).

Menlo Park Deployment—The deployments consisted of various arrays with definitive objectives. A general overall layout of the USGS–Menlo Park (Branch of Engineering Seismology and Geology) deployments is seen in Figure 4.1. The area covered extends from San Francisco to south of Santa Cruz. The boxes in the figure outline Figures 4.2–4.6 that show the deployments in different regions. The Menlo Park effort consisted of deployment of only GEOS recording systems with one or both of the triaxial velocity (Mark Products L–22) transducers or triaxial force-balance accelerometers (Kinemetrics FBA–3). The GEOS units recorded the aftershocks at 200 sps.

Golden Deployment—The Branch of Geologic Risk Assessment of USGS at Golden, Colorado deployed Sprengnether DR–200 portable recorders and S–6000 triaxial velocity transducers particularly in the Santa Cruz area. General description of the Golden deployments is provided in Figure 4.7. These deployments consisted of several arrays in different study areas including the city of Santa Cruz, the city of Los Gatos, Rebecca Ridge and Robinwood Lane study areas. These deployments and locations of the stations are shown in Figures 4.8–4.12.

LDGO Deployments—LDGO deployment was limited to a special purpose dense array consisting of 5 stations in the vicinity of the Cypress Structure in the East San Francisco Bay (Hough, 1990). The array deployment used dual-gain, 2 Hz sensors (Mark Products L–22s) with IRIS/PASCAL digital Reftek recorders. The stations covered by LDGO deployments fall outside the study area of this report.

LLNL Deployments—LLNL deployments consisted of 7 stations, 3 at Livermore and 4 co-located with CDMG stations (Jarpe and others, 1989). Outside of Livermore, the stations were scattered mainly to different sites such as Treasure Island (fill), Redwood Shores (alluvium and fill), Yerba Buena Island (rock site) and Mission San Jose (an alluvium site). The objective was to determine spectral relations from pairs of aftershock records (soil and rock) and compare them with those from strong-motion records. The only station that falls within the study area of this report is the Redwood Shores station.

4.3 Discussion of Results

As summarized in Table 4.1, thousands of (velocity and/or acceleration) seismograms have been recorded by the organizations which attempted to do so. These seismograms have been processed and have been incorporated in data bases of each respective organization. The USGS data is compiled in CD–ROMs and are distributed along with open-file reports that summarize the data.

The aftershock recording stations were re-occupied (as much as possible) to record micro-tremor measurements to be used for comparison of the characteristics derived from both methods (aftershocks versus microtremors).

Selected data has been processed to derive spectral ratios. In processing the records, computer software by Mueller was used. These were done mainly for stations in the peninsula. Similar processing will be performed for the Santa Cruz stations in a revised volume of this report.

The figures below are from four aftershocks (event 3090130 [$M = 3.8$], event 3091337 [$M = 3.8$], event 3112342 [$M = 4.0$], and event 3121345 [$M = 2.4$]). Data available for those stations which recorded these events are processed.

Figure 4.13 shows for event 3090310 the three-component velocity seismograms of **FOX** and **AP7** as well as their Fourier amplitude spectra superimposed for each component and the spectral ratios (**FOX/AP7**). **FOX** is located on fill and bay mud (Qm).

Figure 4.14 shows for event 3091337 the three-component velocity seismograms of **FOX** and **AP7** as well as their Fourier amplitude spectra superimposed for each component and the spectral ratios (**FOX/AP7**).

Figure 4.15 shows for event 3112342 the three-component velocity seismograms of **FOX** and **AP7** as well as their Fourier amplitude spectra superimposed for each component and the spectral ratios (**FOX/AP7**).

These figures show that for the events 1090130 and 3112342, the Fourier amplitude spectra shapes are very similar. The **FOX** and **AP7** amplitudes diverge above approximaely 1 Hz. The ratios are significantly high for frequency bands at 1 Hz, 1.2–1.3 Hz and 1.8 and 2.2 Hz. Event 3091337 on the other hand shows higher amplitudes for **FOX** and higher ratios for the 0.1–0.3 Hz band in addition to those bands up to 2.8 Hz.

Figure 4.16 shows for event 3091337 the three-component velocity seismograms of **MAL** and **AP7** as well as their Fourier amplitude spectra superimposed for each component and the spectral ratios (**MAL/AP7**). **MAL** is located on fill and bay mud (Qm).

Figure 4.17 shows for event 3121345 the three-component velocity seismograms of **MAL** and **AP7** as well as their Fourier amplitude spectra superimposed for each component and the spectral ratios (**MAL/AP7**).

The above two figures distinctly show an order of magnitude variation in amplitude spectra particularly for the horizontal components (higher for event 3091337). This is attributable to the higher magnitude of the 3091337 event. The ratios on the other hand are consistent for the N–S components and present ratios similar in frequency band of 0.3–0.7 Hz and at approximately 1.3 Hz. The E–W components are not very comparable.

Figure 4.18 shows for event 3112342 the three-component velocity seismograms of **AP2** and **AP7** as well as their Fourier amplitude spectra superimposed for each component and the spectral ratios (**AP2/AP7**). **AP2** is located on fill and bay mud (Qm).

This event shows almost the same order of amplitude for all three components. For the horizontal component, amplitudes of AP2 start to be larger at 0.6–0.7 Hz. We note significant ratio peaks at 1 Hz and around 2 Hz.

REFERENCES

Brabb, E. E. (editor) (1979). Progress on seismic zonation in the San Francisco Bay region, *U.S. Geol. Surv. Circular* **807**.

Borcherdt, R. D. and J. F. Gibbs (1976). Effects of local geological conditions in the San Francisco Bay region on ground motions and the intensities of the 1906 earthquake, *Bull. Seism. Soc. Am.*, **66**, 467–500.

Borcherdt, R. D., J. B. Fletcher, E. G. Jensen, G. L. Maxwell, J. R. Van Schaack, R. E. Warrick, E. Cranswick, M. J. S. Johnston, and R. McClear (1985). A General Earthquake Observation System (GEOS), *Bull. Seism. Soc. Am.*, **75**, 1783–1825.

Carver, D., K. W. King, E. Cranswick, D. W. Worley, and P. Spudich (1990). Digital recordings of aftershocks of the October 17, 1989, Loma Prieta earthquake in Santa Cruz, Los Gatos, and surrounding areas, *U.S. Geol. Surv. Open-File Rep.* **90–683**.

Clark, J. C. (1981). Geologic map and sections of the Felton–Santa Cruz area, Santa Cruz County, California, *U.S. Geol. Surv. Prof. Pap.* **1168**, plate 2.

Hensolt, W. H. and E. E. Brabb (1990). Maps showing elevation of bedrock and implications for design of engineered structures to withstand earthquake shaking in San Mateo County, California, *U.S. Geol. Surv. Open-File Rep.* **90–496**.

Hough, S. E. (1990). Constraining sediment thickness in the San Francisco Bay area using observed resonances and p-to-s conversions, *Geophys. Res. Lett.*, **17**, 9, 1469–1472.

Jarpe, S. P., J. L. Hutchings, T. F. Hauk, and A. F. Shakal (1990). LLNL strong and weak motion data from the Loma Prieta sequence, *Seism. Res. Let.*, **60**, 4, 167–176.

Maley, R. and others (1989). U.S. Geological Survey strong-motion records from the northern California (Loma Prieta) earthquake of October 17, 1989, *U.S. Geol. Surv. Open-File Rep.* **89–568**.

Mueller, C. S. and G. Glassmoyer (1990). Digital recordings of aftershocks of the 17 October 1989 Loma Prieta, California, earthquake, *U.S. Geol. Surv. Open-File Rep.* **90–503**.

Mueller, C. S. (1990). Computer programs for analyzing digital seismic data, *U.S. Geol. Surv. Open-File Rep.* **90–351**.

Shakal, A. F. and others (1989). CSMIP strong-motion records from the Santa Cruz Mountains (Loma Prieta), California earthquake of October 17, 1989, *Report OSM* **89–03**, November.

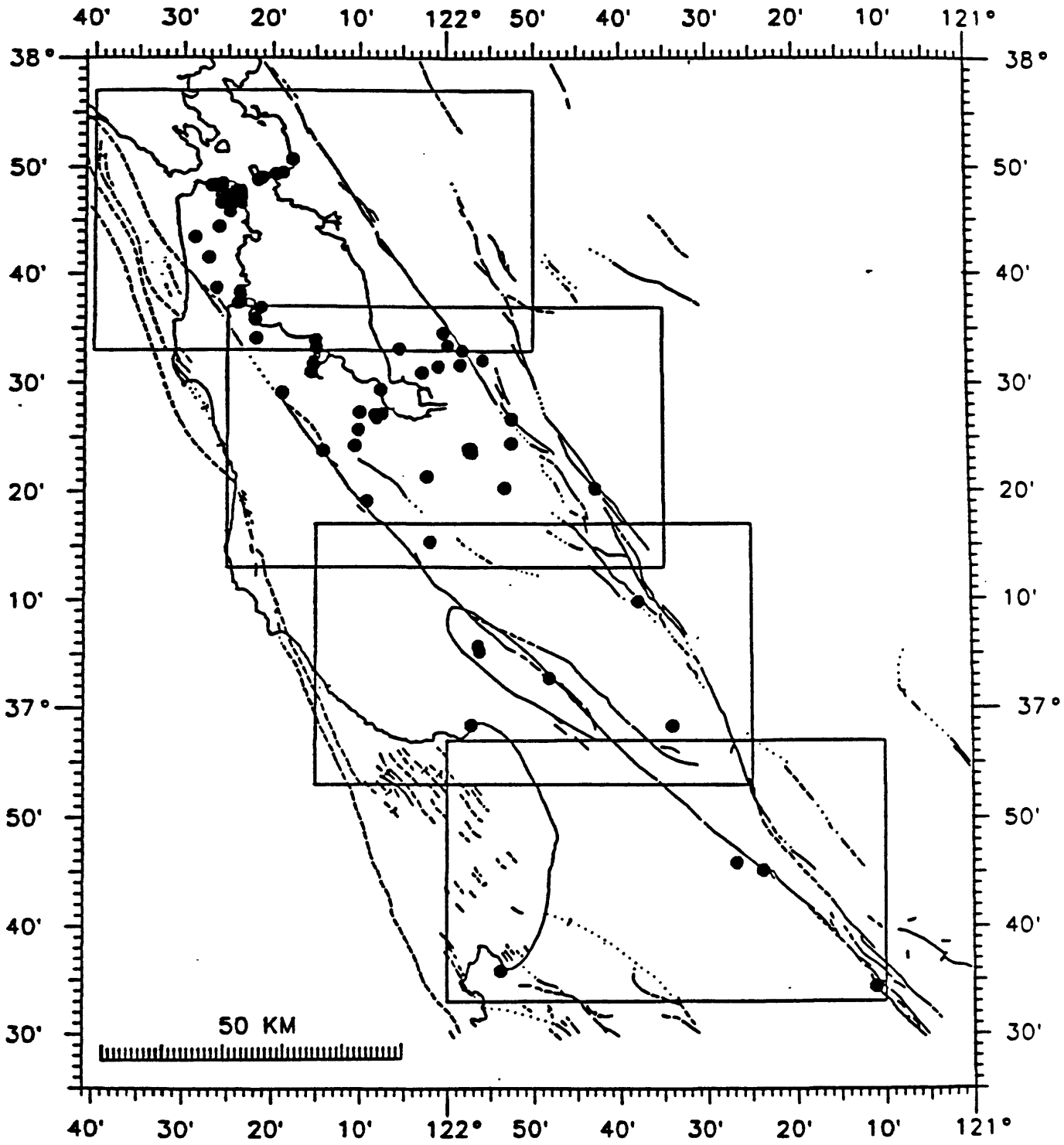

Figure 4.1. GEOS station locations (dots) superimposed on a map of central California showing coastline, faults, and estimated main-shock rupture area (crosshatch). Boxes outline four large scale maps shown in Figures 2, 3, 4, and 5 (from Ref. 10).

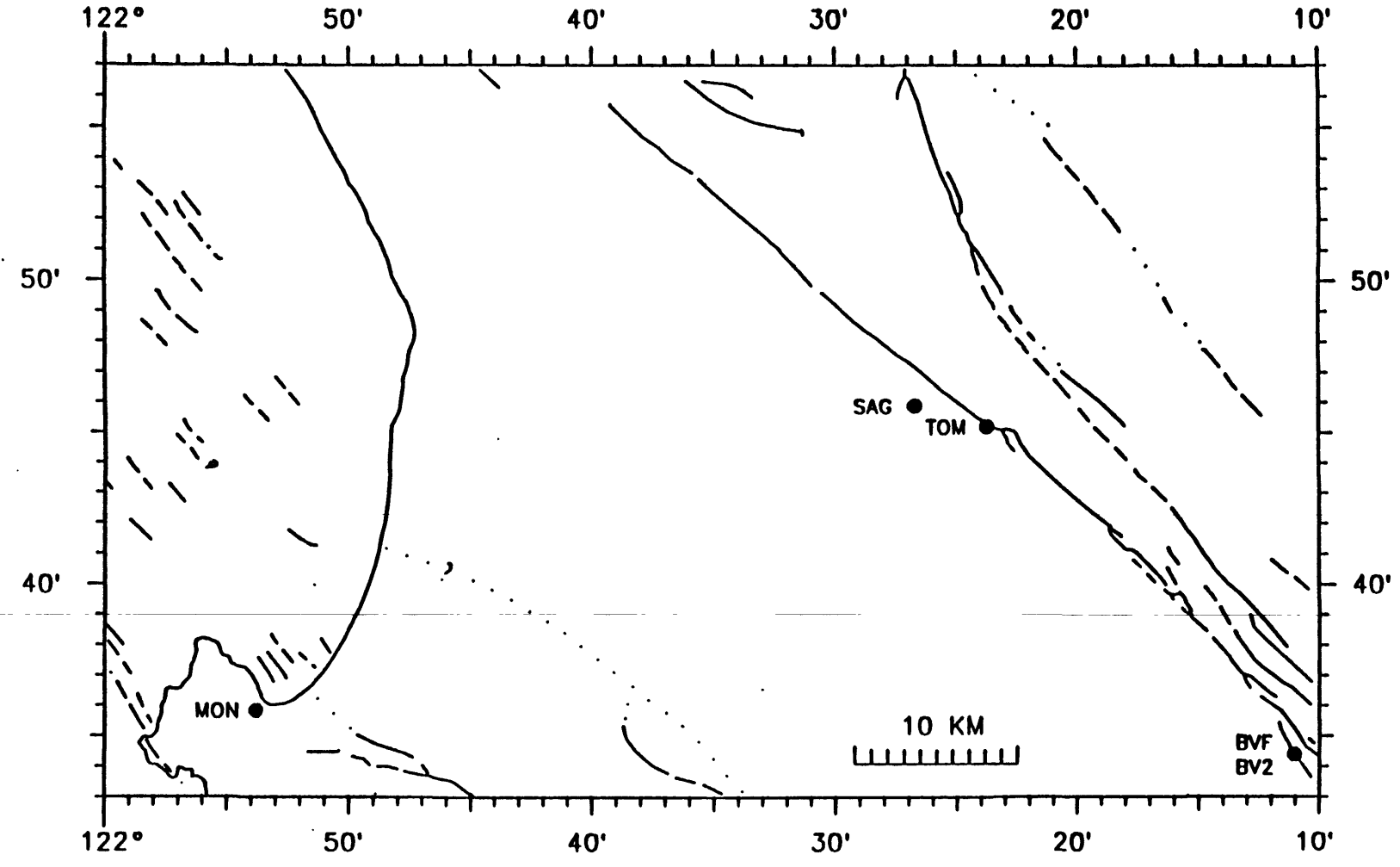

Figure 4.2. GEOS station locations in south region (refer to Figure 1) (from Ref.10).

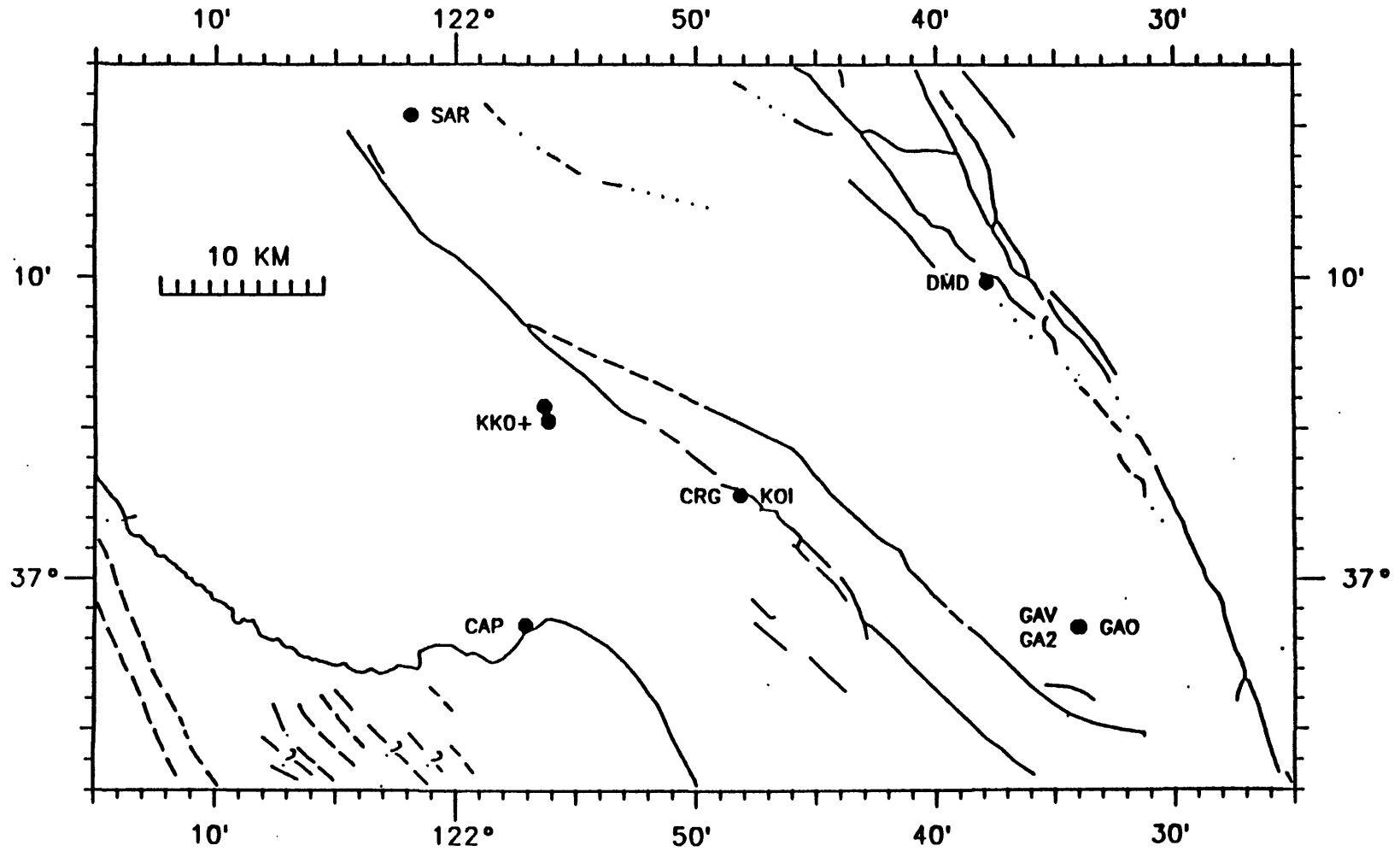

Figure 4.3. GEOS station locations in south-central region (refer to Figure 1) (from Ref. 10).

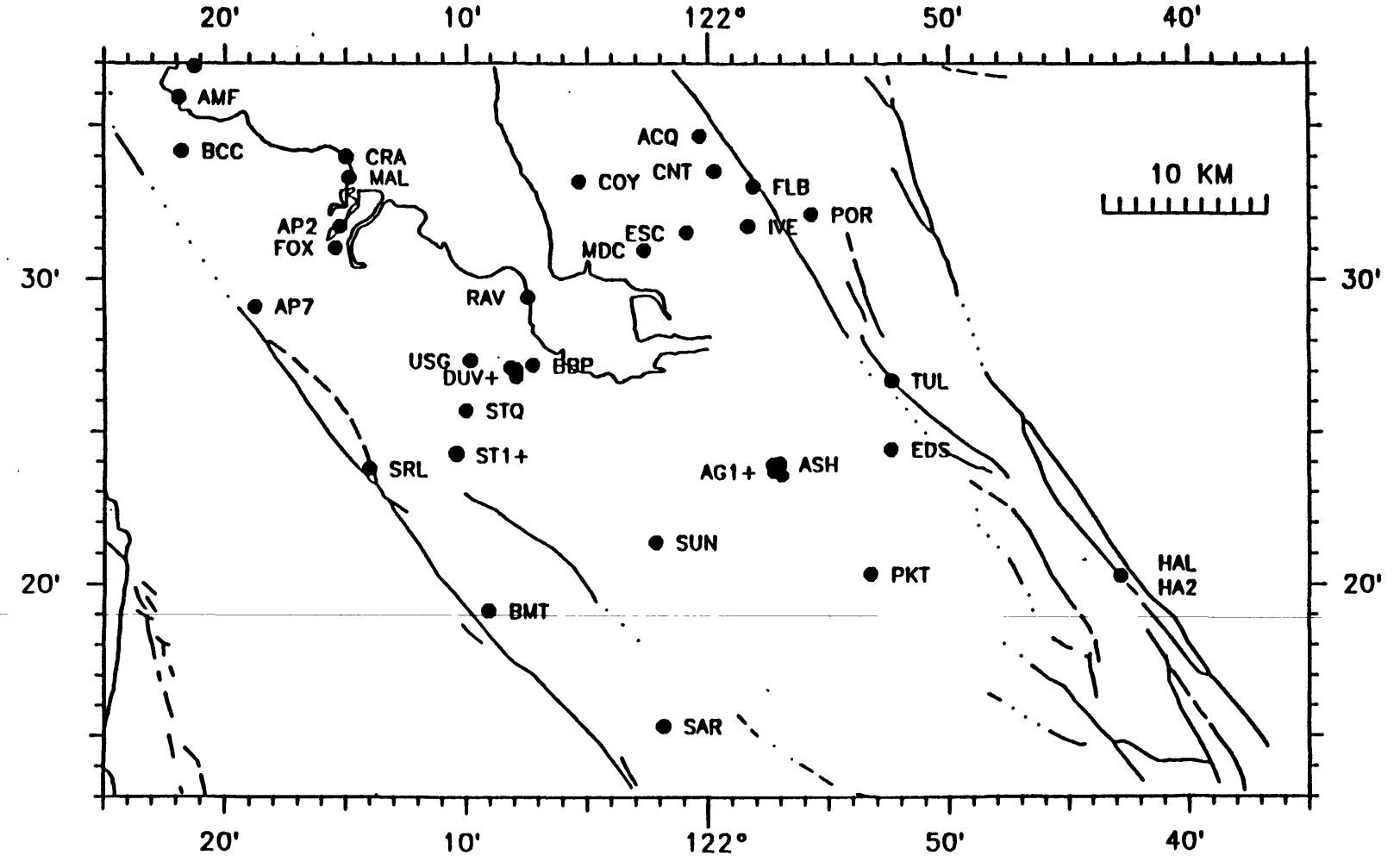

Figure 4.4. GEOS station locations in north-central region (refer to Figure 1) (from Ref. 10).

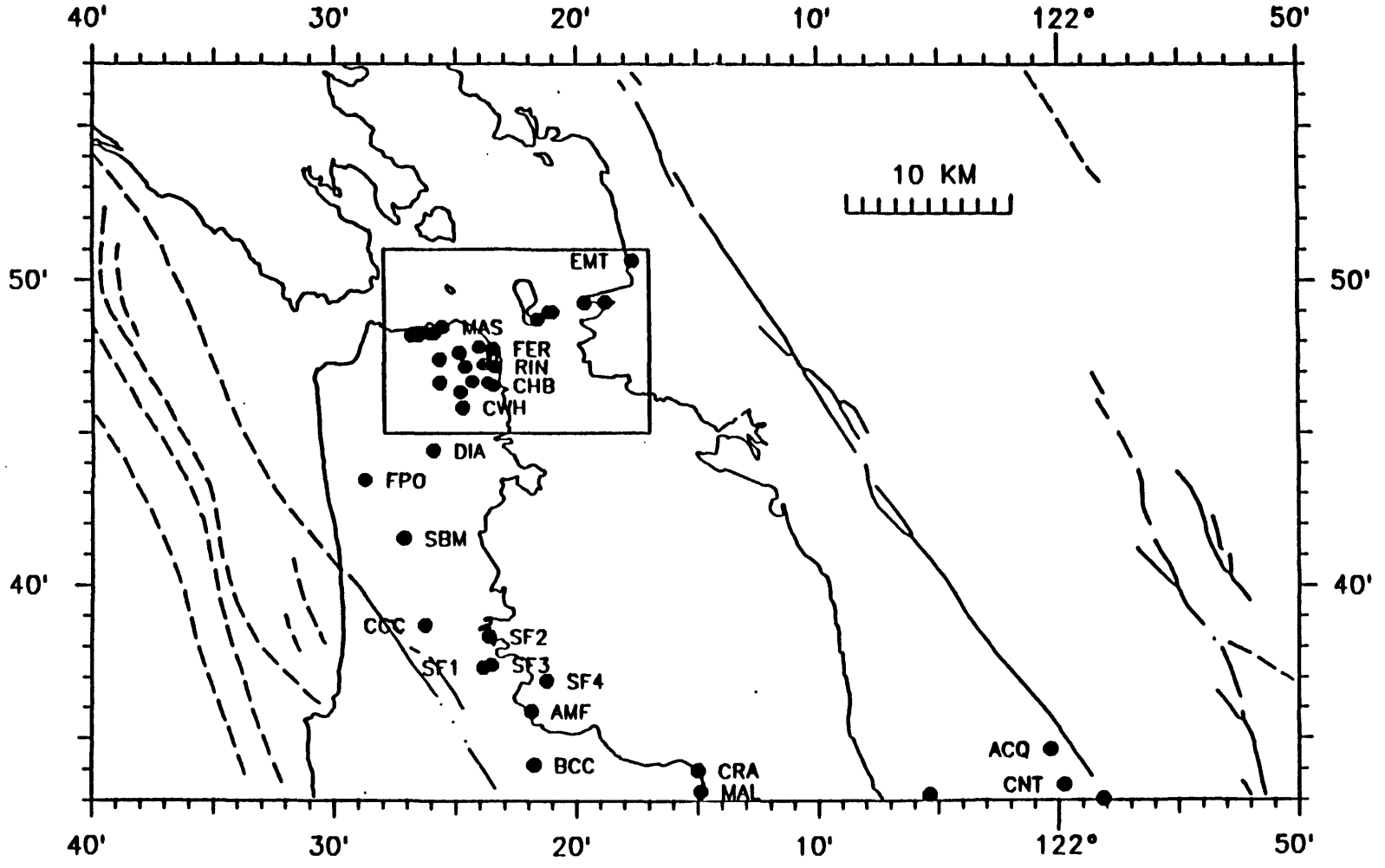

Figure 4.5. GEOS station locations in north region (refer to Figure 1) (from Ref. 10).

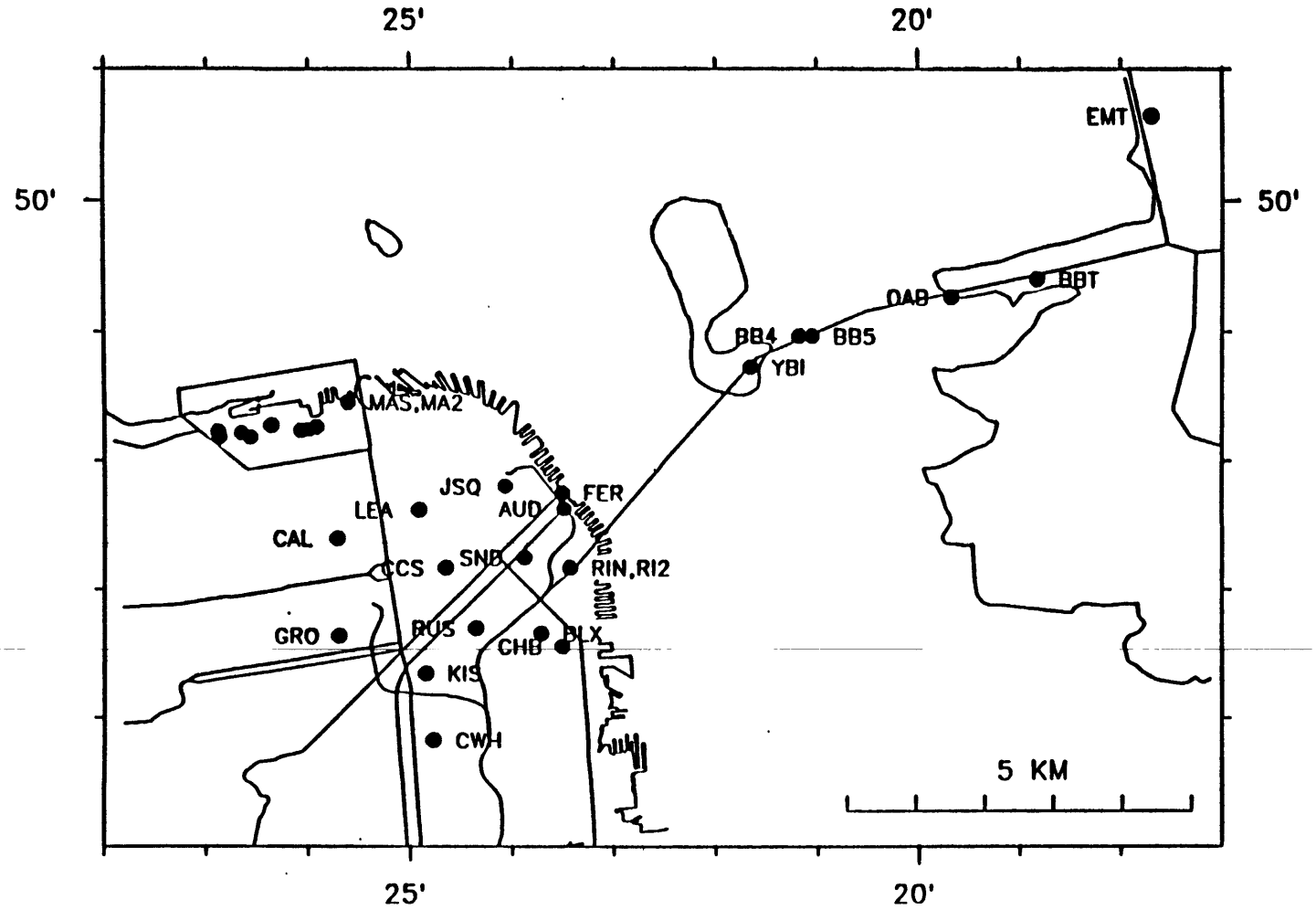

Figure 4.6. GEOS station locations in San Francisco (refer to Figure 5) (from Ref. 10).

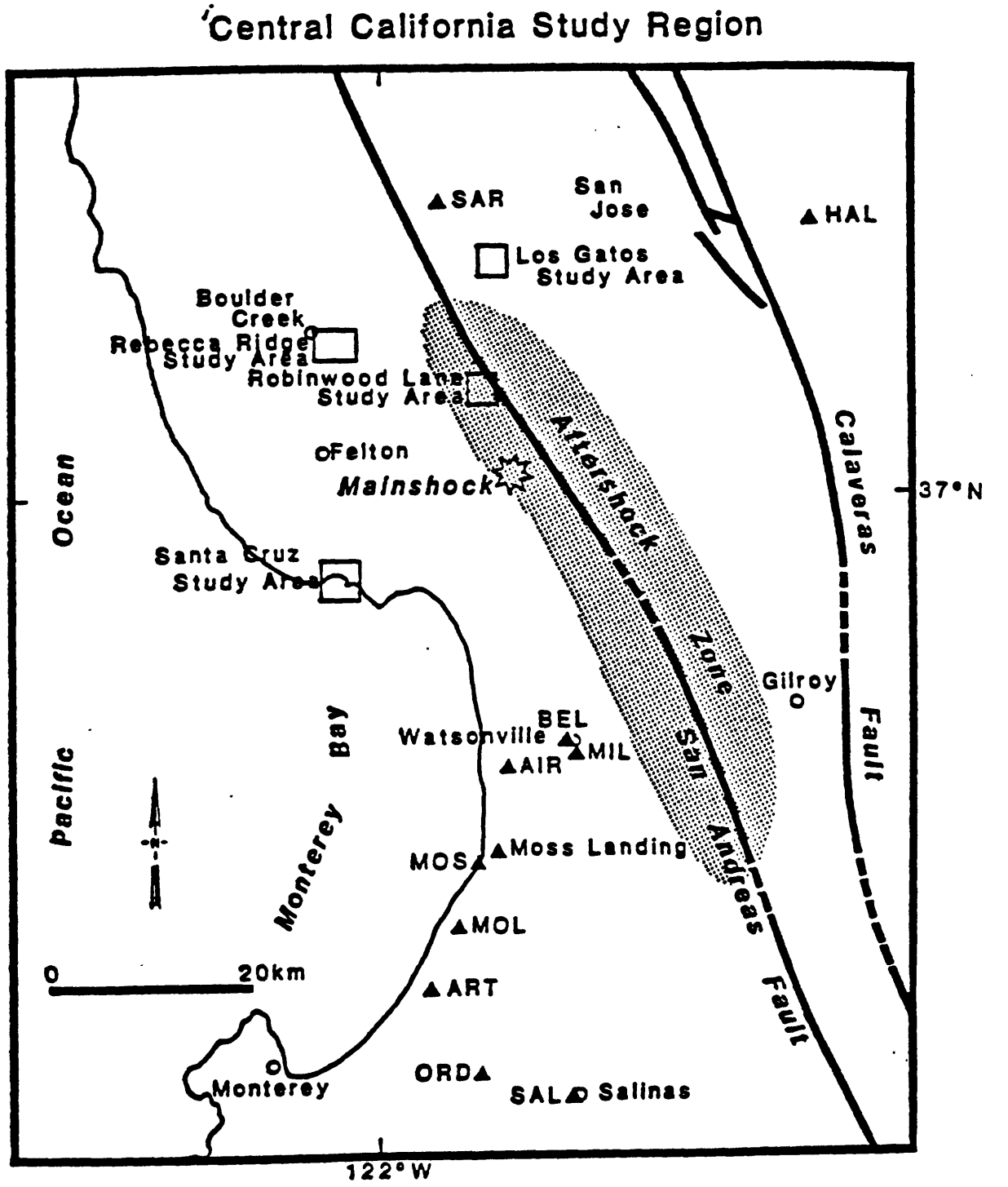

Figure 4.7. Map of central California showing coastline, faults, mainshock, mainshock rupture area, study areas (shown in greater detail in figure 2, 3, 4, 5, and 6) and several outlying station locations. (from Ref. 4).

Santa Cruz Flood Plain Array

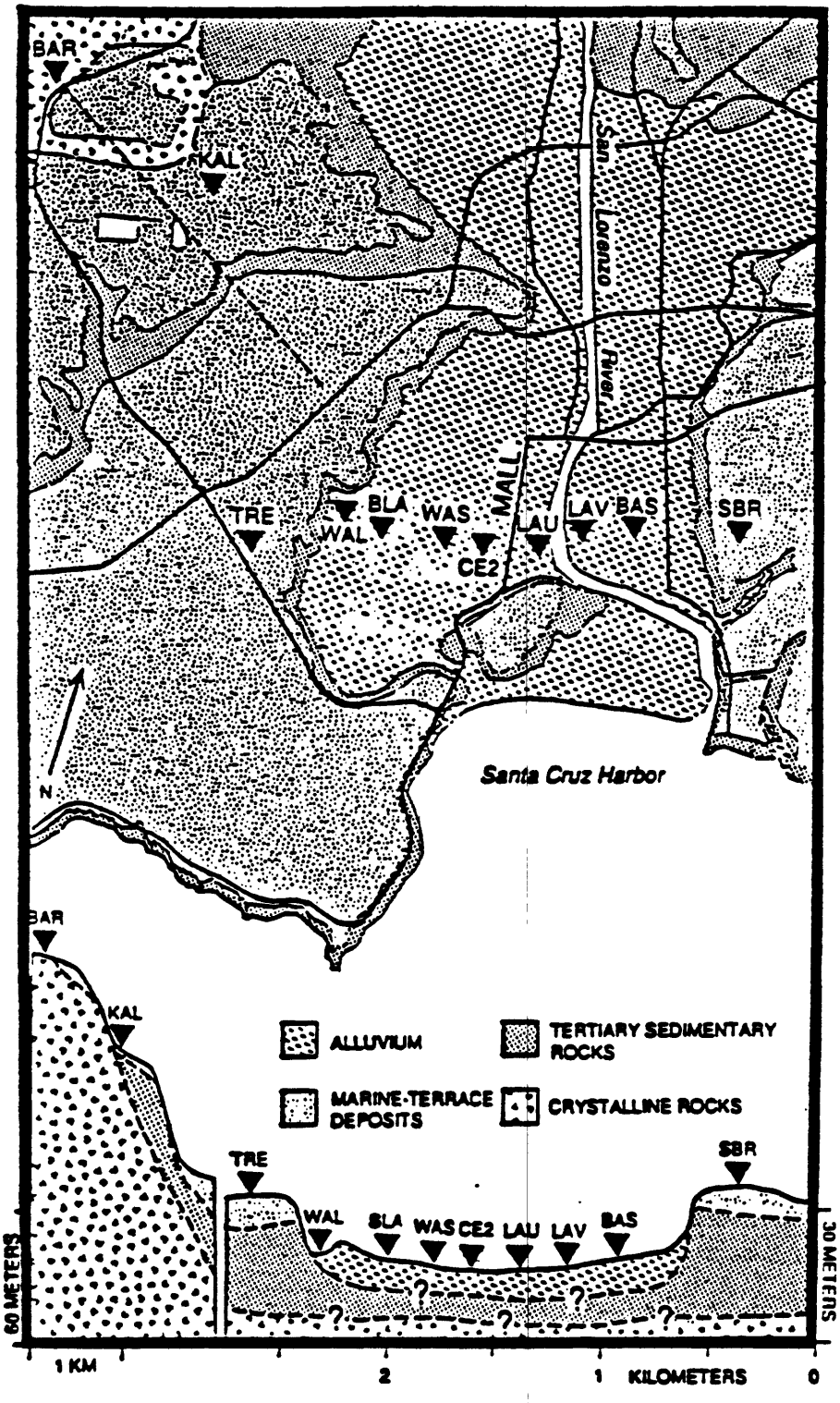

Figure 4.8. Map of the Santa Cruz, California, study area showing seismograph station locations, and general surficial geology (adapted from Clark, 1981) (from Refs. 4 and 5).

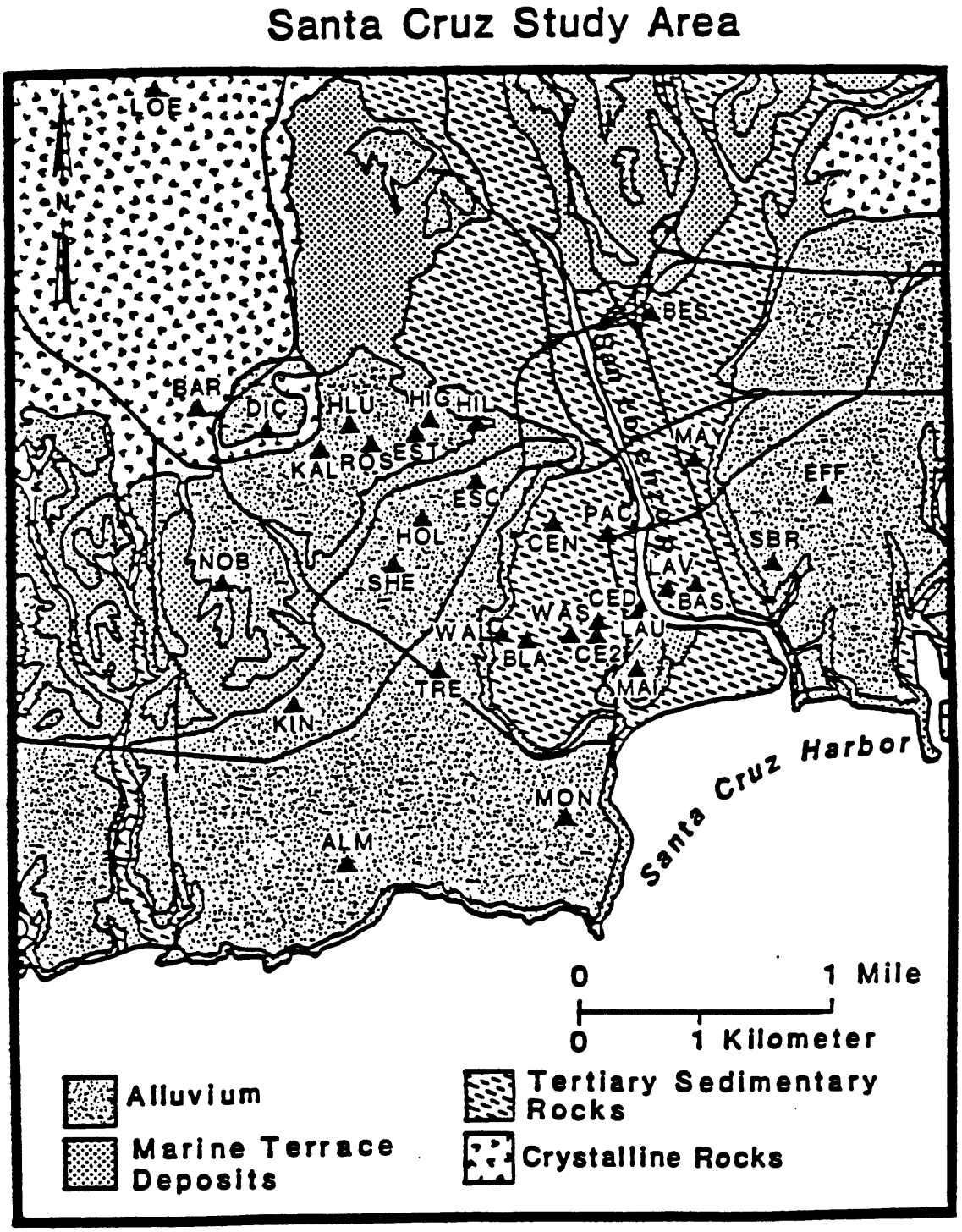

Figure 4.9. Geological map of Santa Cruz, California, showing seismograph station locations. Bottom: Idealized cross-section along the downtown array (from Ref. 4).

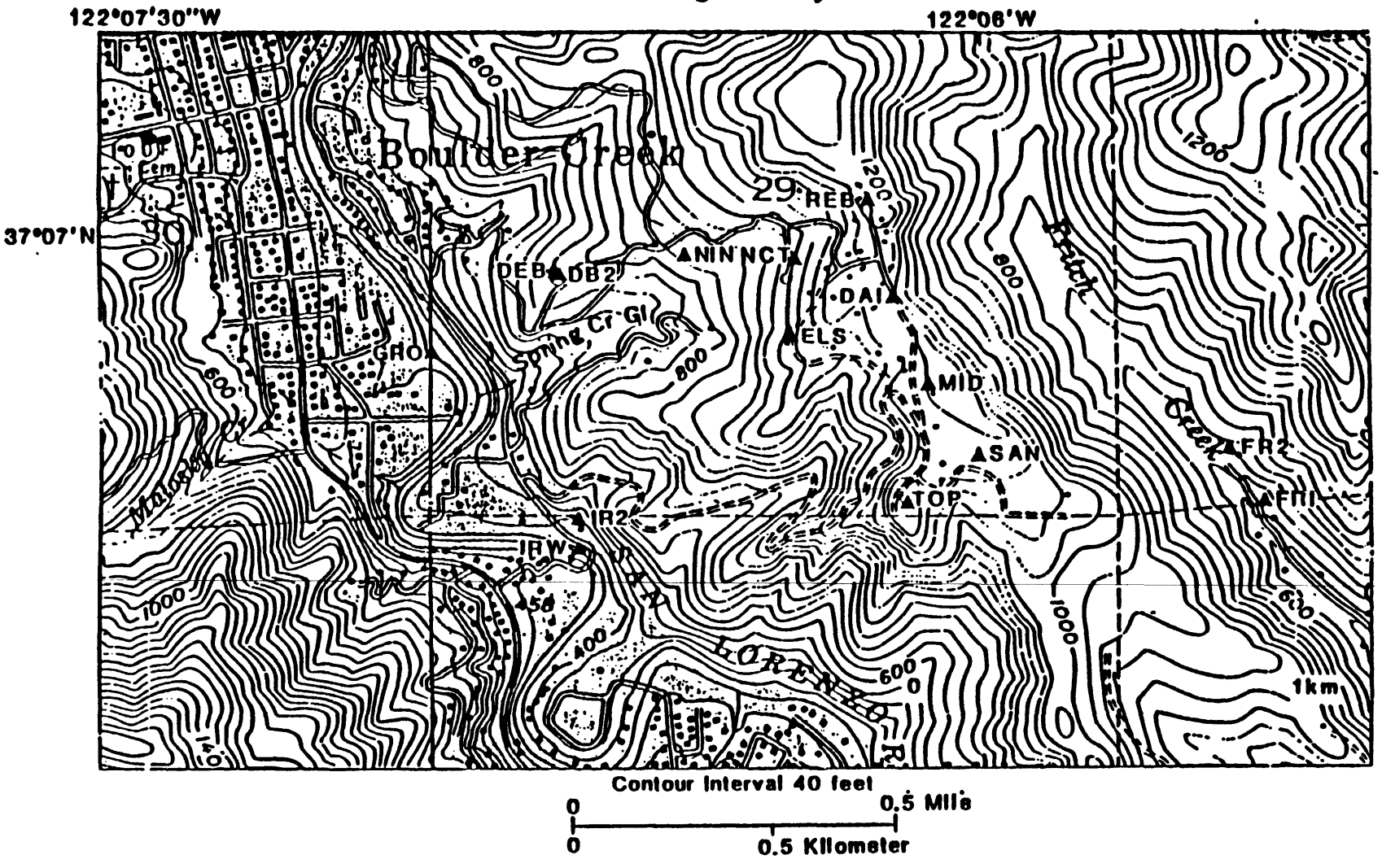

Figure 4.10. Map of the Rebecca Ridge study area showing seismograph station locations (from Ref. 4).

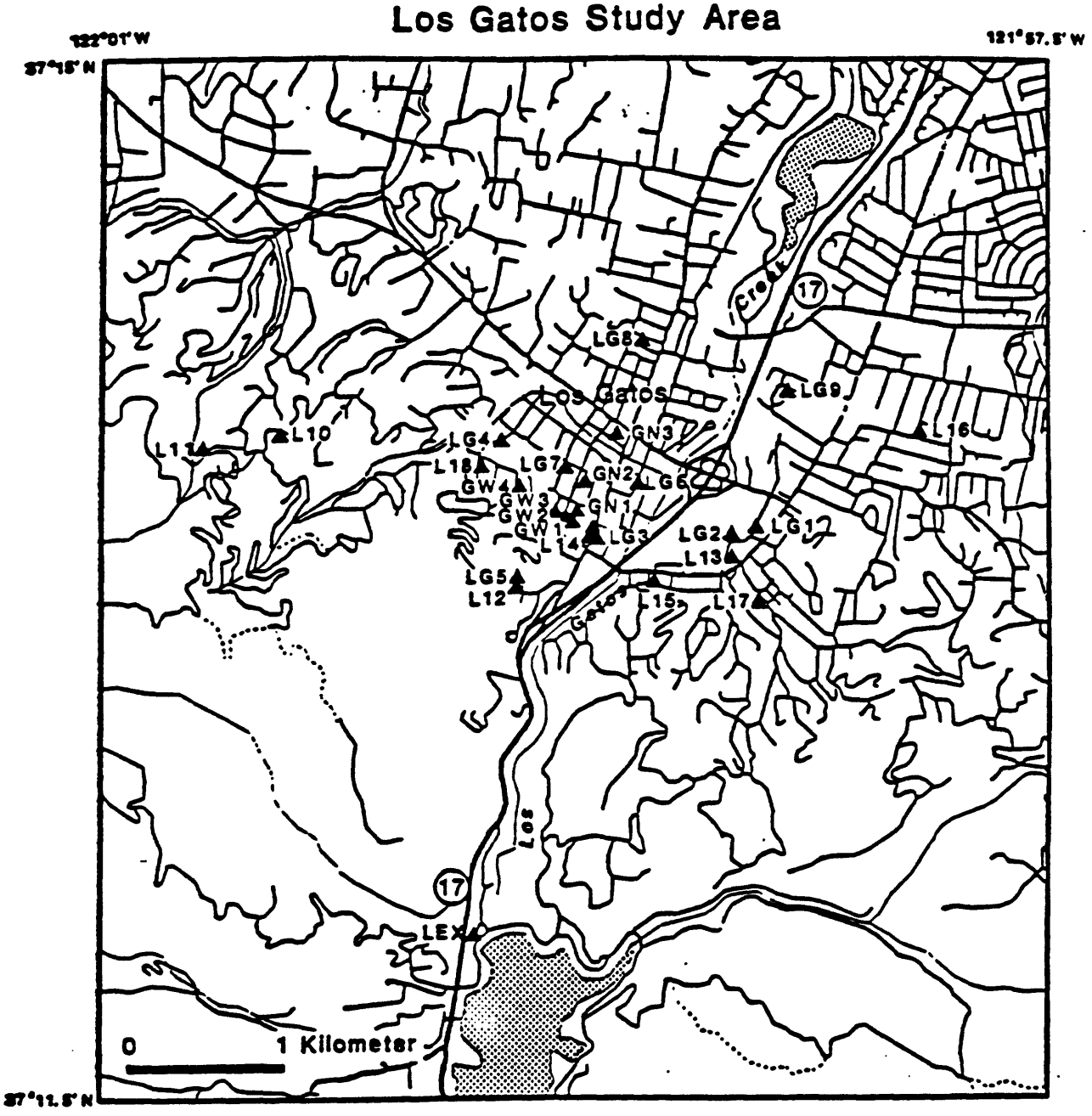

Figure 4.11. Map of Los Gatos seismograph stations (from Ref. 4).

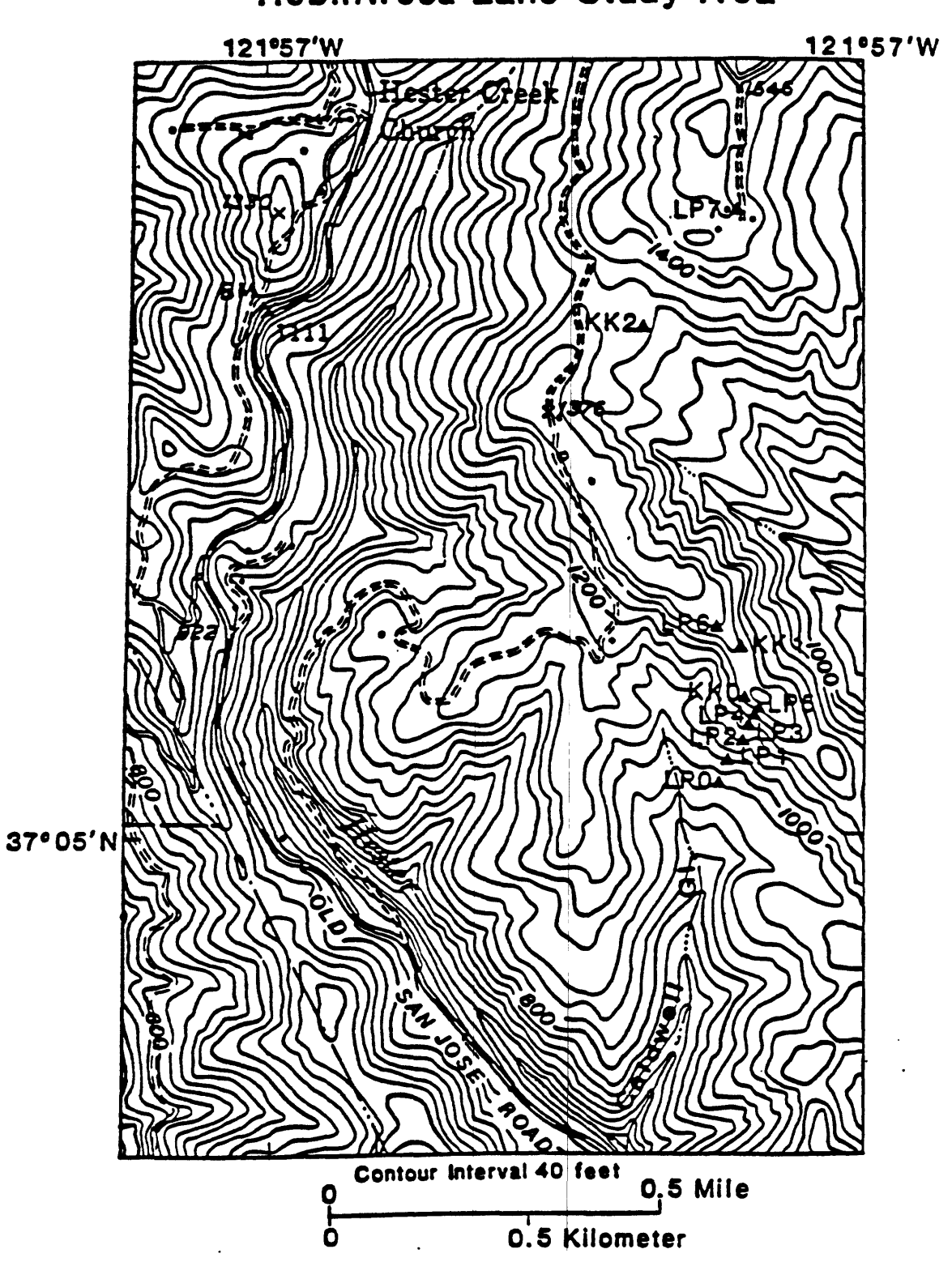

Figure 4.12. Map of Robinwood Lane study area seismograph array (from Ref. 4).

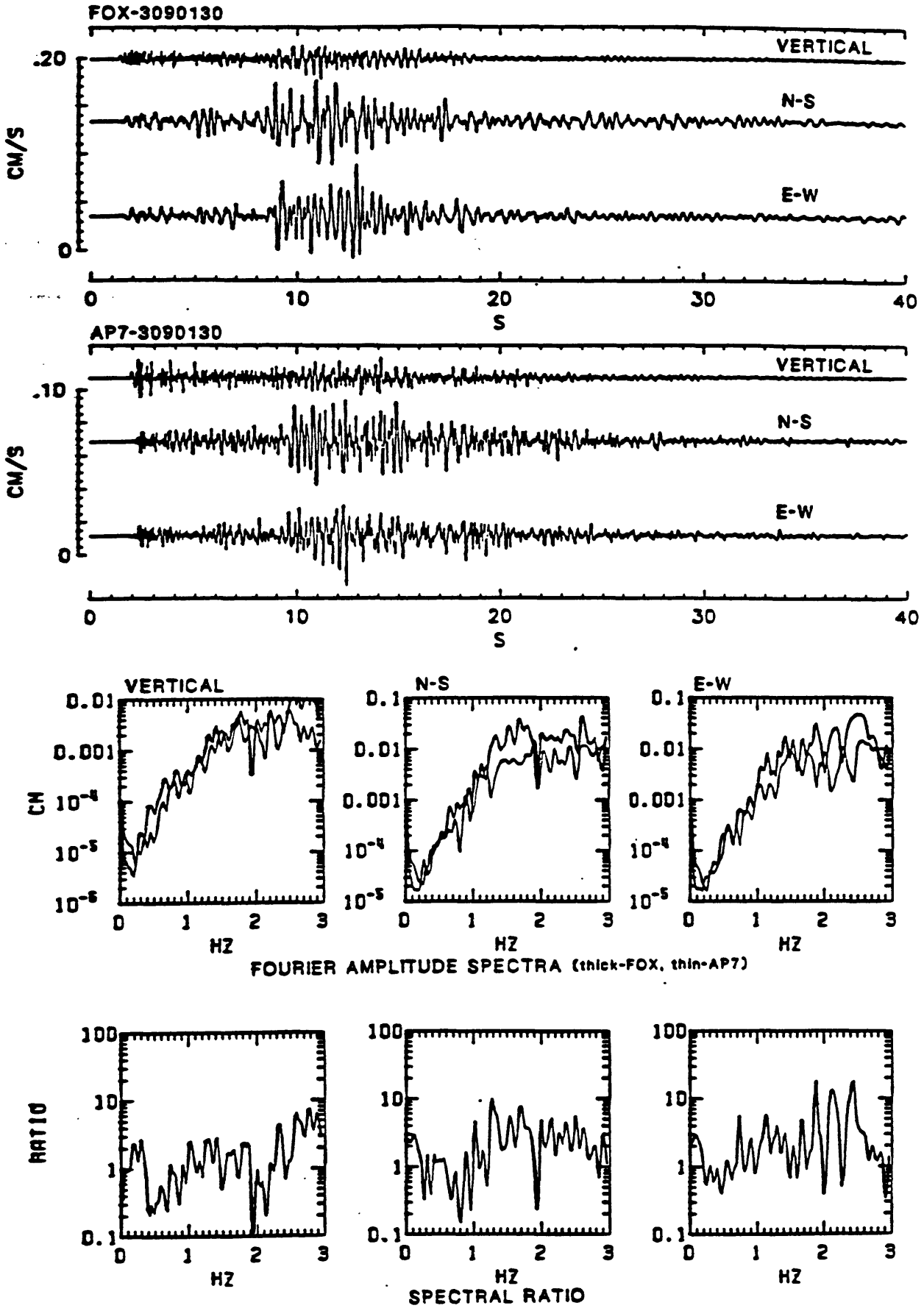

Figure 4.13. Event 3090310. The three-component velocity seismograms of FOX and AP7 as well as their Fourier amplitude spectra superimposed for each component and the spectral ratios (FOX/AP7). FOX is located on fill and bay mud (Qm).

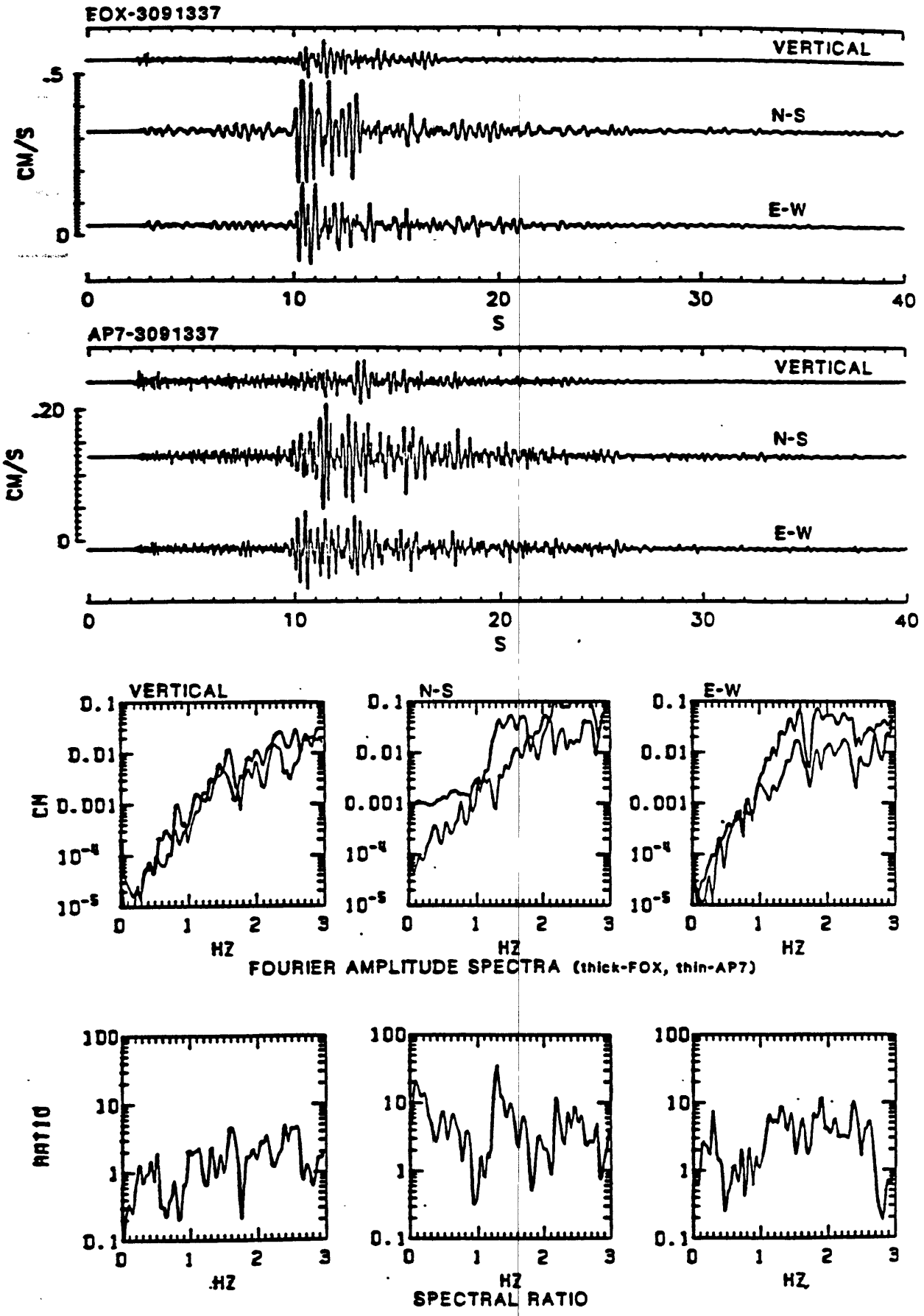

Figure 4.14. Event 3091337. The three-component velocity seismograms of FOX and AP7 as well as their Fourier amplitude spectra superimposed for each component and the spectral ratios (FOX/AP7). FOX is located on fill and bay mud (Qm).

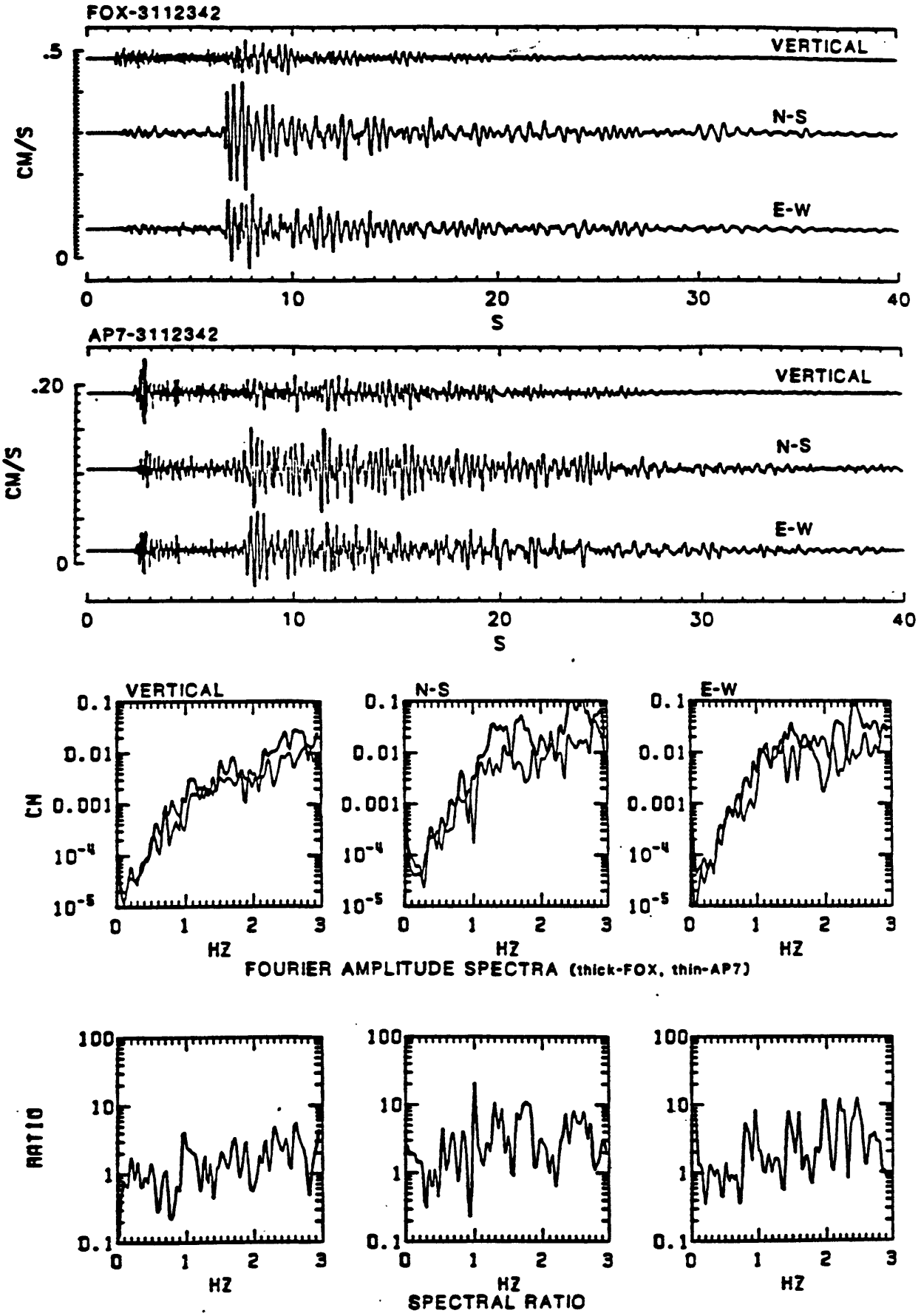

Figure 4.15. Event 3112342. The three-component velocity seismograms of FOX and AP7 as well as their Fourier amplitude spectra superimposed for each component and the spectral ratios (FOX/AP7). FOX is located on fill and bay mud (Qm).

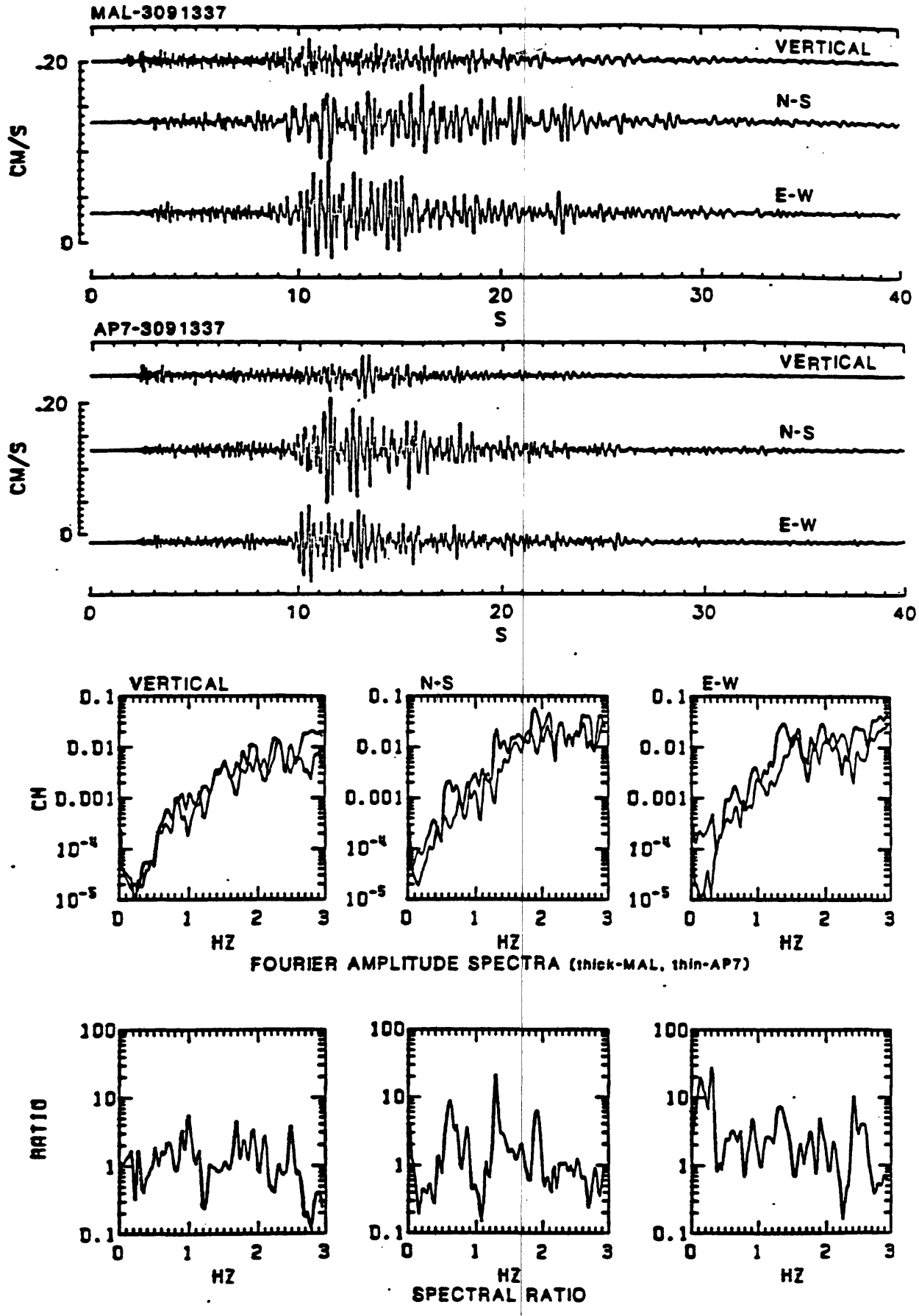

Figure 4.16. Event 3091337. The three-component velocity seismograms of MAL and AP7 as well as their Fourier amplitude spectra superimposed for each component and the spectral ratios (MAL/AP7). MAL is located on fill and bay mud (Qm).

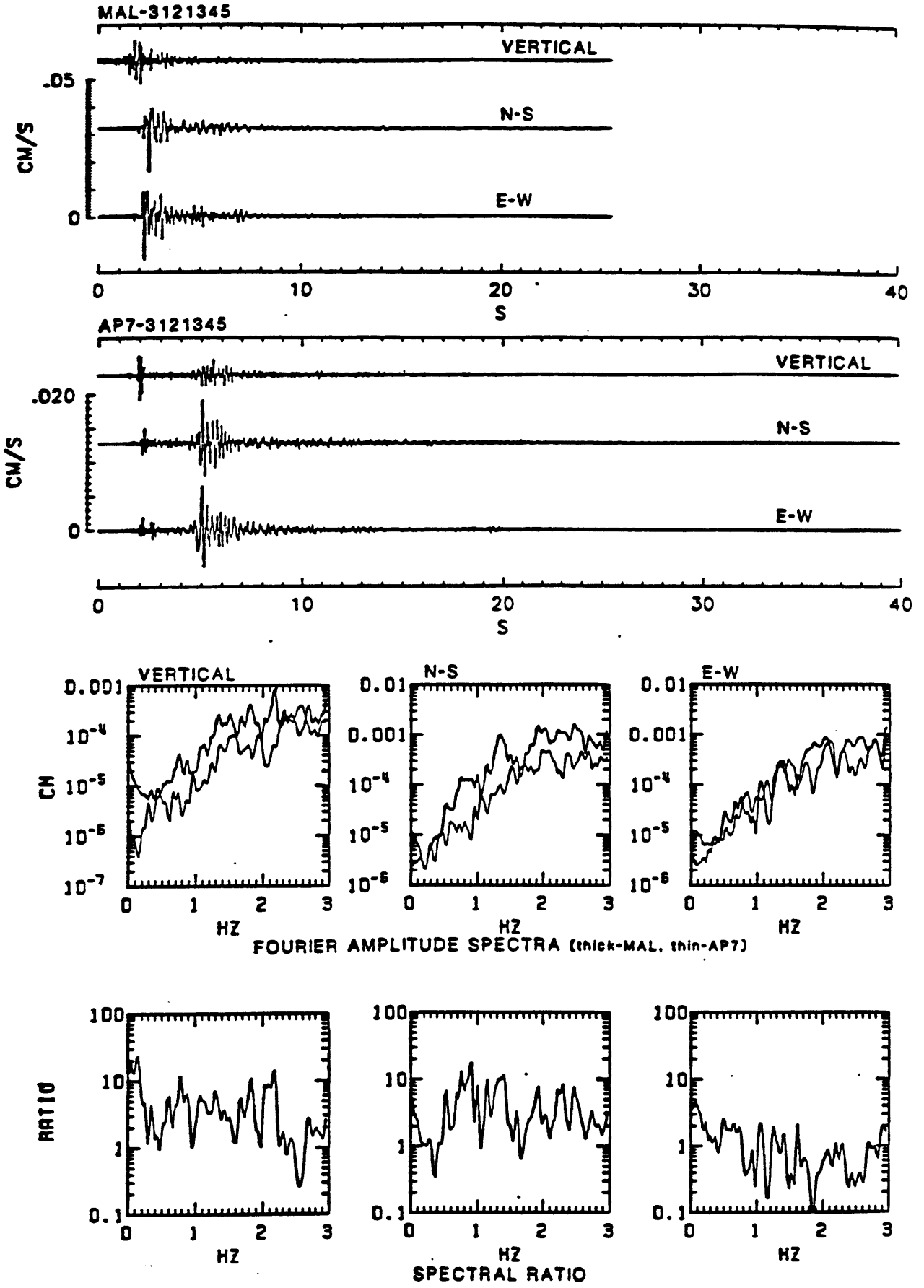

Figure 4.17. Event 3121345. The three-component velocity seismograms of MAL and AP7 as well as their Fourier amplitude spectra superimposed for each component and the spectral ratios (MAL/AP7). MAL is located on fill and bay mud (Qm).

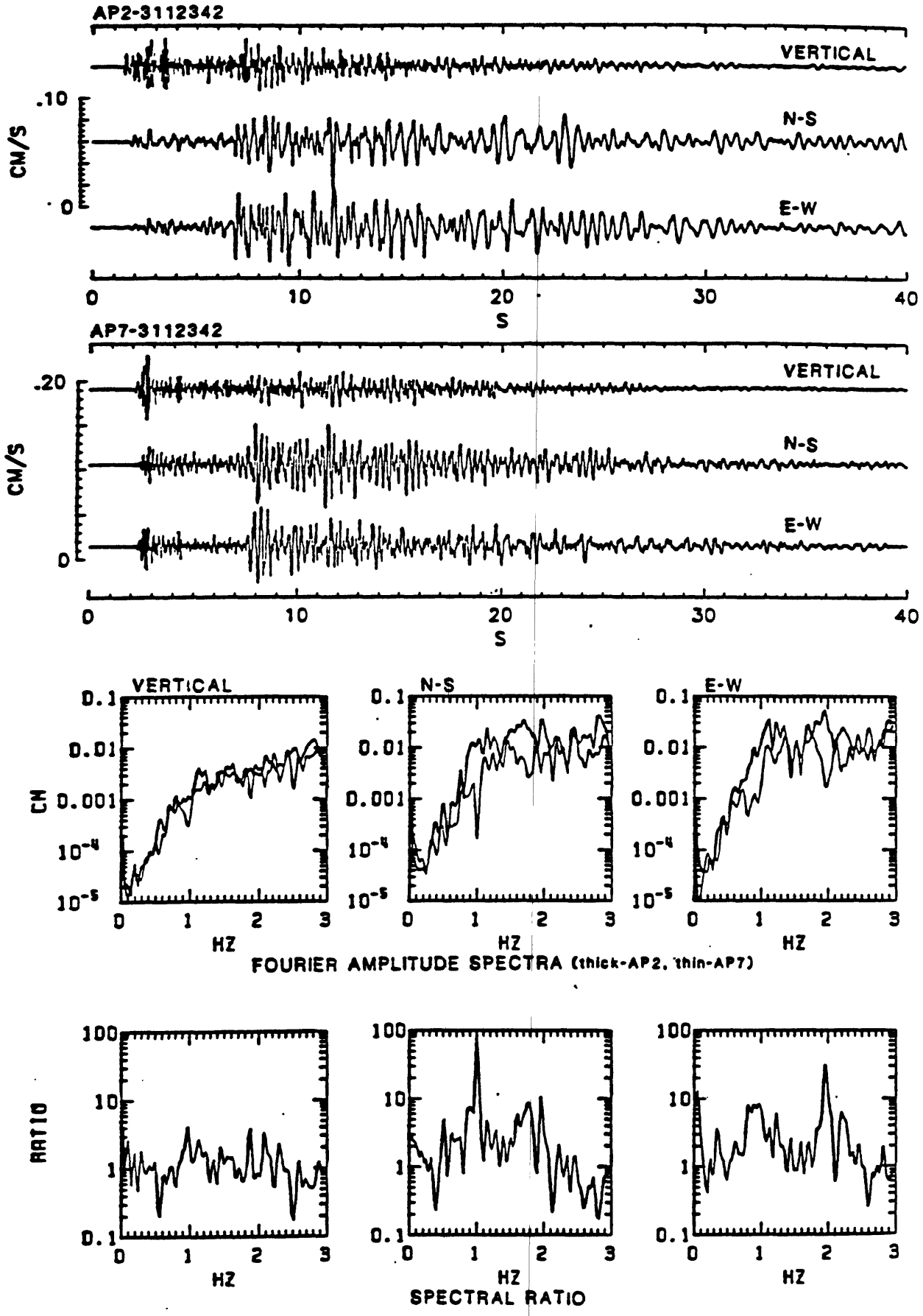

Figure 4.18. Event 3112342. The three-component velocity seismograms of AP2 and AP7 as well as their Fourier amplitude spectra superimposed for each component and the spectral ratios (AP2/AP7). AP2 is located on fill and bay mud (Qm).

5. COMPARATIVE OBSERVATION OF THE RESULTS FROM LONG-PERIOD MICROTREMOR AND EARTHQUAKE RECORDINGS

5.1 Comparison of Microtremors with Strong Motions

In section 2, it was shown that soil amplification for long-period microtremors exhibits systematic variation with site location, reflecting site geological setting. Frequency characteristics in amplification appear to depend not only on soil properties and depth to bedrock but also on configuration of bedrock. In section 3, soil amplifications determined from Loma Prieta strong motions and low-strain motions generated by distant explosions were discussed in terms of surface geology and surface shear-wave velocity. Average amplifications for strong motions are nearly the same as those for low-strain motions with the exception of sites where some liquefactions were suggested. They increase with decreasing mean shear-wave velocity. Overall characteristics of soil amplifications for microtremors and strong motions and their variation with geological units seem consistent to each other.

Table 5.1 compares means of average spectral ratios in the frequency band of 0.2–0.667 Hz (*i.e.*, 1.5–5 s) from microtremors (MT) and Loma Prieta strong motions (SM). Means are calculated using all sites in the Bay area. Averaged spectral ratios for MT in the Santa Clara Valley are taken from those calculated for the assumed attenuating wave field. Soil amplifications for SM are apparently larger than those for MT at sites on units Qal and Qm. The apparent discrepancy in mean amplification between SM and MT is attributable partly to the difference of site locations between SM and MT and consequently to the difference in depth to bedrock. As seen from Figure 4 in section 2, depth to bedrock should affect strongly on seismic amplification in the low frequency range.

Table 5.2 shows comparison of soil amplifications for SM and MT at the same sites. In this case, amplifications for SM are generally smaller than those for MT, especially at sites on unit Qm such as **MAL** and **RSH(RWS)**. However, at site **AP2** on unit Qm, where possible liquefaction is suggested during the Loma Prieta earthquake, the amplifications for SM are larger than those for MT.

The apparent reduction of amplification for SM shown in Table 5.2 should be attributed to the following factors: (1) Possibility of the difference in wave mode between earthquake ground motions and microtremors analyzed. The strong motion data used herein include both surface and S waves within a processing time-window of 40 seconds. Therefore, it is necessary to examine the similarity of site response due to S waves compared with that from surface waves. (2) Possibility of secondary-generated surface waves. It has been suggested that incident S waves produce surface waves at the boundary of sedimentary basin and the secondary-generated surface waves proagate and cause interference in the basin (Bard and Bouchon, 1984). Long durations with large amplitudes during the Loma Prieta earthquake at sites on unit Qal such as **SVL** (Borcherdt and Glassmoyer, 1990) might suggest the importance of the phenomena. In this connection, it is interesting to note that, in the aftershock records at alluvial sites in Santa Cruz (King *et al.*, 1990), there are remarkable later-phases following S phases, which might suggest the secondary

surface waves generated at the boundary. (3) Possible nonlinear effect of soil response. Possible nonlinear response associated with liquefaction at the **AP2** site is suggested from the difference in soil amplification between the Loma Prieta strong motions and the low-strain motions from explosions. At **AP2**, however, difference in amplification between SM and MT are contrary to the feature expected from nonlinear soil response. The evaluation of the nonlinear effects should be made for each wave group separately after decomposing the strong motion seismograms into various wave modes as mentioned above.

It is interesting to note similar studies performed for the Kyoto basin, Japan. Extensive long-period microtremor measurements were carried out for microzoning the basin. Comparative studies with earthquake ground motions have also been made to verify the applicability of microtremor measurement to microzoning. The strong motion event is the 1984 Western Nagano Prefecture earthquake ($M = 6.8$). The main results from comparative studies for different surface wave groups identified from earthquake and long-period microtremors are: Although peak frequencies and peak values of spectral ratios (ground site/rock site) from earthquake ground motions vary from event to event depending on the frequency contents of incident surface waves and directions of wave propagation, each peak value is similar to the spectral ratios determined from microtremors both in vertical and horizontal components (Akamatsu, 1984). In the case of the Western Nagano Prefecture earthquake, ratios of maximum amplitudes for band-pass filtered surface-wave seismograms exhibit similar amplification characteristics to those from microtremors, however, ratios for S-wave seismograms show the different frequency characteristics than those from surface waves and microtremors (Akamatsu *et al.*, 1991). These observations show the importance of decomposition of wave modes for evaluation of soil responses and limitations on applicability of microtremor measurements for mirozoning. However, this result is encouraging, because long-period components in strong motion seismograms are considered to be composed of surface waves (Mamura *et al.*, 1984).

5.2 Comparison of Microtremors with Aftershock Recordings

Comparative study of aftershock recordings (AS) versus microtremors (MT) are also made. Although extensive aftershock recordings are provided, six recordings obtained at sites on unit Qm in Foster City have so far been analyzed. At **FOX**, soil amplification for the horizontal components occurs in the frequeny range higher than 0.8 Hz, and 1.5 Hz resonance is suggested from MT. In this frequency range, large amplifications for AS are also observed (events 3090130, 3091337, and 3112342), although there are many other peaks. At **MAL**, soil amplification for horizontal MT occurs from 0.5 Hz and peaks around 0.6–1.0 Hz. These features are very similar to those of NS component for AS (events 3091337 and 3121345), whereas EW amplifications show different characteristics. At **AP2**, horizontal amplification for MT increases from 0.7 Hz to 1.0 Hz rapidly. Spectral ratios of AS have peaks around 1.0 Hz both in NS and EW components, showing the similar amplification characteristics to those for MS. The processing time-window for AS include P-, S- and surface-wave groups, which could cause additional peaks when compared

with those determined by MT. In general terms, however, frequency characteristics of soil amplifications determined from AS in the frequency range of 0.5–1.5 Hz appear similar to those from MT at these sites. Since the frequency contents of AS are weak in this low frequency range and microtremor measurements are focused on the frequency range lower than 1 Hz, direct comparison should be made carefully with a larger data set.

From microtremor measurements directional soil amplifications are observed in the marginal area in the sedimentary basin/valley. This is considered very important for engineering seismology and earthquake engineering, because directional site responses were observed from the 1989 Loma Prieta earthquake (Borcherdt and Glassmoyer, 1990) and the 1987 Whittier Narrows earthquake and its aftershock (Vidale *et al.*, 1991).

REFERENCES

Akamatsu, J. (1984). Seismic amplification by soil deposits inferred from vibrational characteristics of microseisms, *Bull. Disas. Prev. Res. Inst.*, Kyoto Univ., **34**, 105–127.

Akamatsu, J., M. Fujita, and K. Nishimura (1991). Vibrational characteristics of microseisms and their applicability to microzoning in a sedimentary basin, *J. Phys. Earth,* in press.

Bard, P. Y. and M. Bouchon (1984). The two-dimensional response of sediment-filled valley, *Bull. Seism. Soc. Am.*, **75**, 519–541.

Borcherdt, R. D. and G. Glassmoyer (1990). On the influence of local geologic deposits and crustal structure on ground motions generated by the Loma Prieta earthquake in the San Francisco Bay region, California, *Bull. Seism. Soc. Am.*, submitted.

King, K., D. Carver, R. Williams, D. Worley, E. Cranswick, and M. Meremonte (1990). Santa Cruz seismic investigations following the October 17, 1989 Loma Prieta earthquake, *U.S. Geol. Surv. Open-File Rep.* **90–307**.

Mamura, L., K. Kudo, and E. Shima (1984). Distribution of ground-motion amplification factors as a function of period (3–15 sec), in Japan, *Bull. Earthq. Res. Inst.*, Univ. of Tokyo, **59**, 467–500.

Vidale, J. E., O. Bonamassa, and H. Houston (1991). Directional site resonances observed from the 1 October 1987 Whittier Narrows, California, earthquake and the 4 October aftershock, *Earthq. Spectra*, **7**, 107–125.

Table 5.1 Comparison of soil amplifications for the Loma Prieta strong motions (SM) and microtremors (MT) in the Bay area. The values are means of averaged spectral ratios for the frequency band of 0.2 - 0.667 Hz (i.e. 1.5 - 5 s). The values for MT in the Santa Clara Valley are from those for the attenuating wave field.

		UD	Radial/N40W	Transverse/N50E	Sites
Qal	SM	1.56±0.57	2.84±1.84	1.83±1.03	HWB OOF FRE MSJ MUR SVL ASH
	MT	0.97±0.22	1.75±0.86	1.85±1.15	SYL CHE OT2 SNV AGN SJ1
Qm	SM	1.70±1.72	4.49±2.98	4.09±2.70	EMT OHW SF1 MAL AP2 TRI RSH
	MT	1.02±0.30	2.86±1.66	2.22±1.29	OTA FOX AP2 ARG CHA MAL LON RWS

Table 5.2 Comparison of soil amplifications for the Loma Prieta strong motions (SM) and microtremors (MT) at the same sites in the Bay area. The values are averaged spectral ratios for the frequency band of 0.2 - 0.667 Hz (i.e. 1.5 - 5 s). The values for MT in the Santa Clara Valley are from those for the attenuating wave field.

		Site	UD	Radial/N40W	Transverse/N50E
Qal	SM	SNV	2.05	3.43	1.99
	MT	SNV	0.92	1.78	3.33
	SM/MT		2.23	1.93	0.60
	SM	ASH	1.47	1.81	1.32
	MT	AGN	0.70	2.13	2.33
	SM/MT		2.10	0.85	0.57
Qm	SM	AP2	0.78	1.67	2.13
	MT	AP2	0.81	1.18	0.88
	SM/MT		0.96	1.42	2.42
	SM	MAL	1.00	2.44	1.75
	MT	MAL	1.28	4.43	3.55
	SM/MT		0.78	0.55	0.49
	SM	RSH	0.99	4.32	3.29
	MT	RWS	1.66	5.71	6.52
	SM/MT		0.60	0.76	0.50

6. CONCLUSIONS

The objective of this study was to compile field data recordings of long-period microtremors in the San Francisco Bay area and Santa Cruz, the areas affected by the Loma Prieta earthquake of October 17, 1989 ($M_s = 7.1$). The data set was recorded with long-period seismometers at 38 locations. In all cases, reference rock sites were used to calculate spectral ratios. Such results from microtremors have been compared with those spectral ratios calculated from the main event strong motion records and aftershock records whenever applicable.

The results permit us to make the following conclusions:

1) Microtremor measurements are useful in identifying significant frequency bands of low-frequency surface waves that cause amplification of soft soil sites.

2) The frequency bands of low-frequency strong motions contain contributions from both S-waves and surface waves. Only spectral ratios from those portions due to surface waves compare well with those from microtremor measurements.

3) Low amplification in the low-frequency region in the Santa Cruz area compared to Peninsula cities and Santa Clara Valley is attributable to the shallow depth to bedrock and small dimension of geography as well.

4) The study confirms once again that all other conditions are the same, depth to bedrock and the geological material usually defined by shear-wave velocities are key variables in defining the frequency bands of resonance (and therefore amplification).

5) Directional amplification demonstrated for strong motion recordings of the Loma Prieta earthquake is once again demonstrated for the microtremor measurement in this study.

6) Difference in amplification calculated from strong motions and from microtremors is attributed to difference in wave modes, generation of secondary surface waves and possible nonlinear soil effects. The nonlinear soil effects should be carefully evaluated for same wave groups.

7) We have accumulated experiences in the United States and in Japan. In order to extrapolate to other areas without strong motion data, we should establish the reliability of the method.

Appendix

Velocity seismograms, amplitude spectra and spectral ratios (soil site/rock site) of microtremors at each site are shown.

Peninsula Cities

Santa Clara Valley

Santa Cruz City

Geologic Unit:

- KJf = Cretaceous and Jurassic Franciscan assemblage
- TMzs = Tertiary and Mesozoic sedimentary rocks
- QTs = Quaternary and Tertiary sedimentary rocks
- Qal = Quaternary alluvium
- Qm = Holocene estuarine mud (fill on bay mud)
- sch = Metasedimentary rocks
- m = Marble
- Qt = Marine terrace deposits

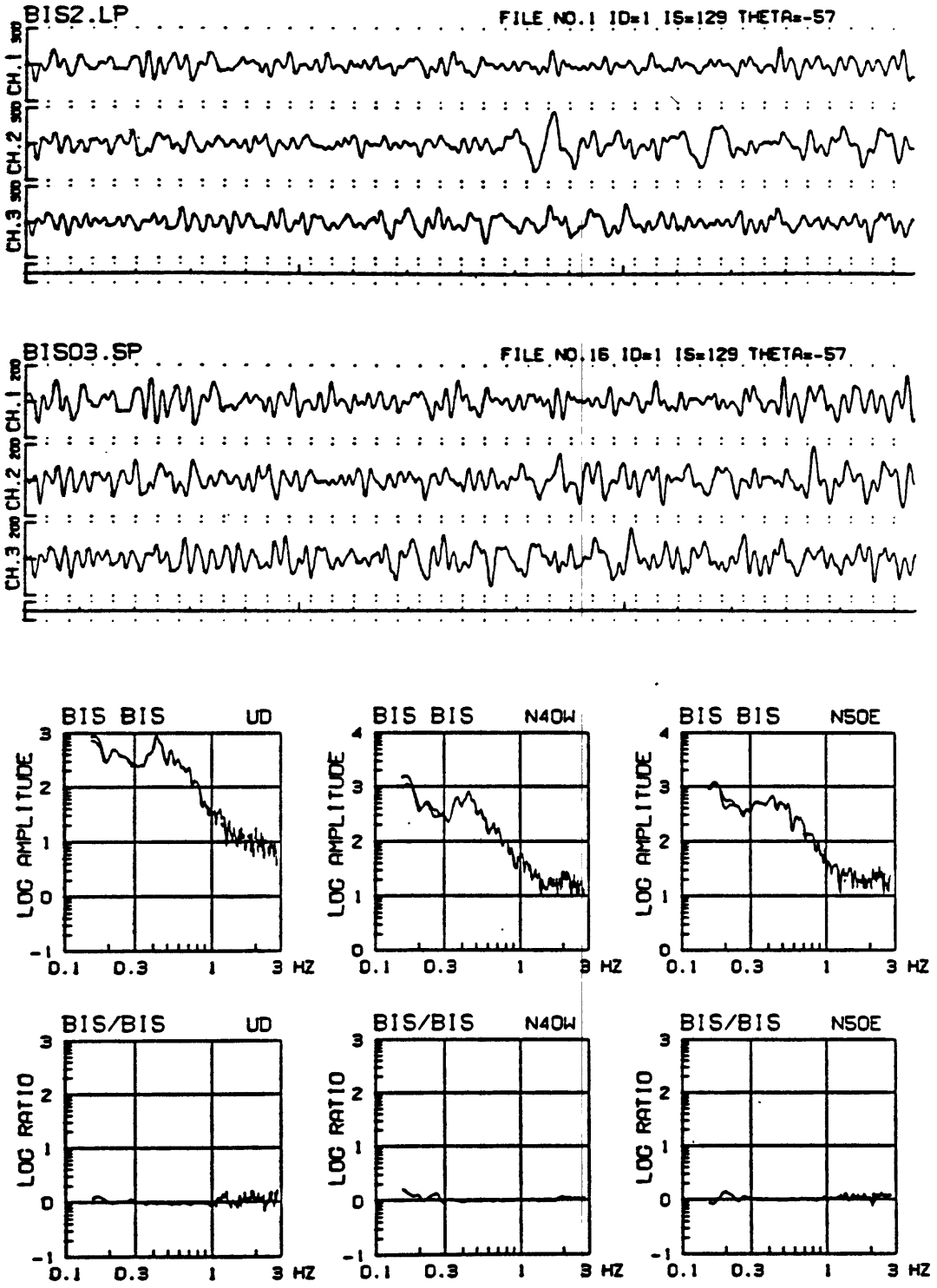

Fig. A.1 Velocity seismograms at **BIS**, amplitude spectra and their ratios (LP system/SP system), showing the same responses of the two systems. Seismogram scale is in 10^{-8} m/s and spectra in 10^{-8} m. **BIS** is the Franciscan assemblage (KJf).

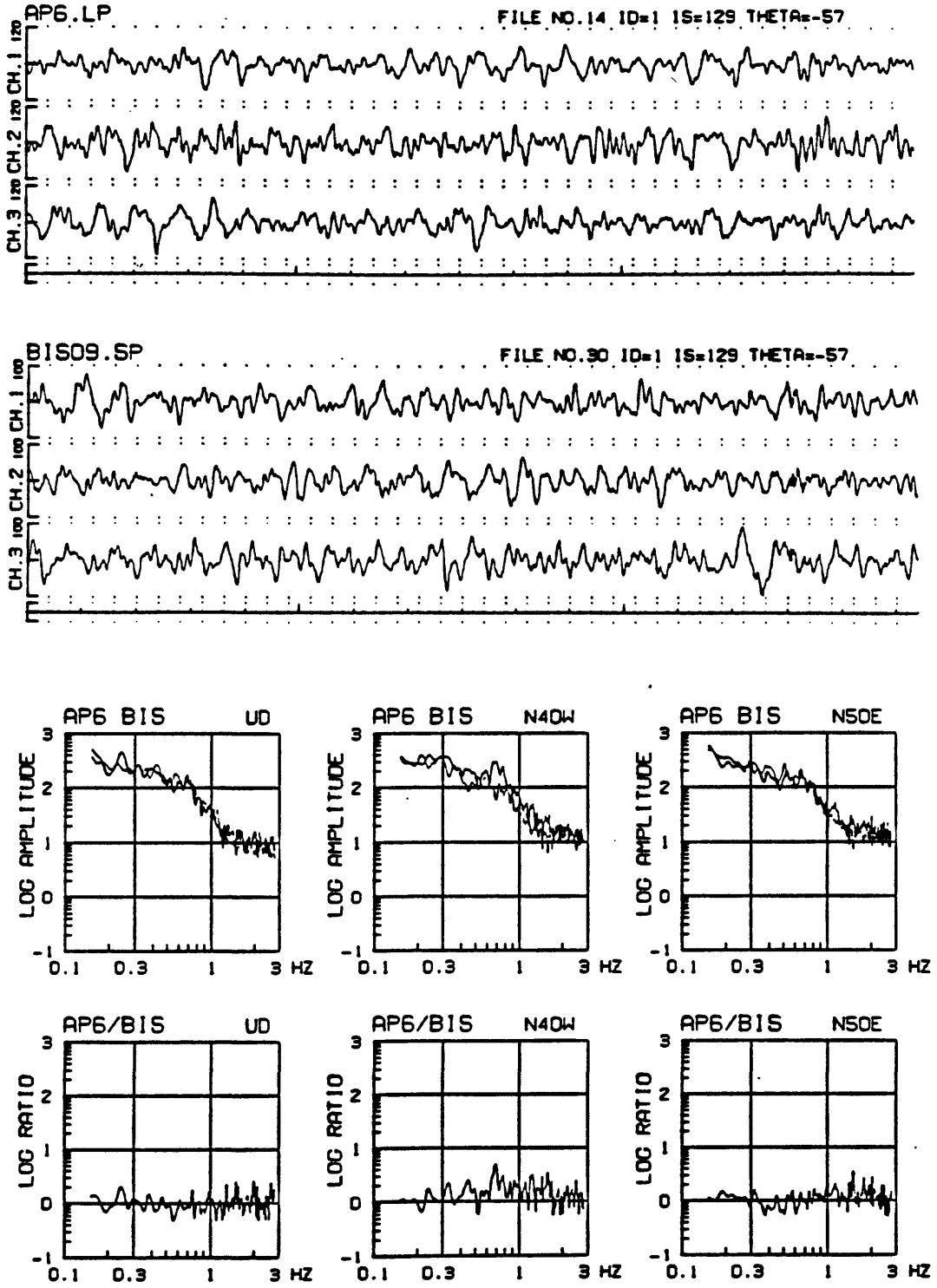

Fig. A.2 Velocity seismograms at **AP6** and **BIS**, amplitude spectra and their ratios (**AP6/BIS**). Seismogram scale is in 10^{-8} m/s and spectra in 10^{-8} m. Horizontal components are rotated to longitudinal and transverse directions to the general trend of geological divisions. **AP6** is the Franciscan assemblage (KJf).

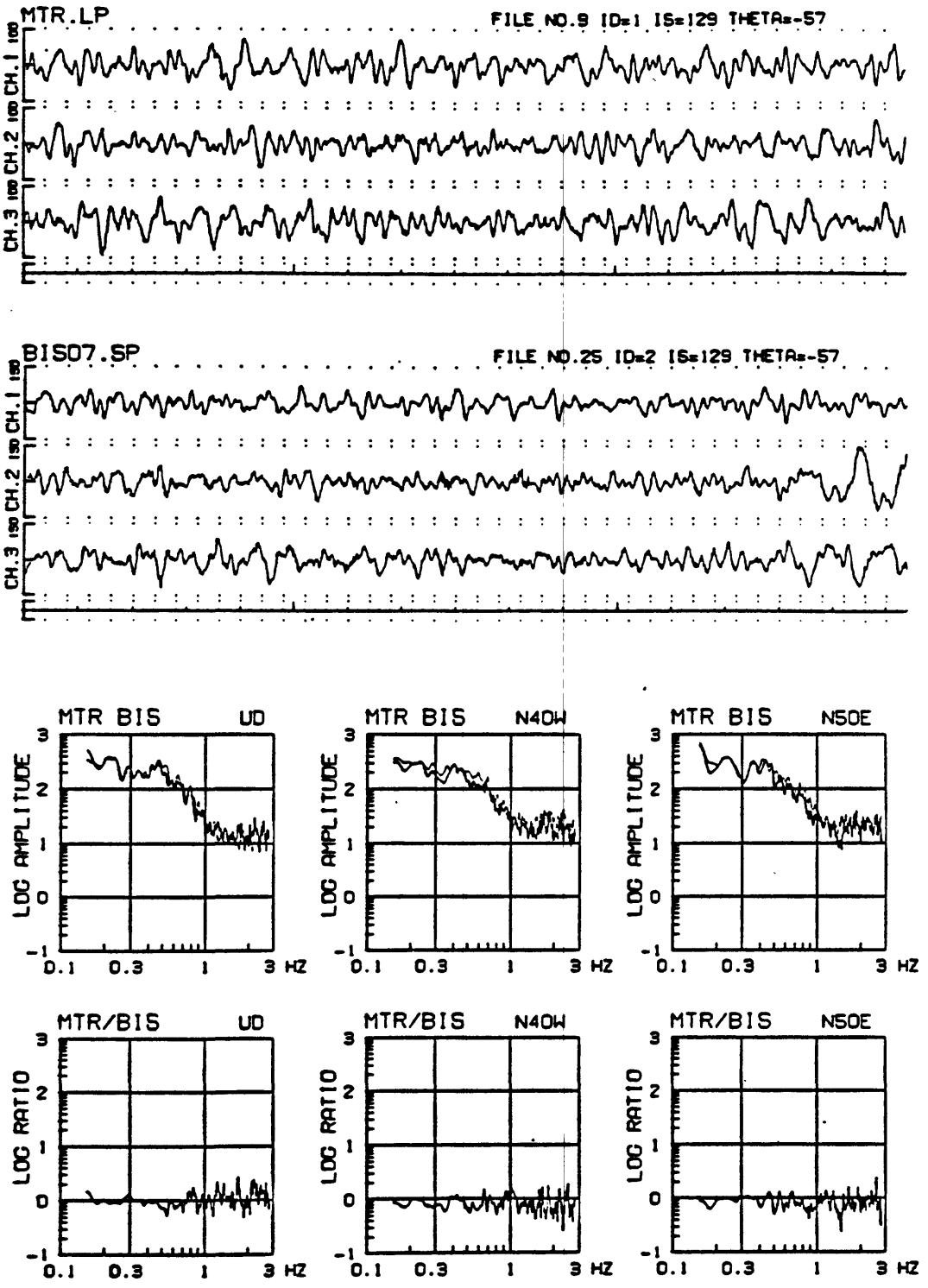

Fig. A.3 Velocity seismograms at **MTR** and **BIS**, amplitude spectra and their ratios (**MTR/BIS**). Seismogram scale is in 10^{-8} m/s and spectra in 10^{-8} m. Horizontal components are rotated to longitudinal and transverse directions to the general trend of geological divisions. **MTR** is the Franciscan assemblage (KJf).

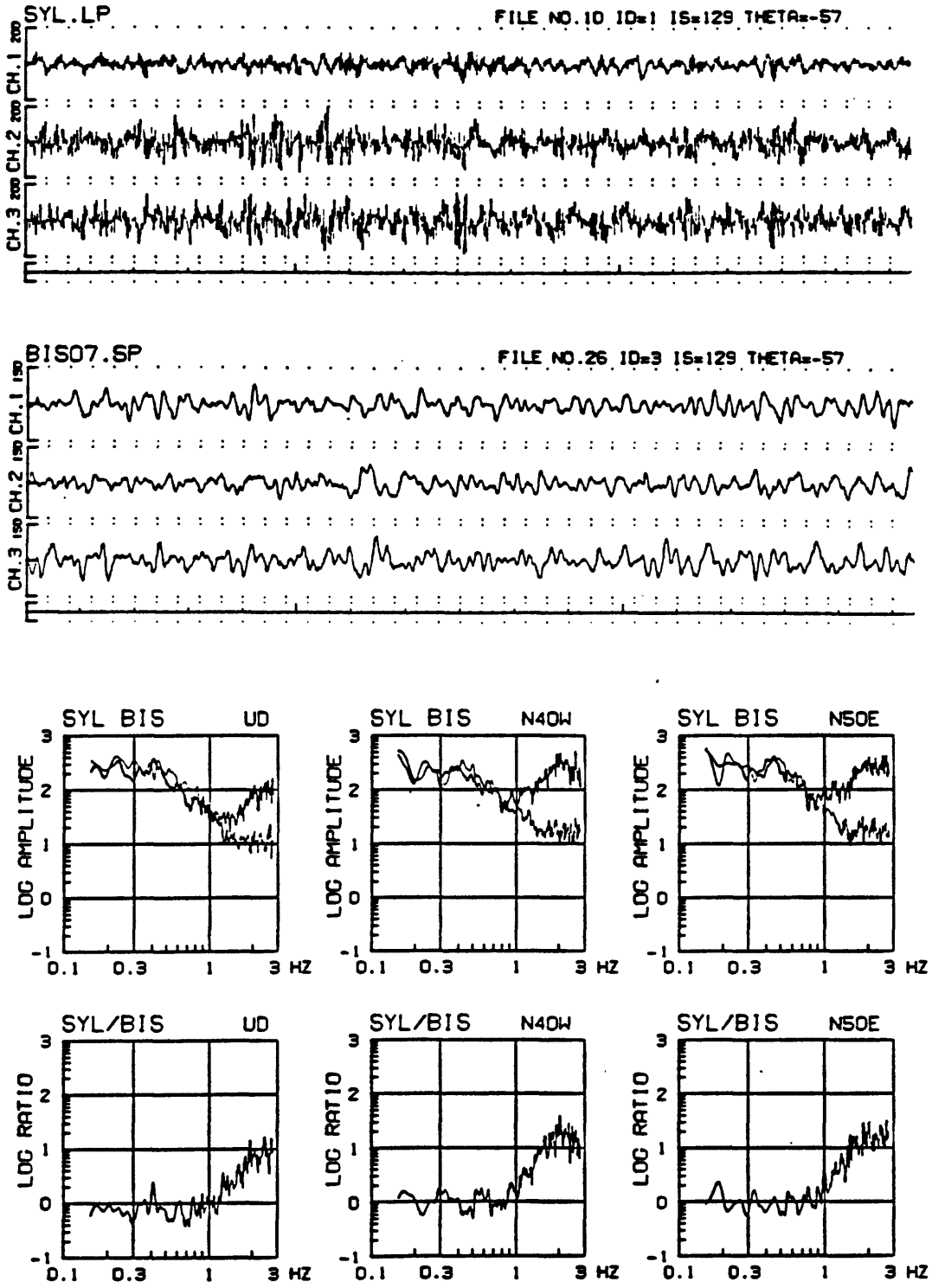

Fig. A.4 Velocity seismograms at **SYL** and **BIS**, amplitude spectra and their ratios (**SYL/BIS**). Seismogram scale is in 10^{-8} m/s and spectra in 10^{-8} m. Horizontal components are rotated to longitudinal and transverse directions to the general trend of geological divisions. **SYL** is alluvium (Qal).

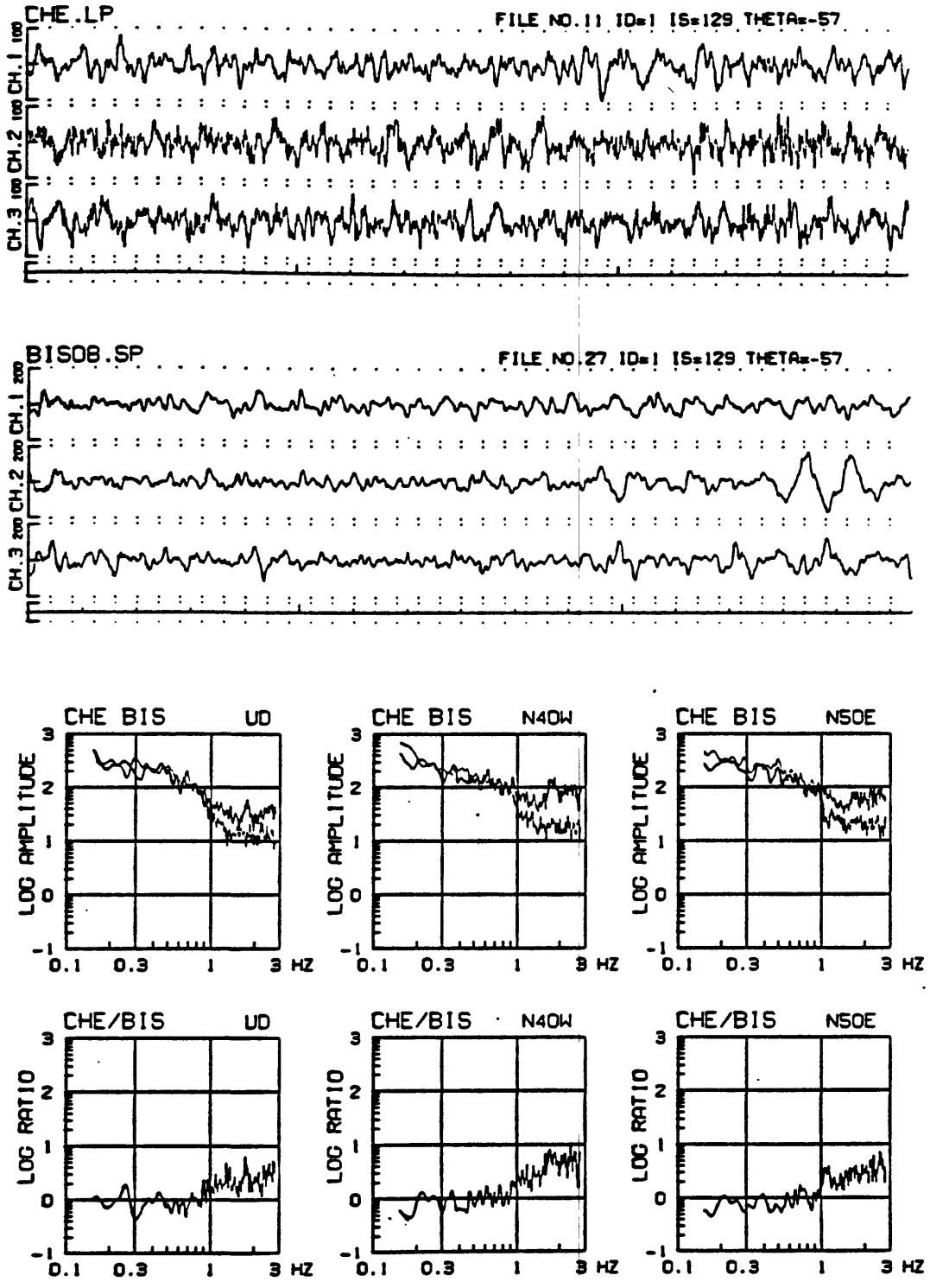

Fig. A.5 Velocity seismograms at **CHE** and **BIS**, amplitude spectra and their ratios (**CHE/BIS**). Seismogram scale is in 10^{-8} m/s and spectra in 10^{-8} m. Horizontal components are rotated to longitudinal and transverse directions to the general trend of geological divisions. **CHE** is alluvium (Qal).

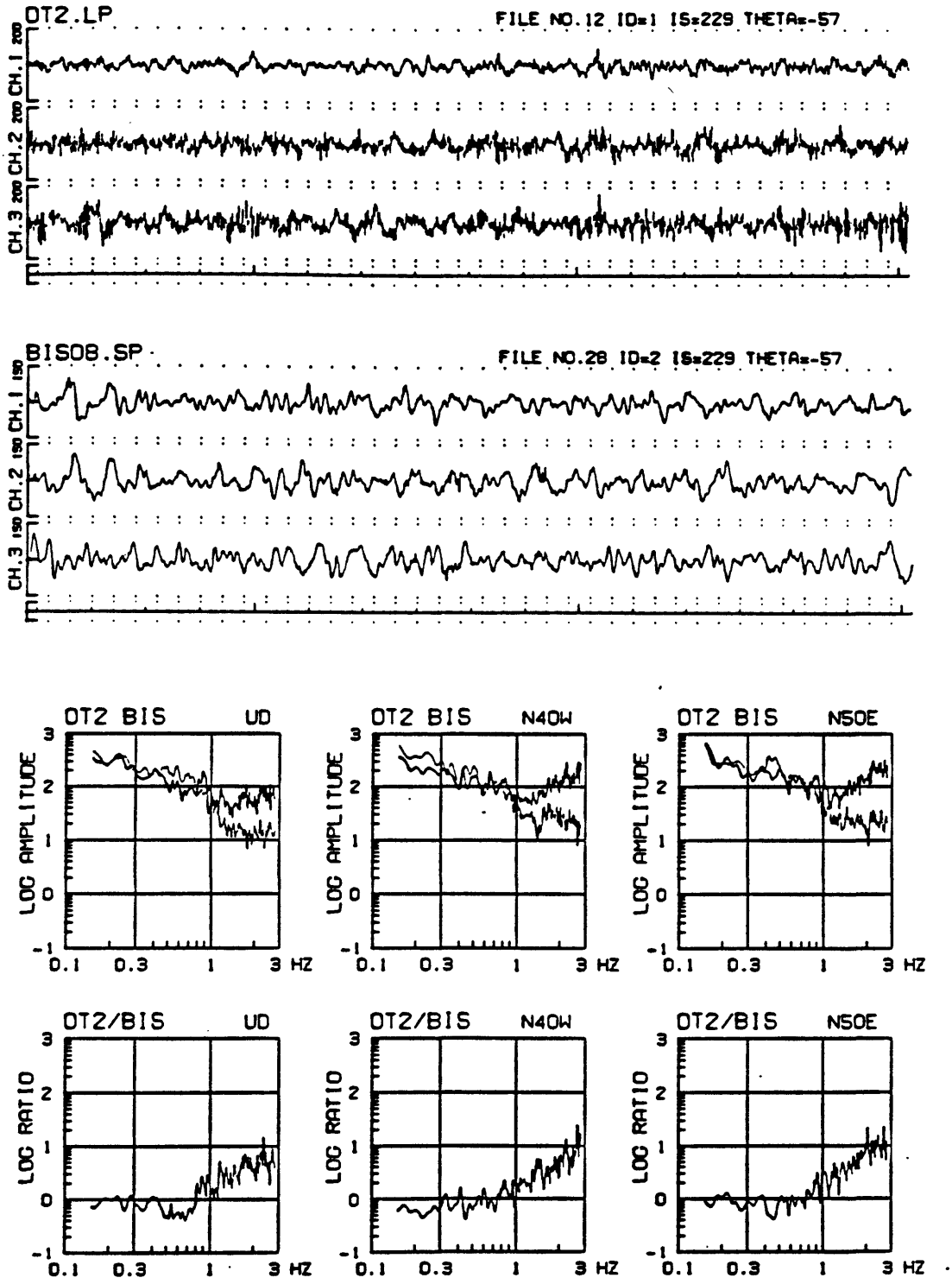

Fig. A.6 Velocity seismograms at **OT2** and **BIS**, amplitude spectra and their ratios (**OT2/BIS**). Seismogram scale is in 10^{-8} m/s and spectra in 10^{-8} m. Horizontal components are rotated to longitudinal and transverse directions to the general trend of geological divisions. **OT2** is alluvium (Qal).

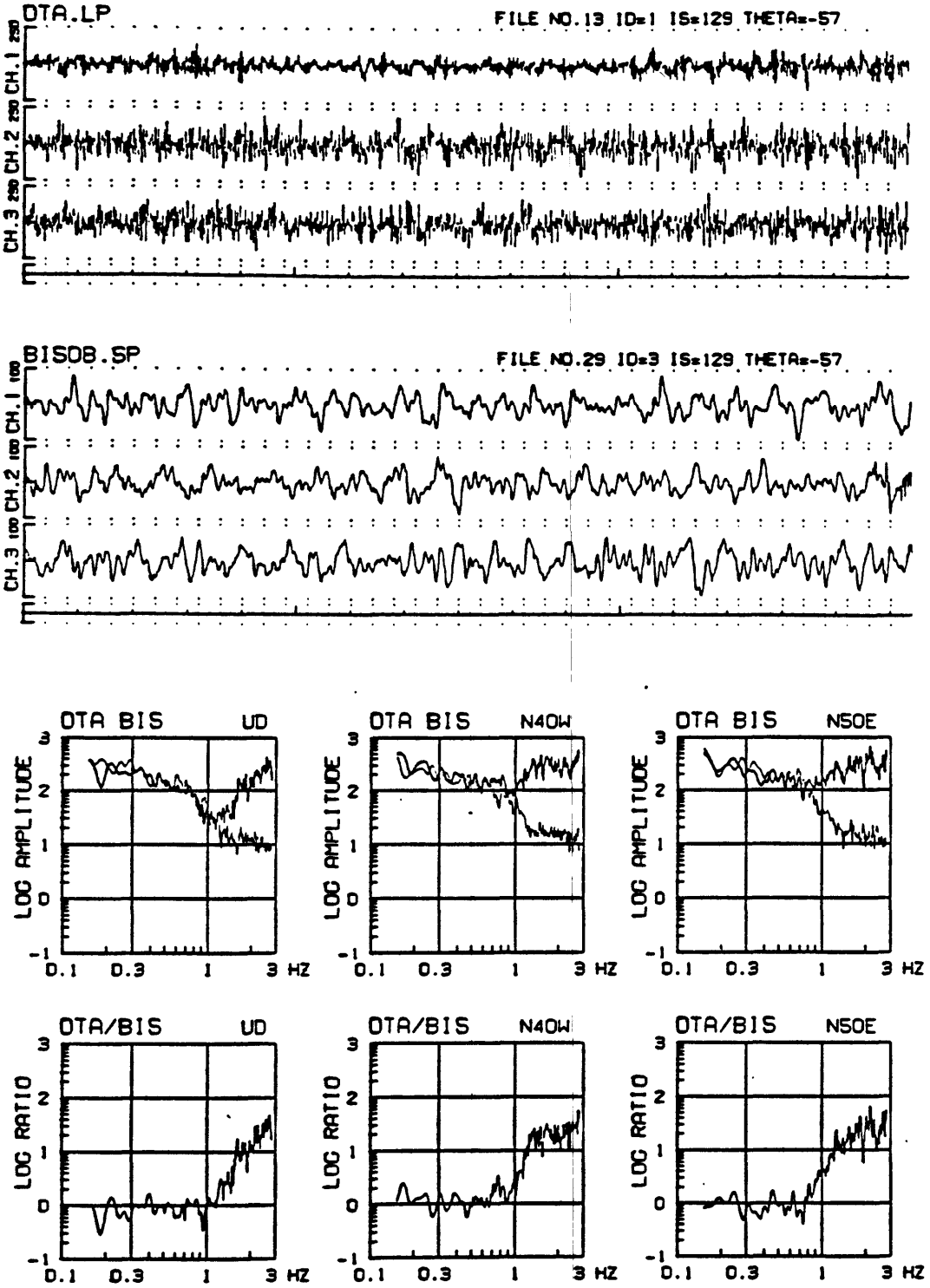

Fig. A.7 Velocity seismograms at **OTA** and **BIS**, amplitude spectra and their ratios (**OTA/BIS**). Seismogram scale is in 10^{-8} m/s and spectra in 10^{-8} m. Horizontal components are rotated to longitudinal and transverse directions to the general trend of geological divisions. **OTA** is located on fill and bay mud (Qm).

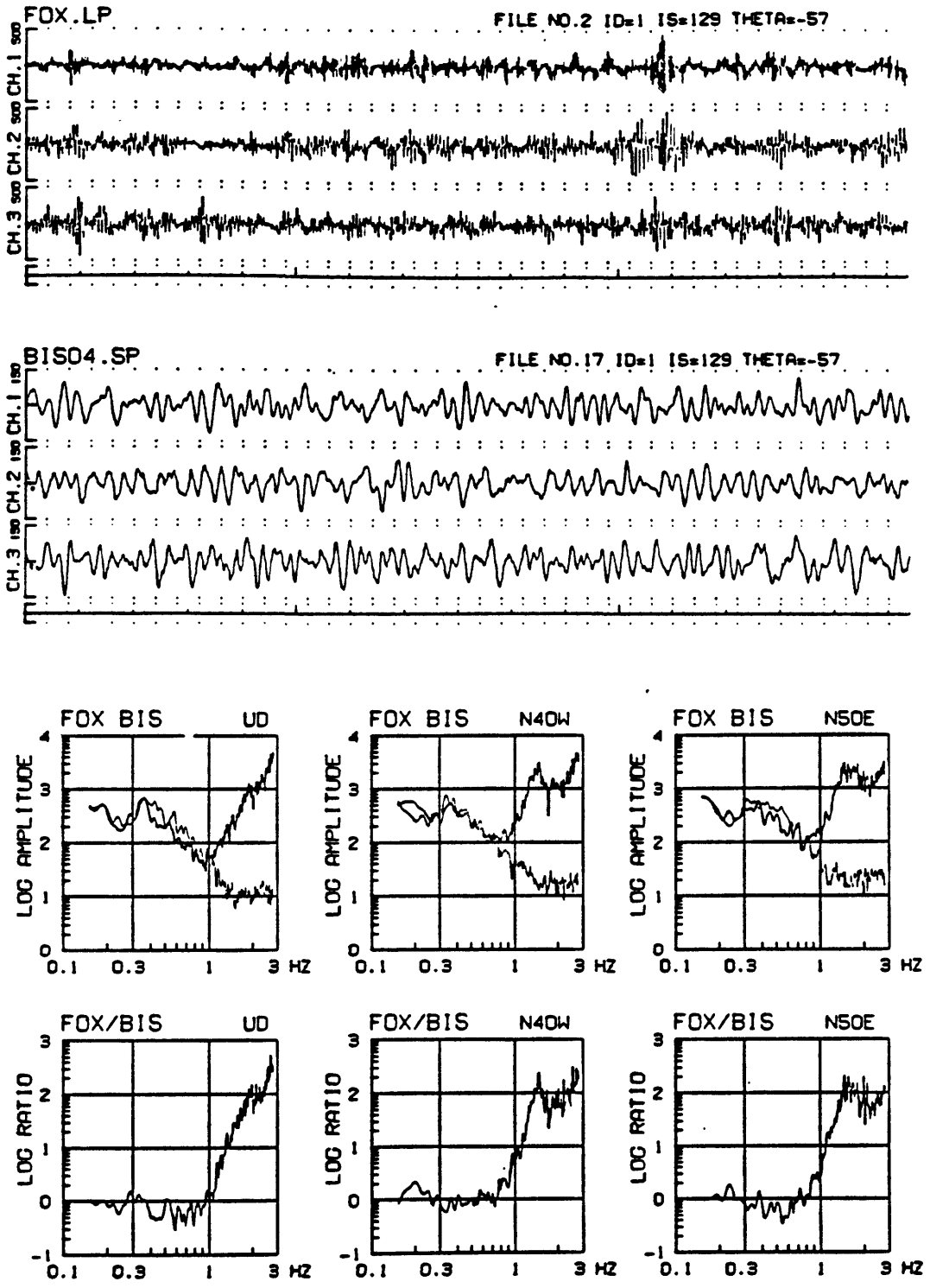

Fig. A.8 Velocity seismograms at **FOX** and **BIS**, amplitude spectra and their ratios (**FOX/BIS**). Seismogram scale is in 10^{-8} m/s and spectra in 10^{-8} m. Horizontal components are rotated to longitudinal and transverse directions to the general trend of geological divisions. **FOX** is located on fill and bay mud (Qm).

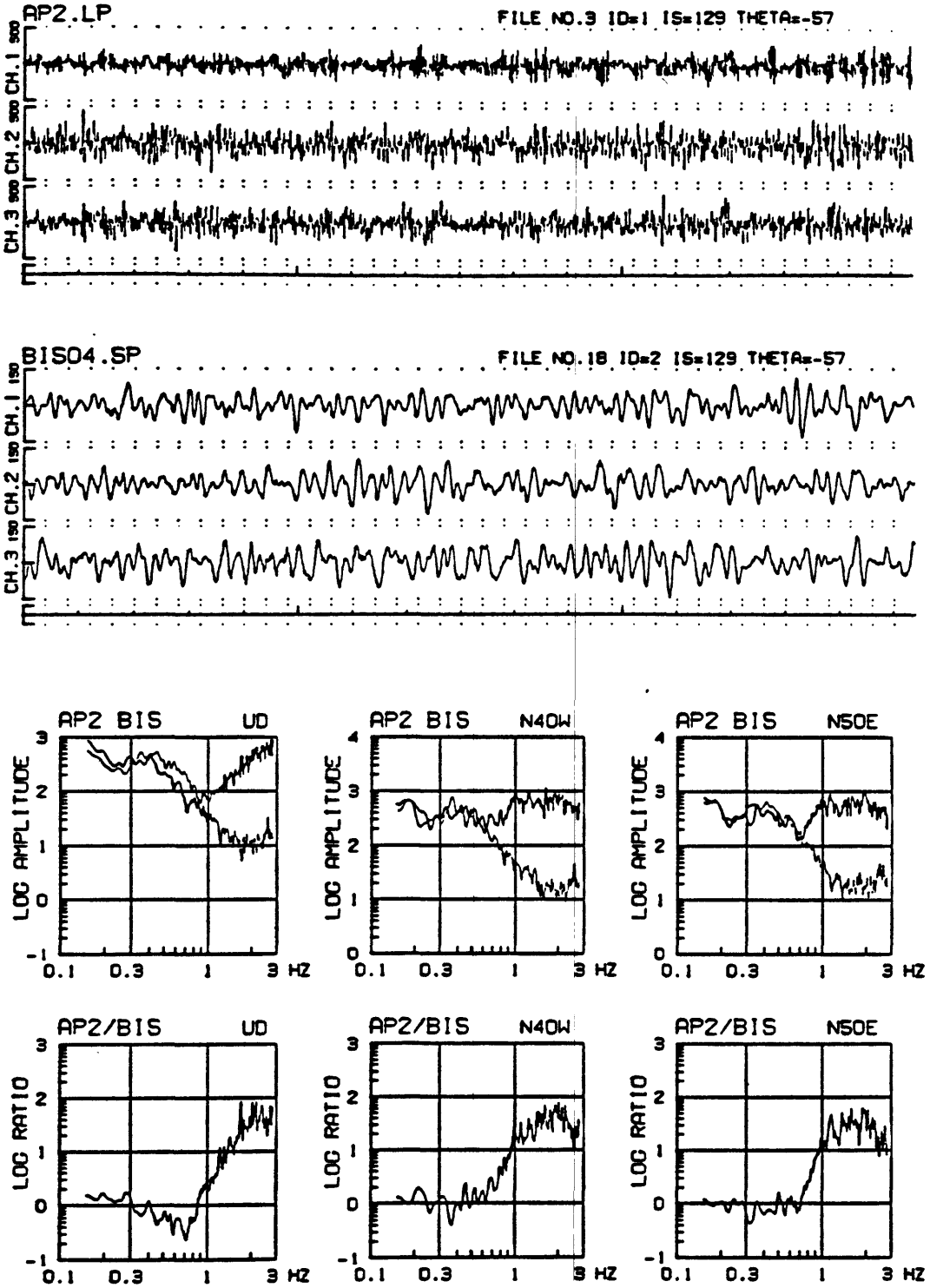

Fig. A.9 Velocity seismograms at **AP2** and **BIS**, amplitude spectra and their ratios (**AP2/BIS**). Seismogram scale is in 10^{-8} m/s and spectra in 10^{-8} m. Horizontal components are rotated to longitudinal and transverse directions to the general trend of geological divisions. **AP2** is located on fill and bay mud (Qm).

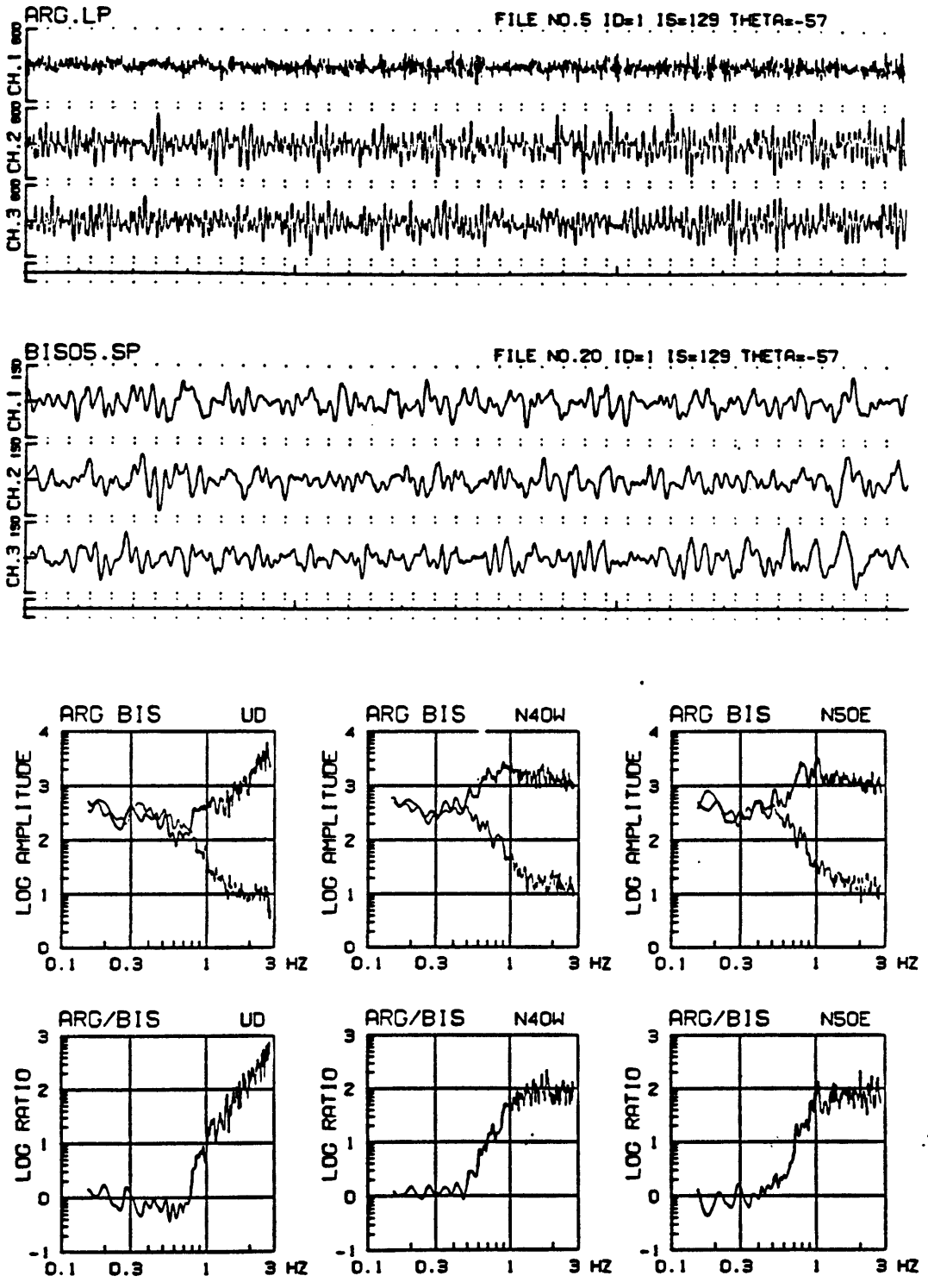

Fig. A.10 Velocity seismograms at **ARG** and **BIS**, amplitude spectra and their ratios (**ARG/BIS**). Seismogram scale is in 10^{-8} m/s and spectra in 10^{-8} m. Horizontal components are rotated to longitudinal and transverse directions to the general trend of geological divisions. **ARG** is located on fill and bay mud (Qm).

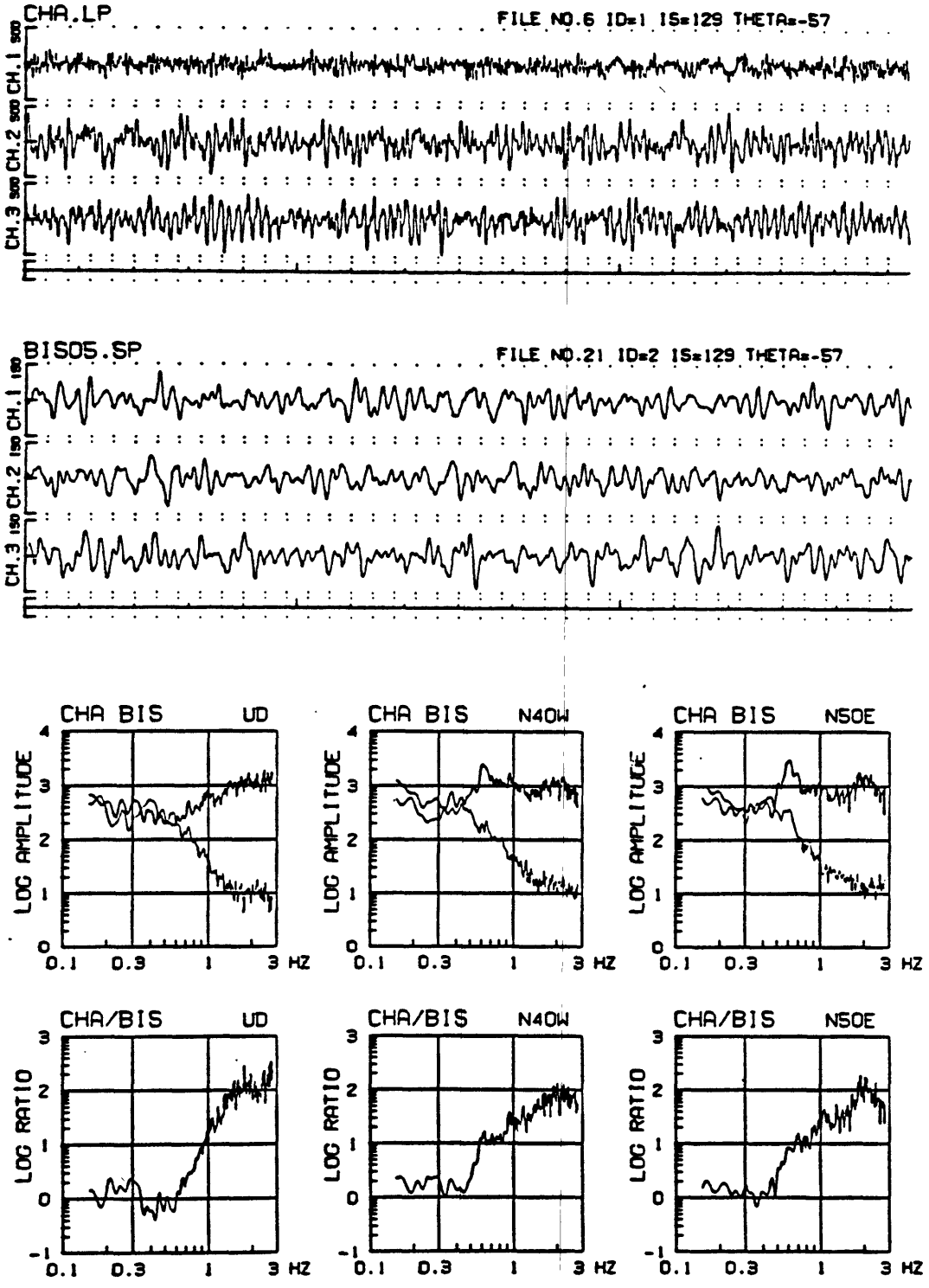

Fig. A.11 Velocity seismograms at **CHA** and **BIS**, amplitude spectra and their ratios (**CHA/BIS**). Seismogram scale is in 10^{-8} m/s and spectra in 10^{-8} m. Horizontal components are rotated to longitudinal and transverse directions to the general trend of geological divisions. **CHA** is located on fill and bay mud (Qm).

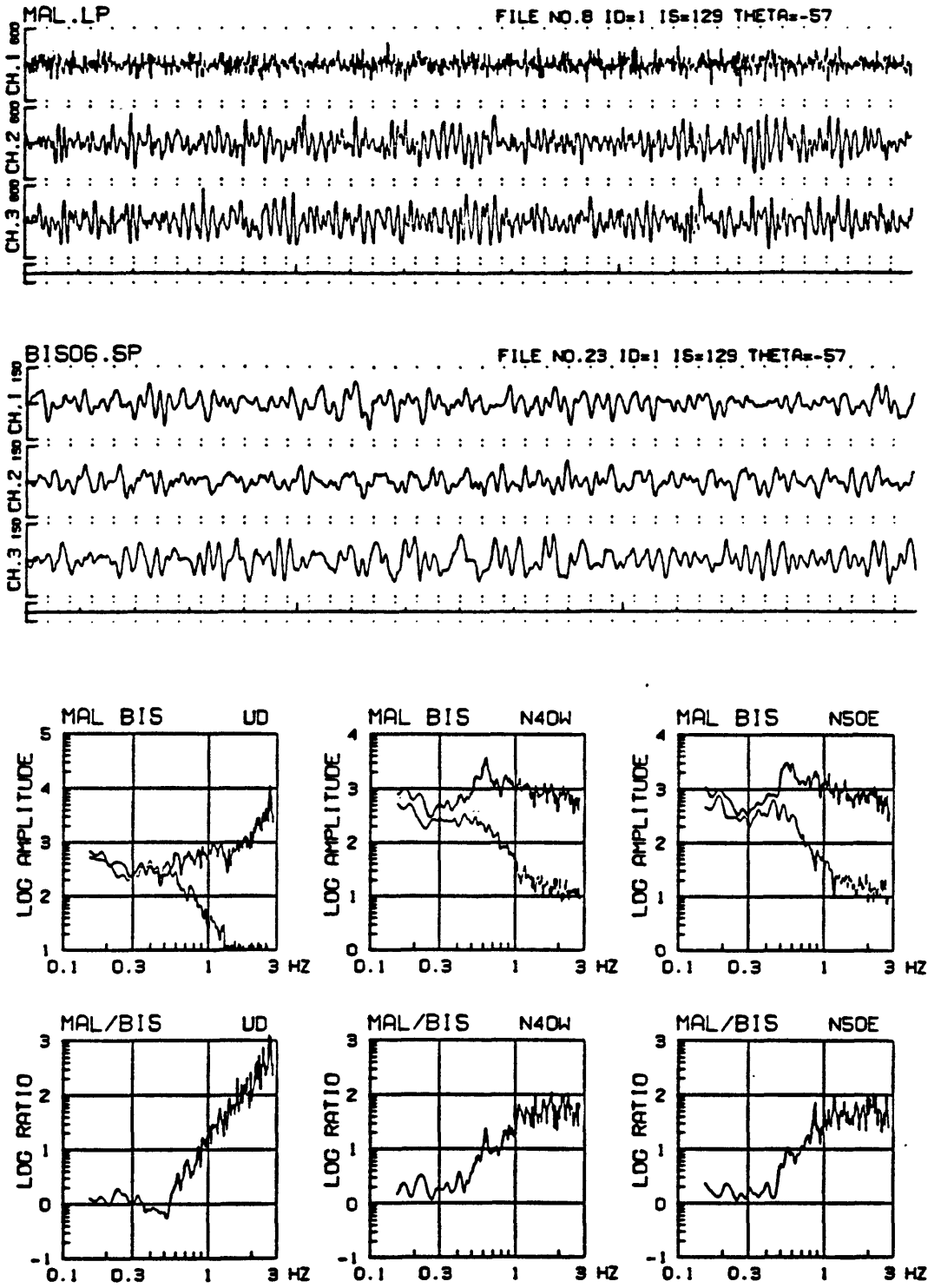

Fig. A.12 Velocity seismograms at **MAL** and **BIS**, amplitude spectra and their ratios (**MAL/BIS**). Seismogram scale is in 10^{-8} m/s and spectra in 10^{-8} m. Horizontal components are rotated to longitudinal and transverse directions to the general trend of geological divisions. **MAL** is located on fill and bay mud (Qm).

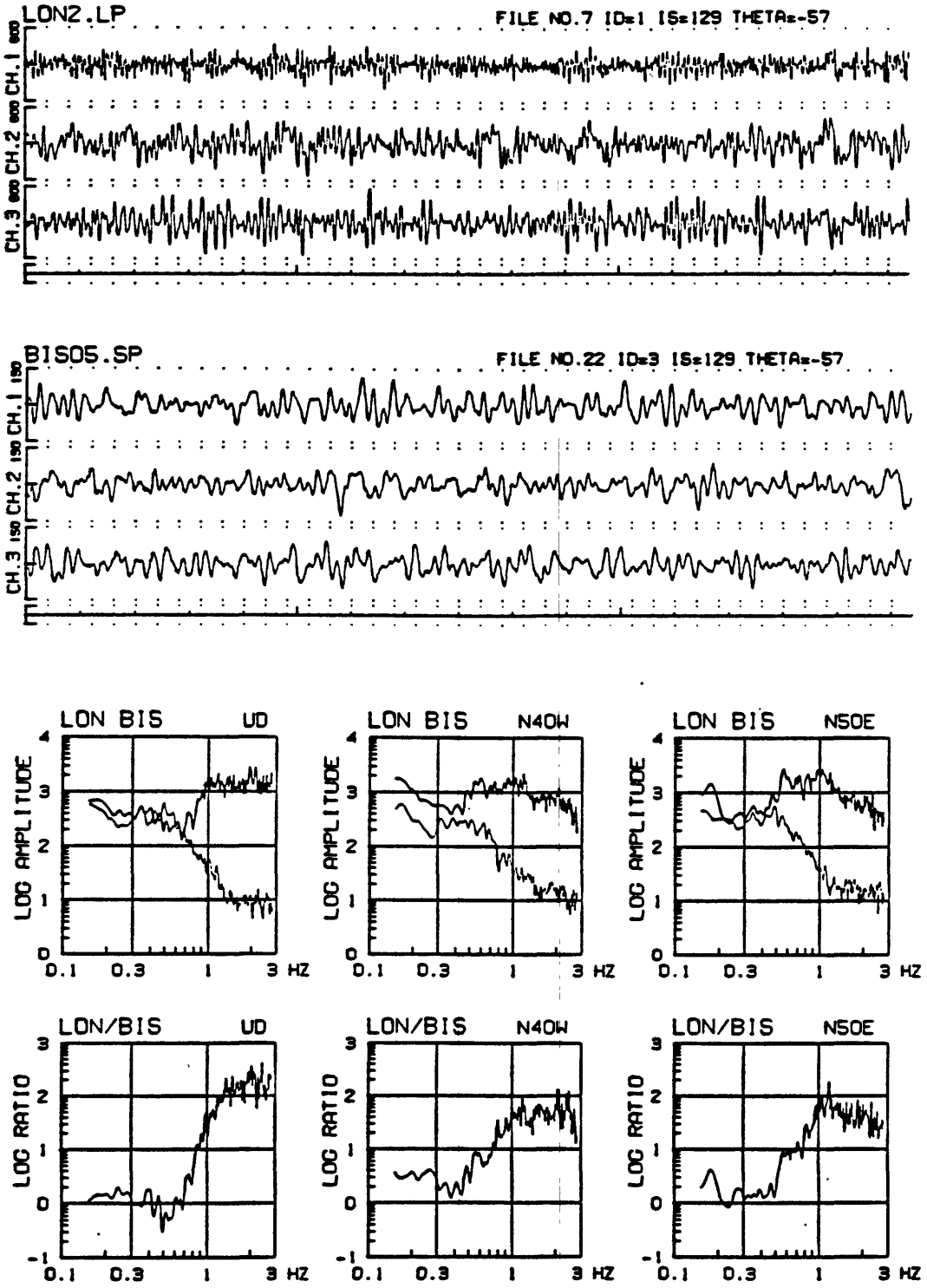

Fig. A.13 Velocity seismograms at **LON** and **BIS**, amplitude spectra and their ratios (**LON/BIS**). Seismogram scale is in 10^{-8} m/s and spectra in 10^{-8} m. Horizontal components are rotated to longitudinal and transverse directions to the general trend of geological divisions. **LON** is located on fill and bay mud (Qm).

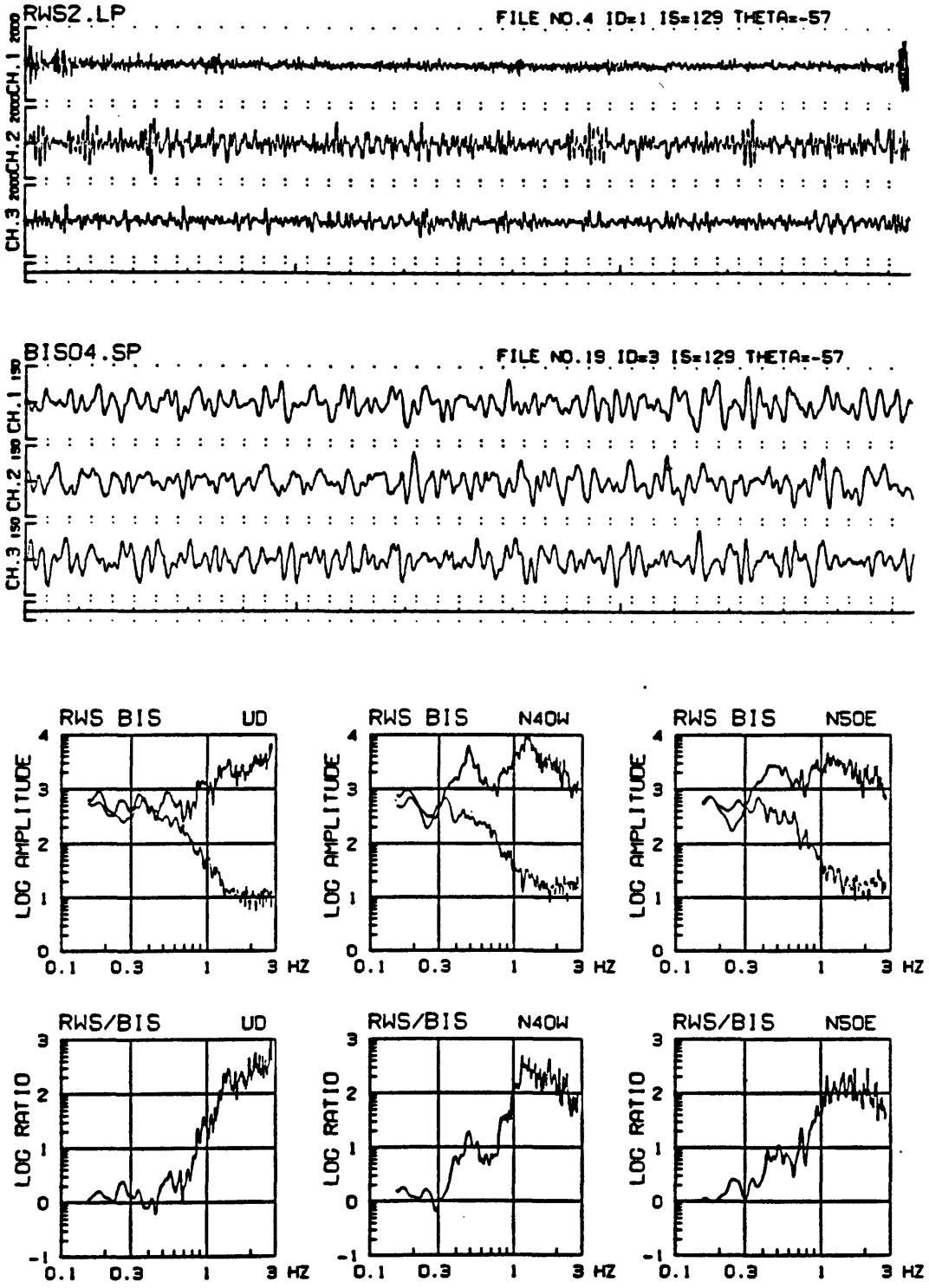

Fig. A.14 Velocity seismograms at **RWS** and **BIS**, amplitude spectra and their ratios (**RWS/BIS**). Seismogram scale is in 10^{-8} m/s and spectra in 10^{-8} m. Horizontal components are rotated to longitudinal and transverse directions to the general trend of geological divisions. **RWS** is located on fill and bay mud (Qm).

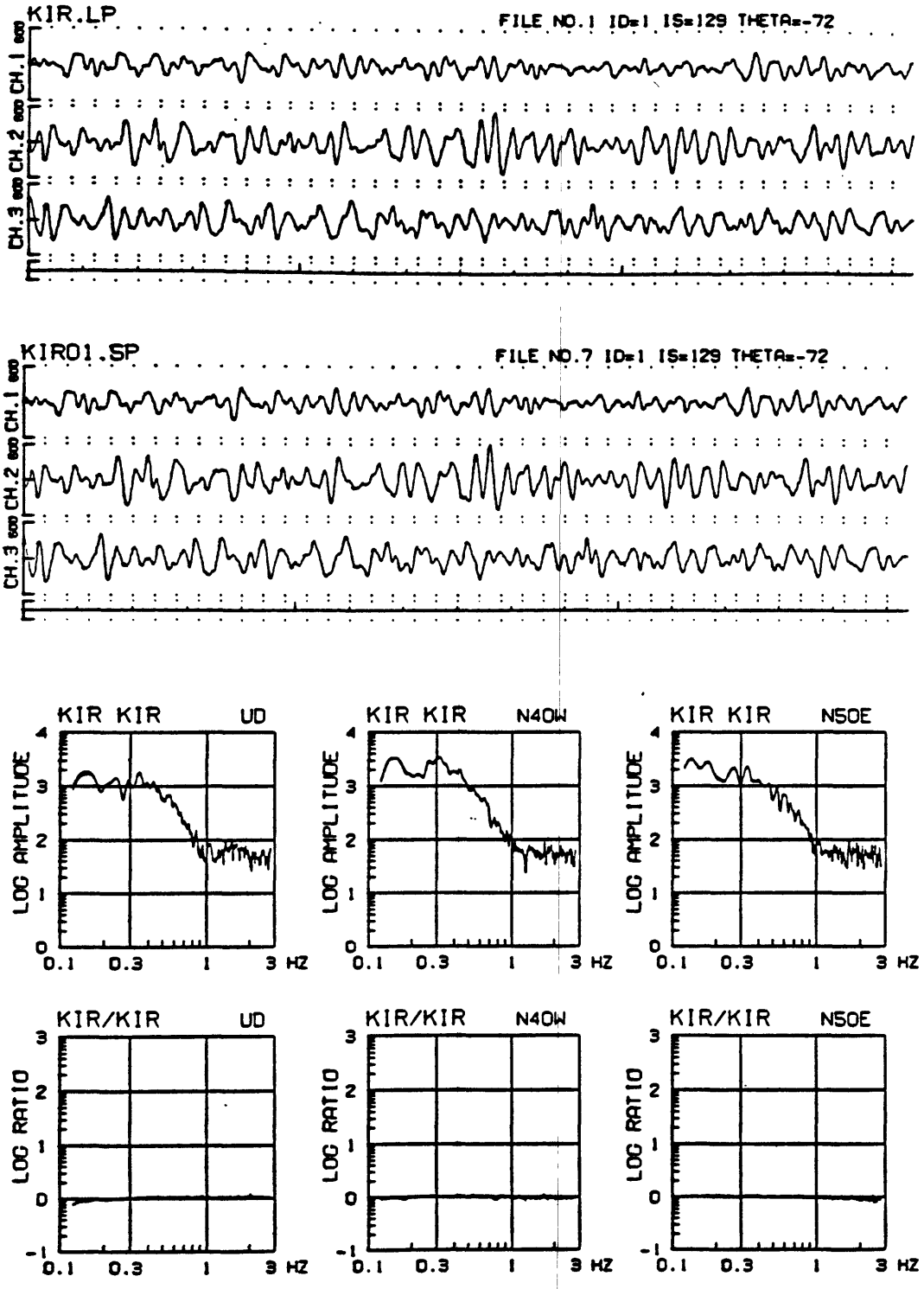

Fig. A.15 Velocity seismograms at **KIR**, amplitude spectra and their ratios (LP system/SP system), showing the same responses of the two systems. Seismogram scale is in 10^{-8} m/s and spectra in 10^{-8} m. **KIR** is located on sedimentary rocks (QTs).

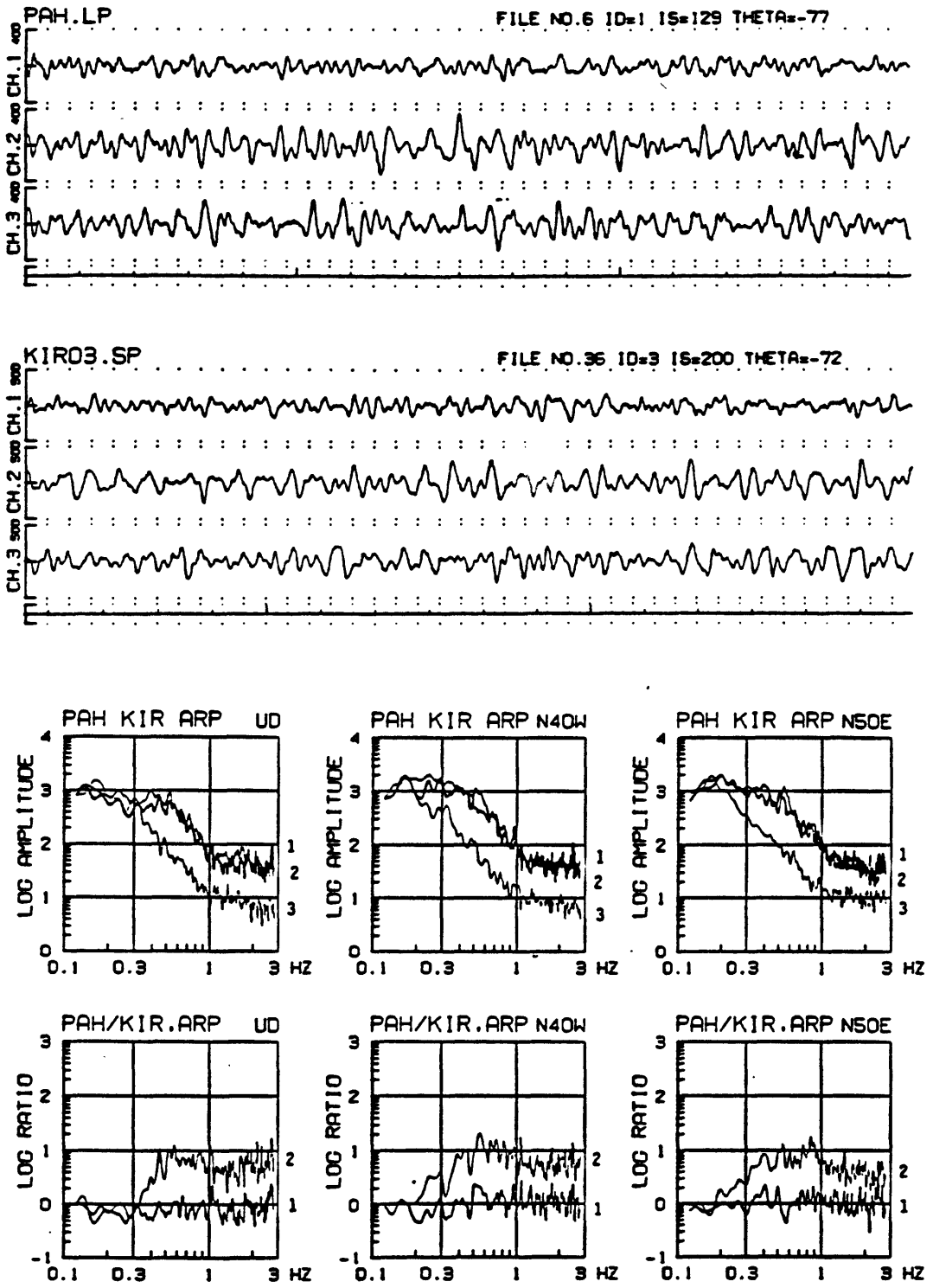

Fig. A.16 Velocity seismograms at **PAH** and **KIR**, amplitude spectra (1: **PAH**, 2: **KIR**, 3: **ARP**) and their ratios (1: **PAH/KIR**, 2: **PAH/ARP**). Seismogram scale is in 10^{-8} m/s and spectra in 10^{-8} m. Horizontal components are rotated to longitudinal and transverse directions to the long axis of the valley. **PAH** is located on sedimentary rocks (**QTs**).

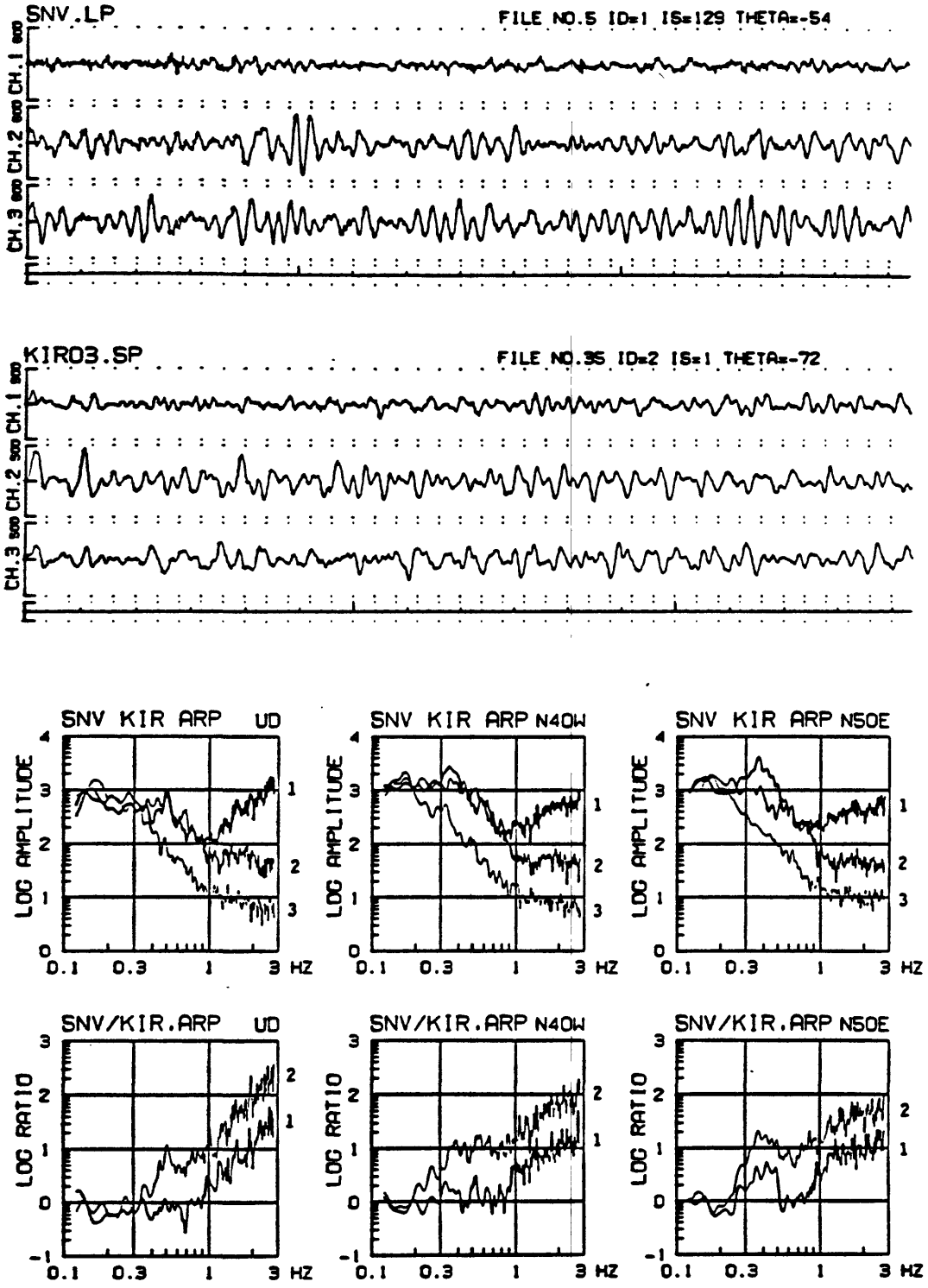

Fig. A.17 Velocity seismograms at **SNV** and **KIR**, amplitude spectra (1: **SNV**, 2: **KIR**, 3: **ARP**) and their ratios (1: **SNV/KIR**, 2: **SNV/ARP**). Seismogram scale is in 10^{-8} m/s and spectra in 10^{-8} m. Horizontal components are rotated to longitudinal and transverse directions to the long axis of the valley. **SNV** is located on thick deposits of alluvium (Qal).

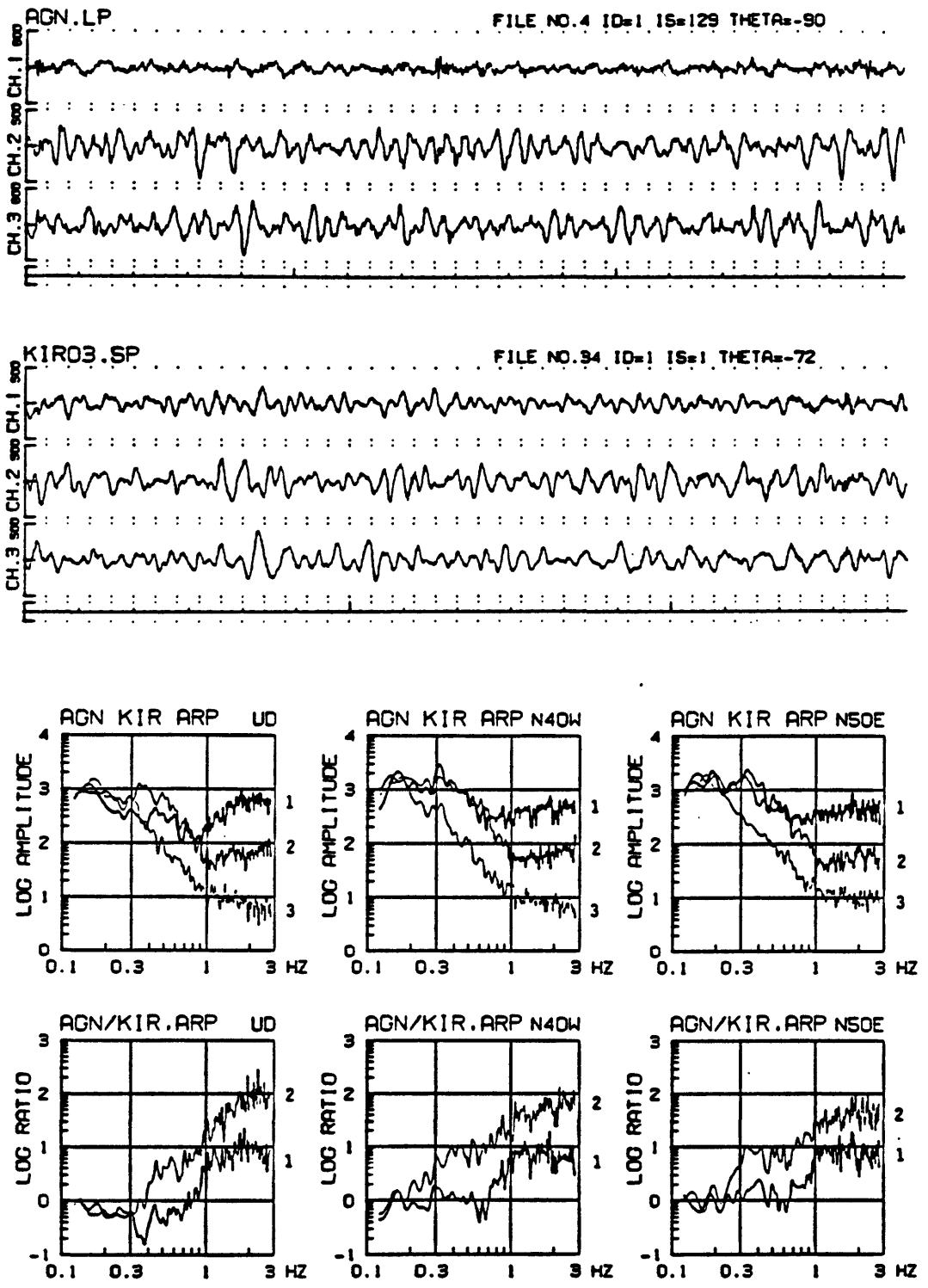

Fig. A.18 Velocity seismograms at **AGN** and **KIR**, amplitude spectra (1: **AGN**, 2: **KIR**, 3: **ARP**) and their ratios (1: **AGN/KIR**, 2: **AGN/ARP**). Seismogram scale is in 10^{-8} m/s and spectra in 10^{-8} m. Horizontal components are rotated to longitudinal and transverse directions to the long axis of the valley. **AGN** is located on thick deposits of alluvium (Qal).

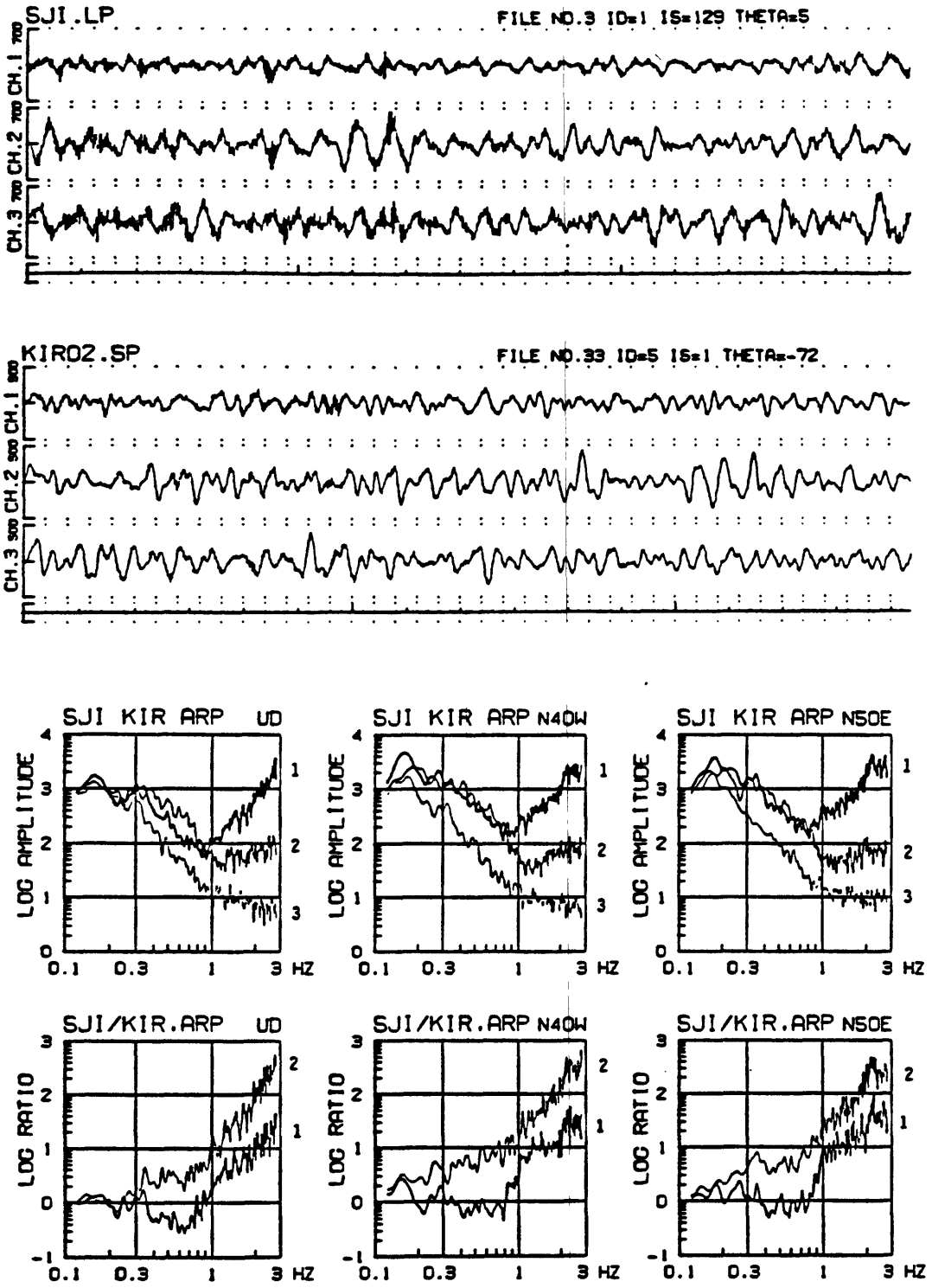

Fig. A.19 Velocity seismograms at **SJI** and **KIR**, amplitude spectra (1: **SJI**, 2: **KIR**, 3: **ARP**) and their ratios (1: **SJI/KIR**, 2: **SJI/ARP**). Seismogram scale is in 10^{-8} m/s and spectra in 10^{-8} m. Horizontal components are rotated to longitudinal and transverse directions to the long axis of the valley. **SJI** is located on thick deposits of alluvium (Qal).

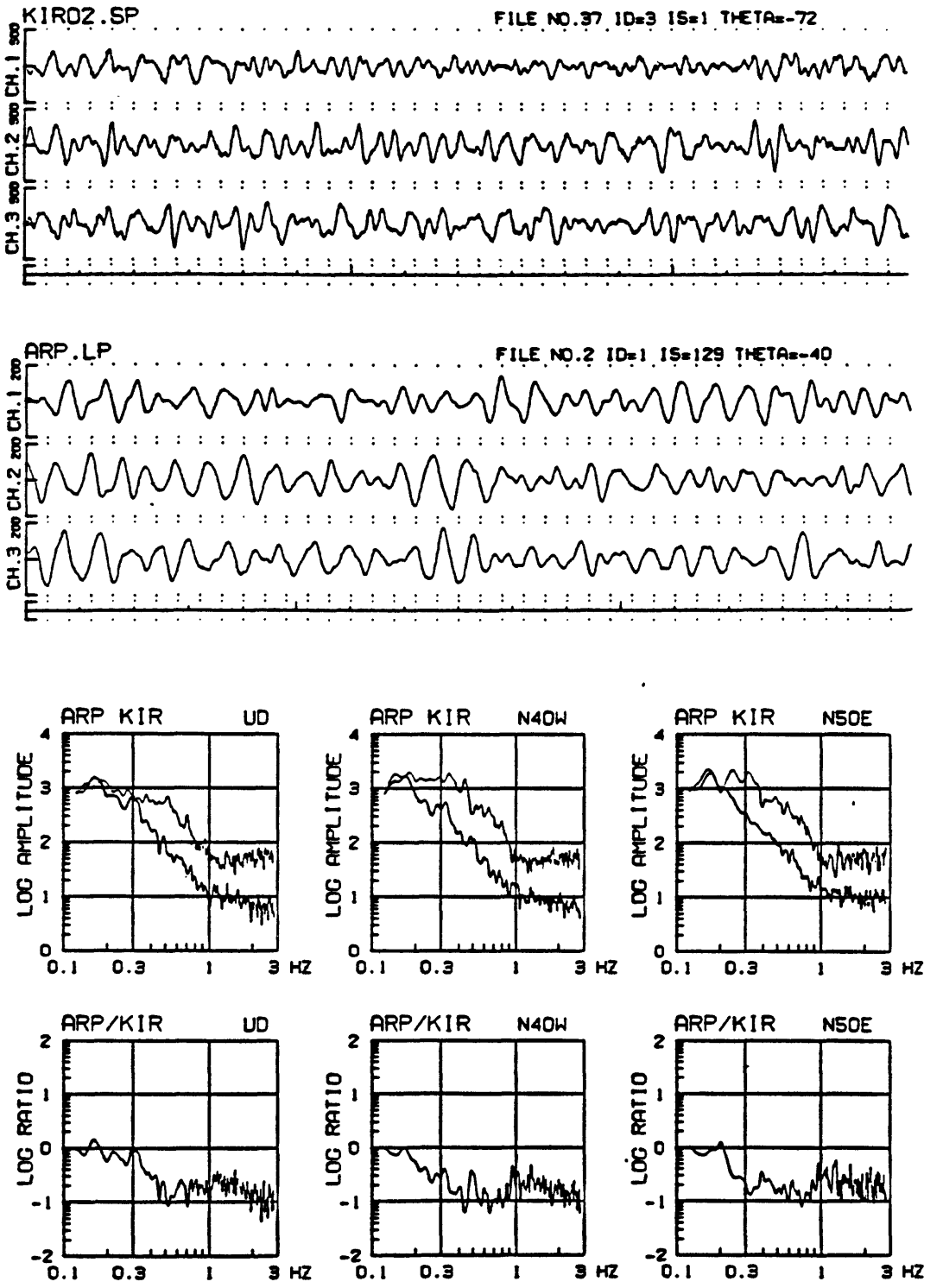

Fig. A.20 Velocity seismograms at **ARP** and **KIR**, amplitude spectra (thick: **ARP**, thin: **KIR**) and their ratios (**ARP/KIR**). Seismogram scale is in 10^{-8} m/s and spectra in 10^{-8} m. Horizontal components are rotated to longitudinal and transverse directions to the long axis of the valley. **ARP** is located on sedimentary rocks (TMzs).

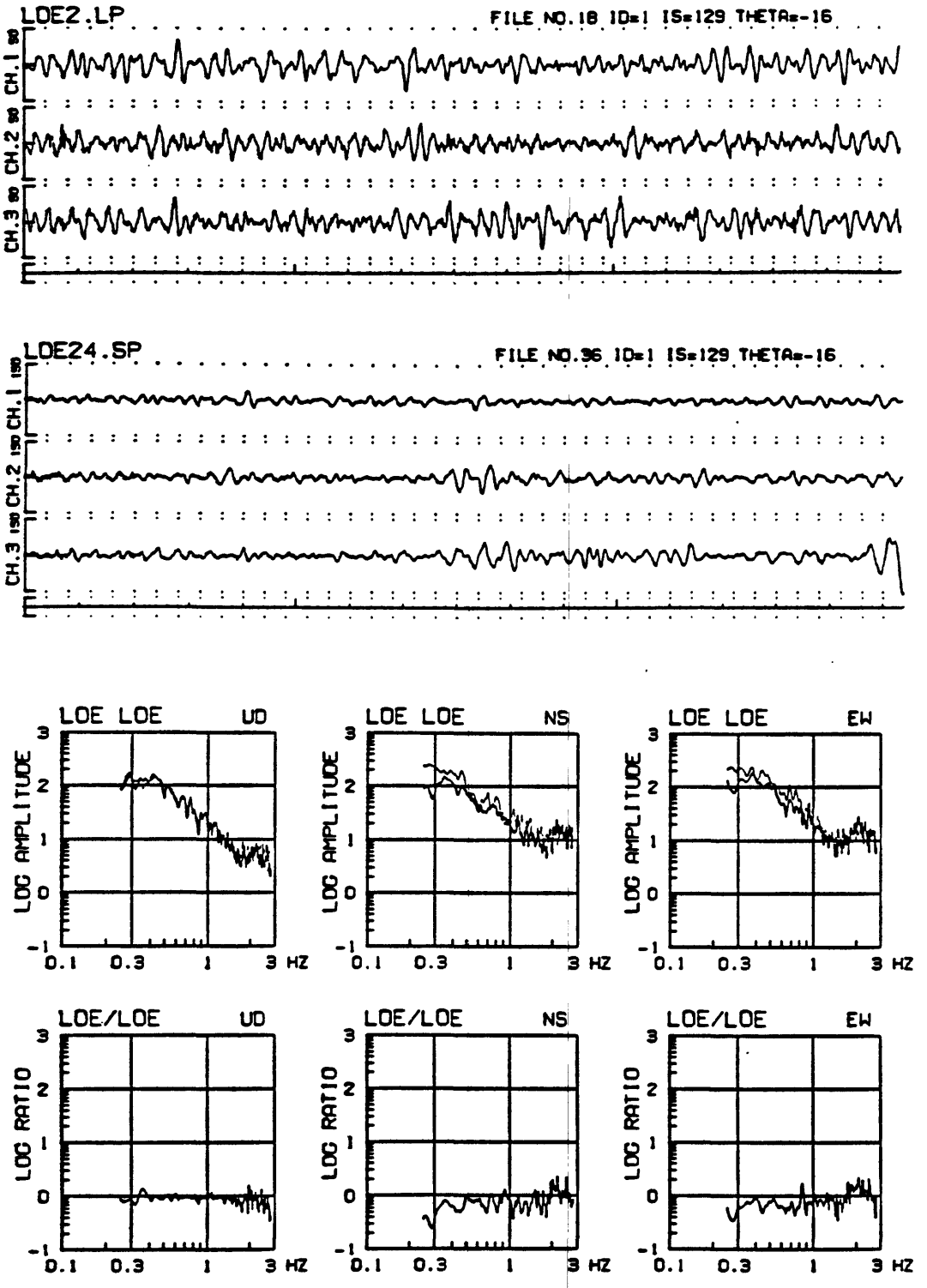

Fig. A.21 Velocity seismograms at **LOE**, amplitude spectra (LP system/SP system), showing the reliability of the two systems. Seismogram scale is in 10^{-8} m/s and spectra in 10^{-8} m. **LOE** is located on metasedimentary rocks (sch).

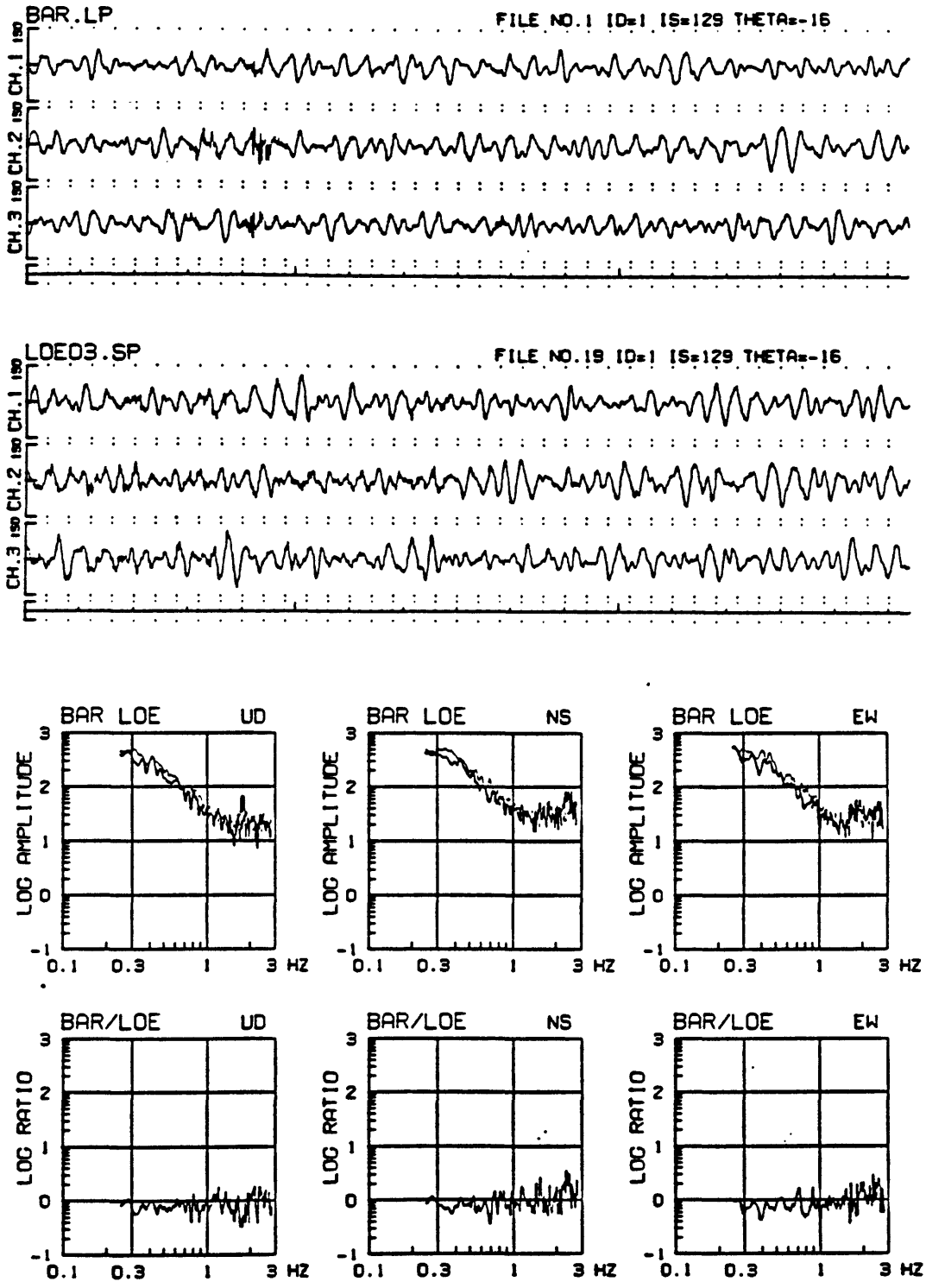

Fig. A.22 Velocity seismograms at **BAR** and **LOE**, amplitude spectra and their ratios (**BAR/LOE**). Seismogram scale is in 10^{-8} m/s and spectra in 10^{-8} m. **BAR** is located on marble (m).

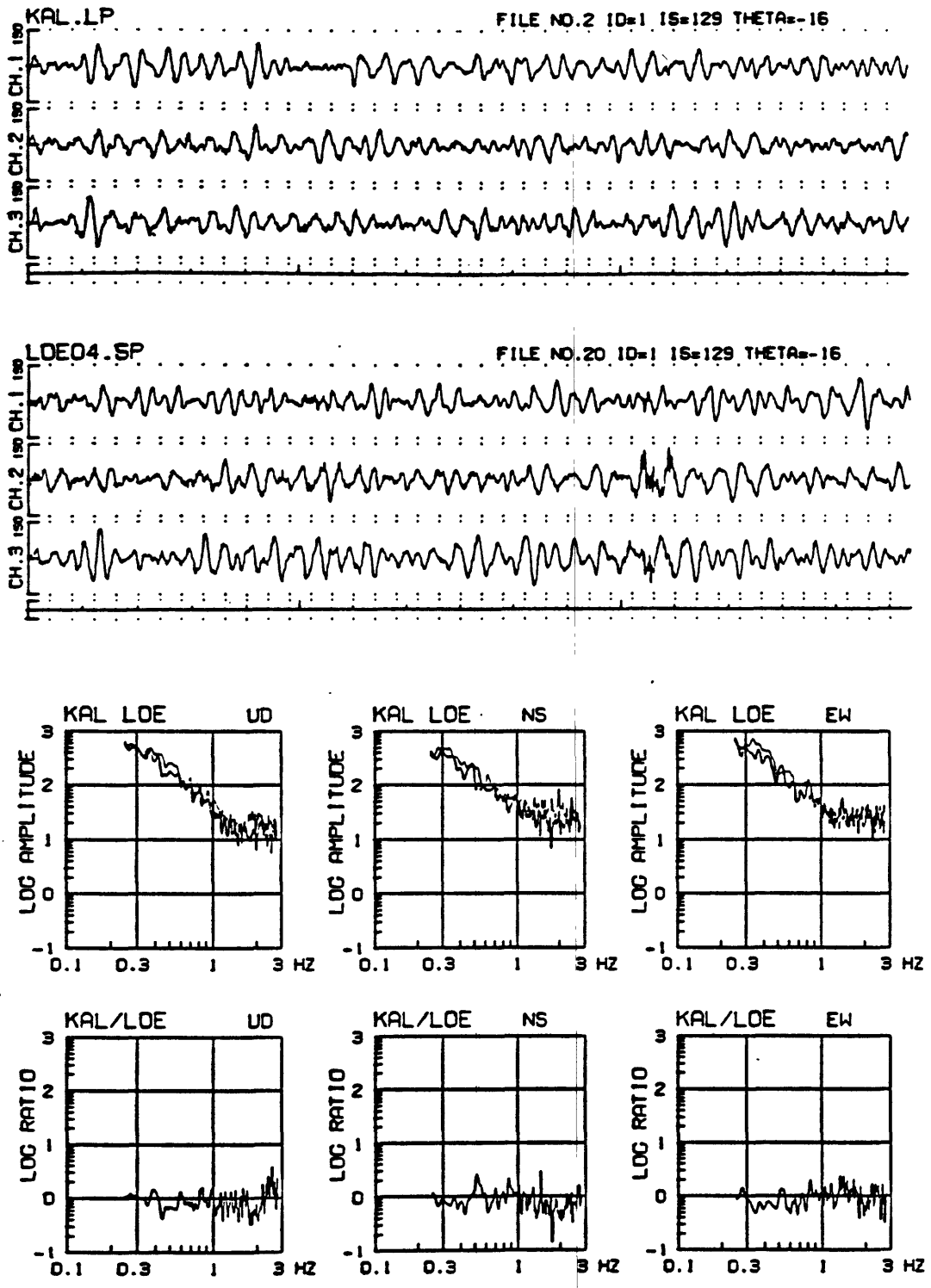

Fig. A.23 Velocity seismograms at **KAL** and **LOE**, amplitude spectra and their ratios (**KAL/LOE**). Seismogram scale is in 10^{-8} m/s and spectra in 10^{-8} m. **KAL** is located on marine terrace deposits (Qt).

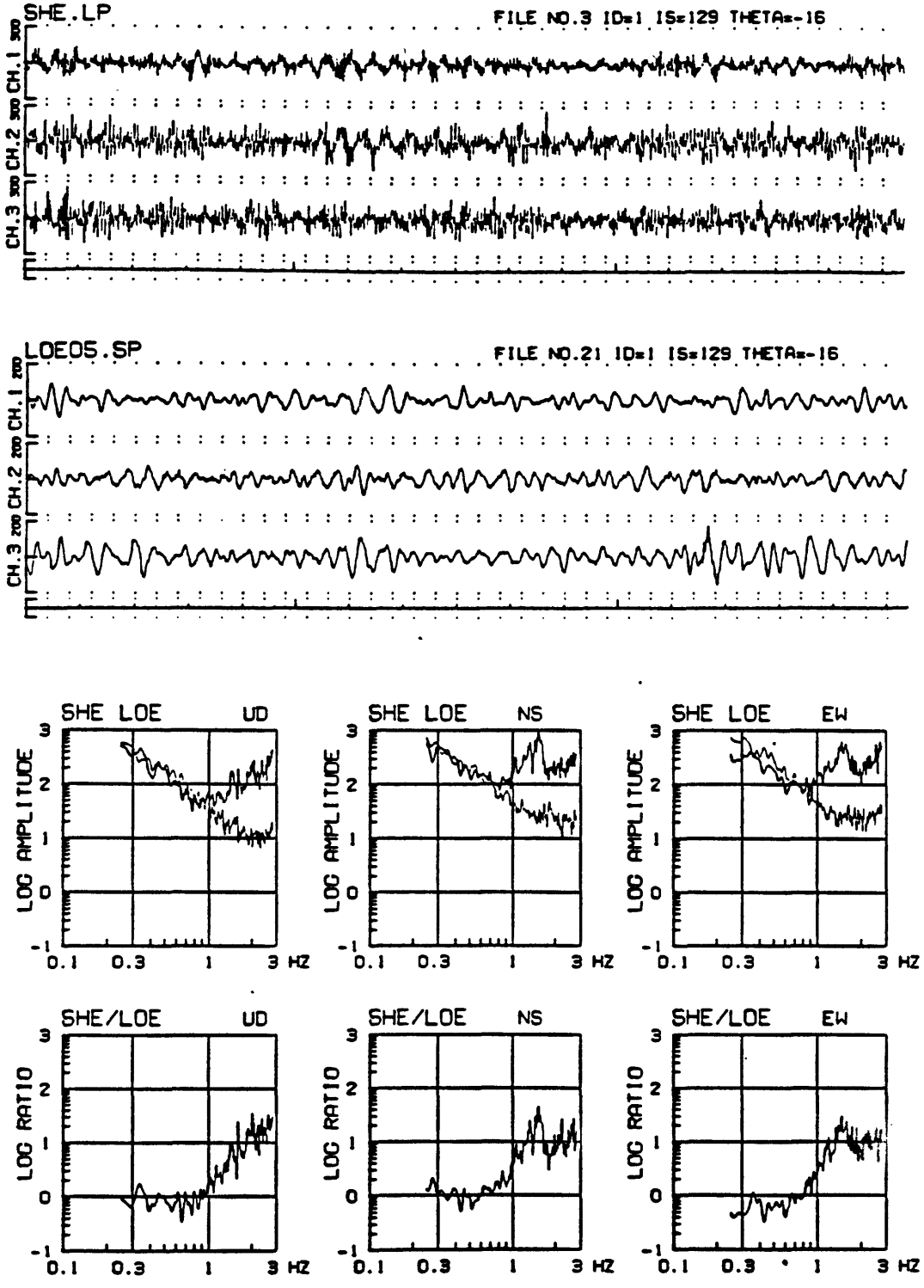

Fig. A.24 Velocity seismograms at **SHE** and **LOE**, amplitude spectra and their ratios (**SHE/LOE**). Seismogram scale is in 10^{-8} m/s and spectra in 10^{-8} m. **SHE** is located on marine terrace deposits (Qt).

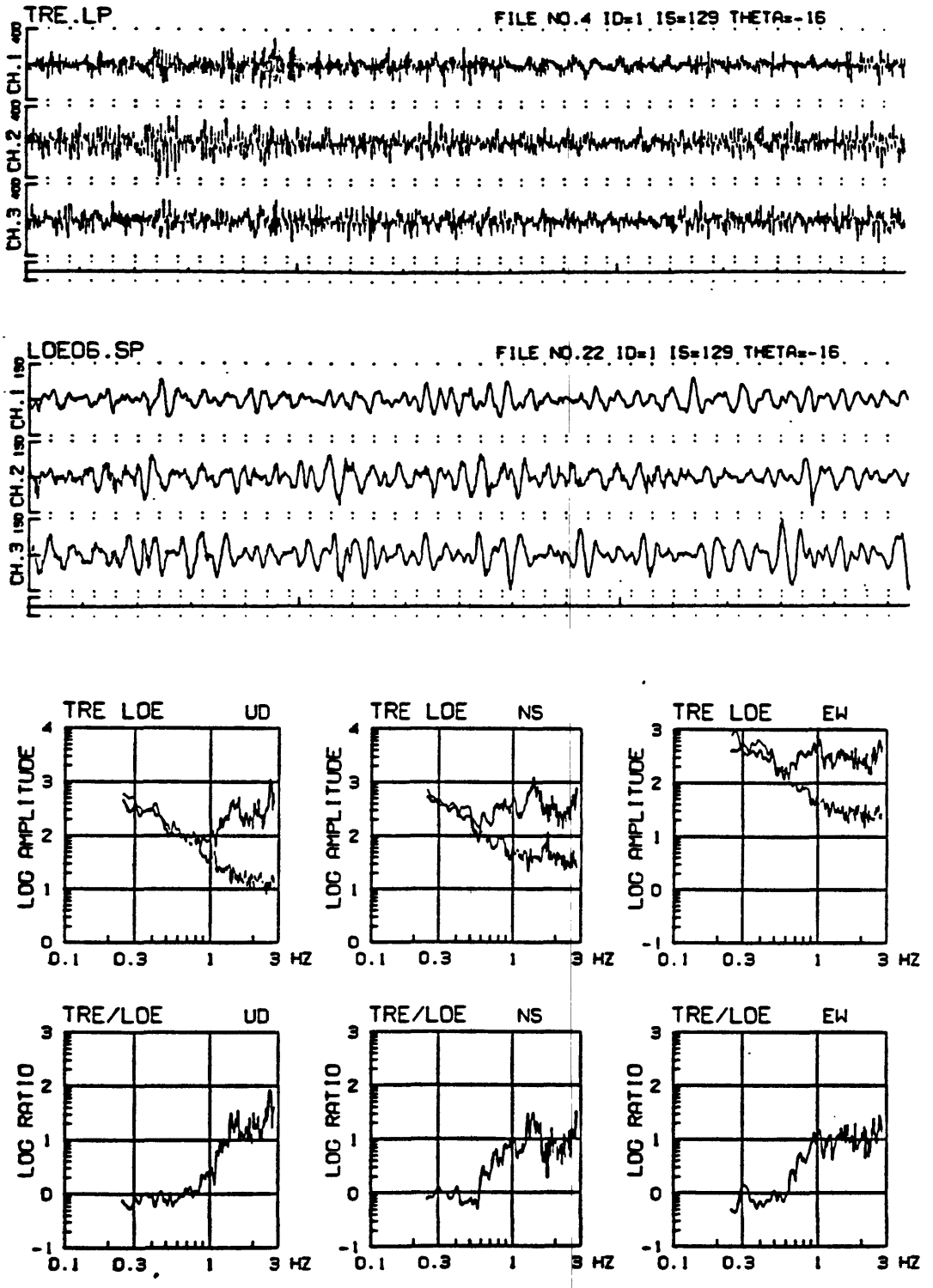

Fig. A.25 Velocity seismograms at **TRE** and **LOE**, amplitude spectra and their ratios (**TRE/LOE**). Seismogram scale is in 10^{-8} m/s and spectra in 10^{-8} m. **TRE** is located on marine terrace deposits (Qt).

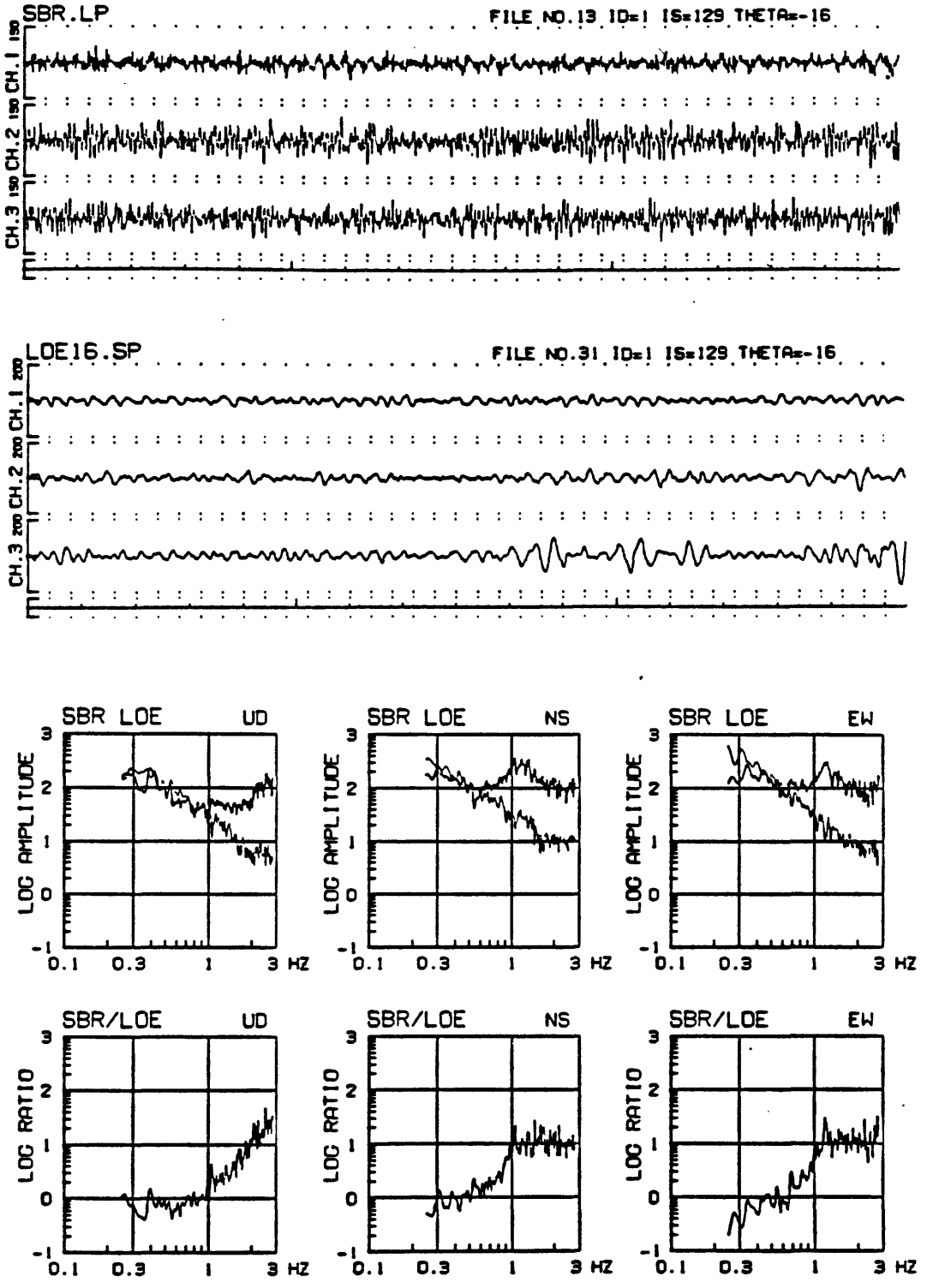

Fig. A.26 Velocity seismograms at **SBR** and **LOE**, amplitude spectra and their ratios (**SBR/LOE**). Seismogram scale is in 10^{-8} m/s and spectra in 10^{-8} m. **SBR** is located on marine terrace deposits (Qt).

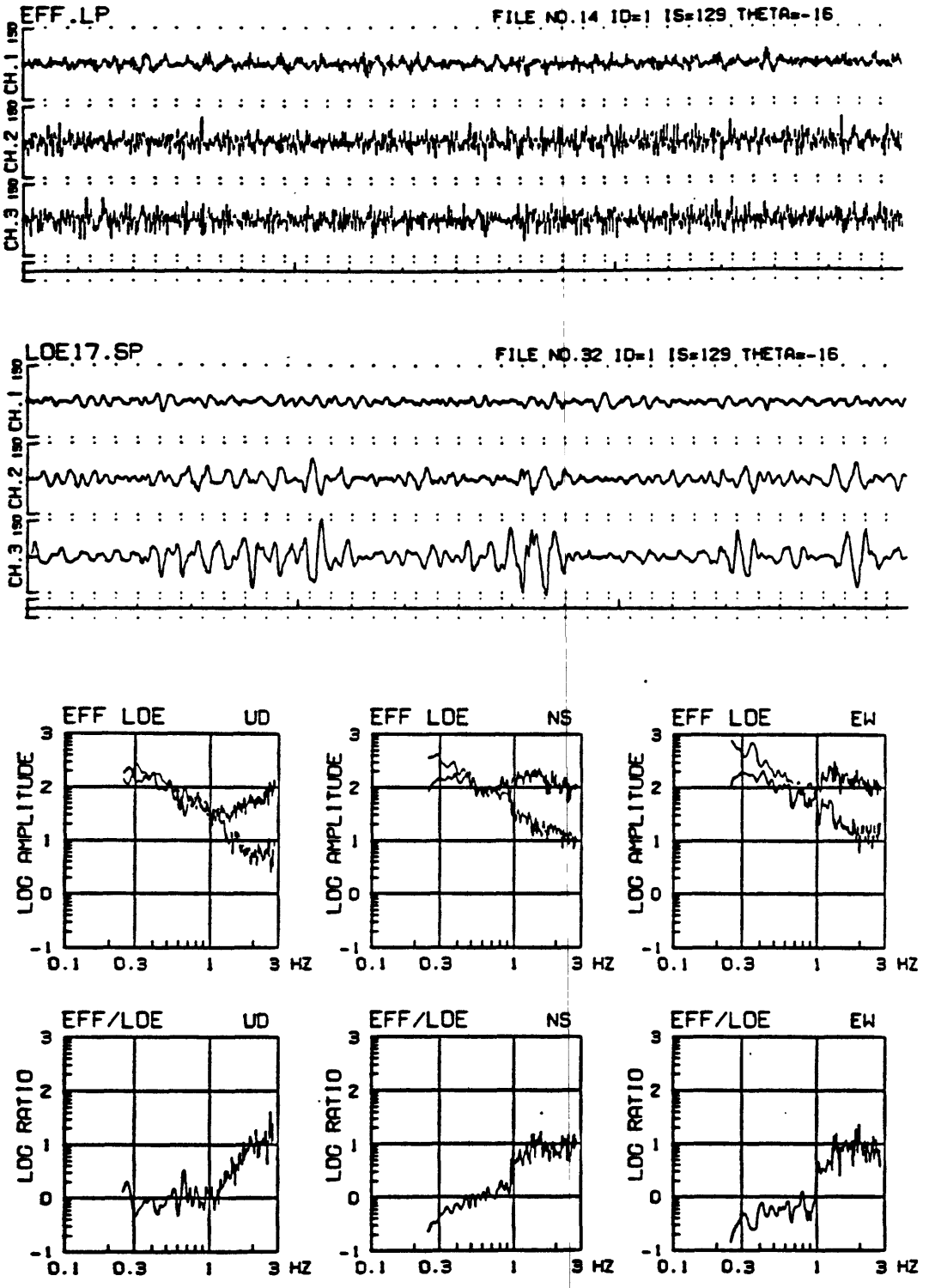

Fig. A.27 Velocity seismograms at **EFF** and **LOE**, amplitude spectra and their ratios (**EFF/LOE**). Seismogram scale is in 10^{-8} m/s and spectra in 10^{-8} m. **EFF** is located on marine terrace deposits (Qt).

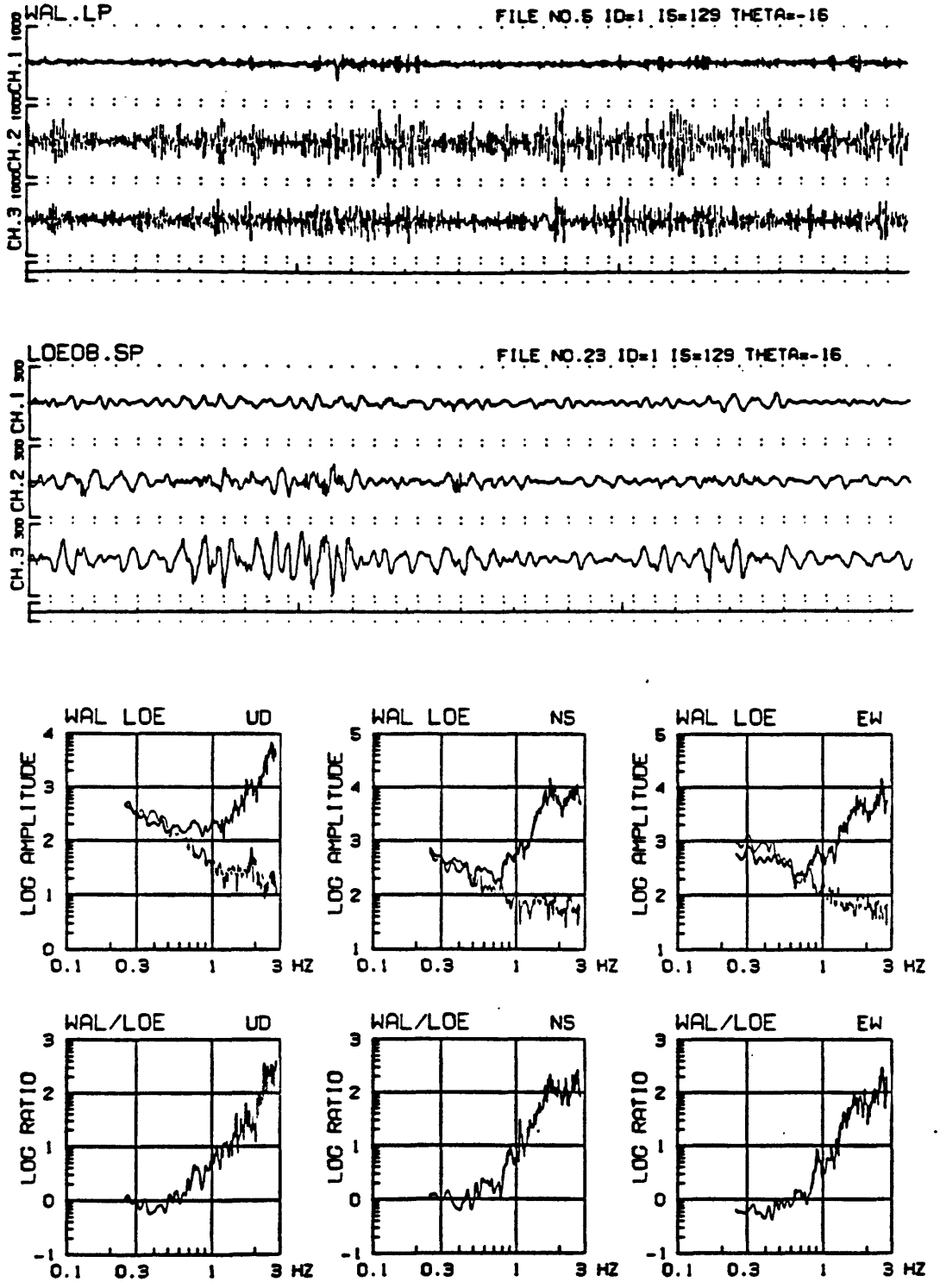

Fig. A.28 Velocity seismograms at **WAL** and **LOE**, amplitude spectra and their ratios (**WAL/LOE**). Seismogram scale is in 10^{-8} m/s and spectra in 10^{-8} m. **WAL** is located on alluvium (Qal).

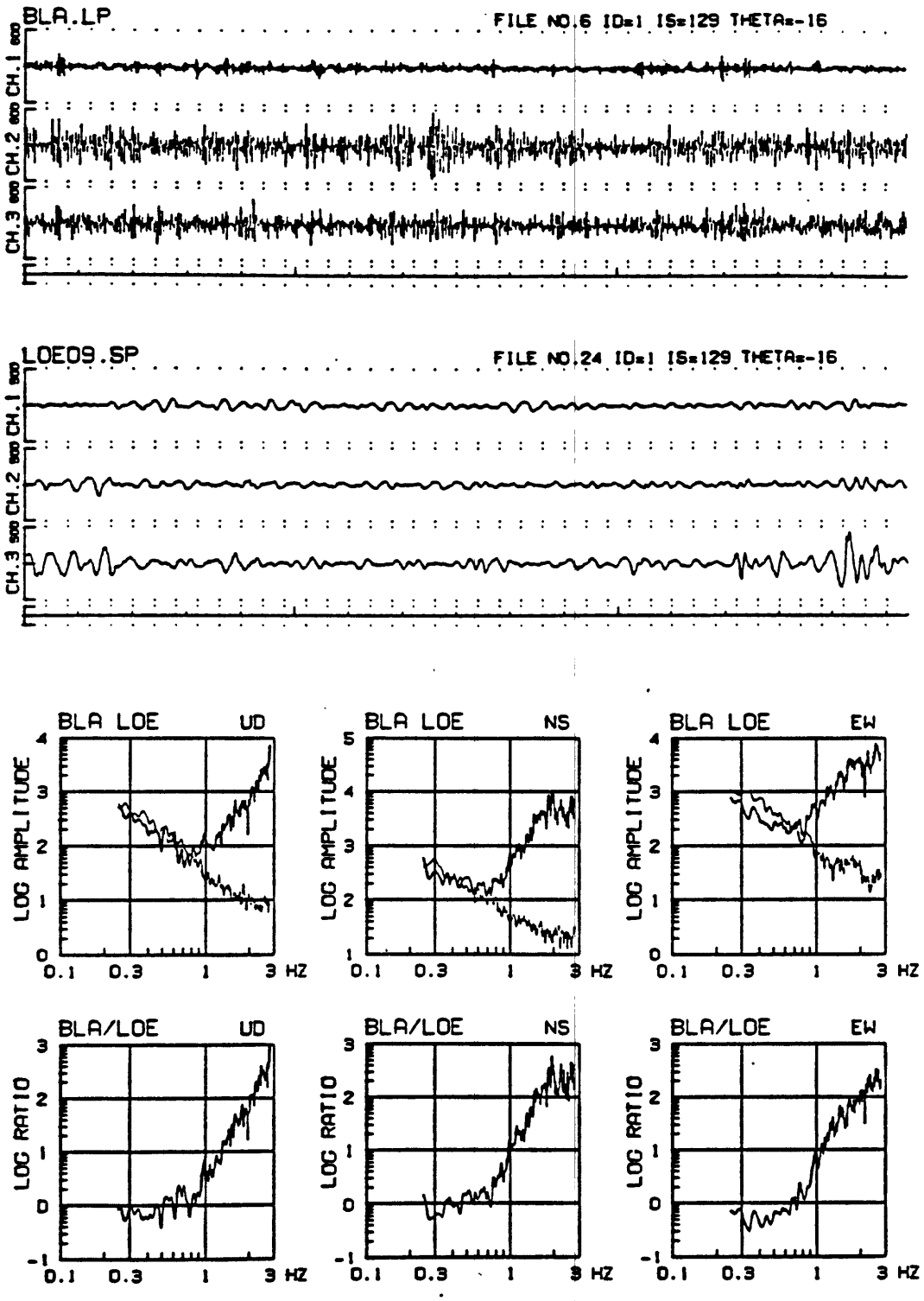

Fig. A.29 Velocity seismograms at **BLA** and **LOE**, amplitude spectra and their ratios (**BLA/LOE**). Seismogram scale is in 10^{-8} m/s and spectra in 10^{-8} m. **BLA** is located on alluvium (Qal).

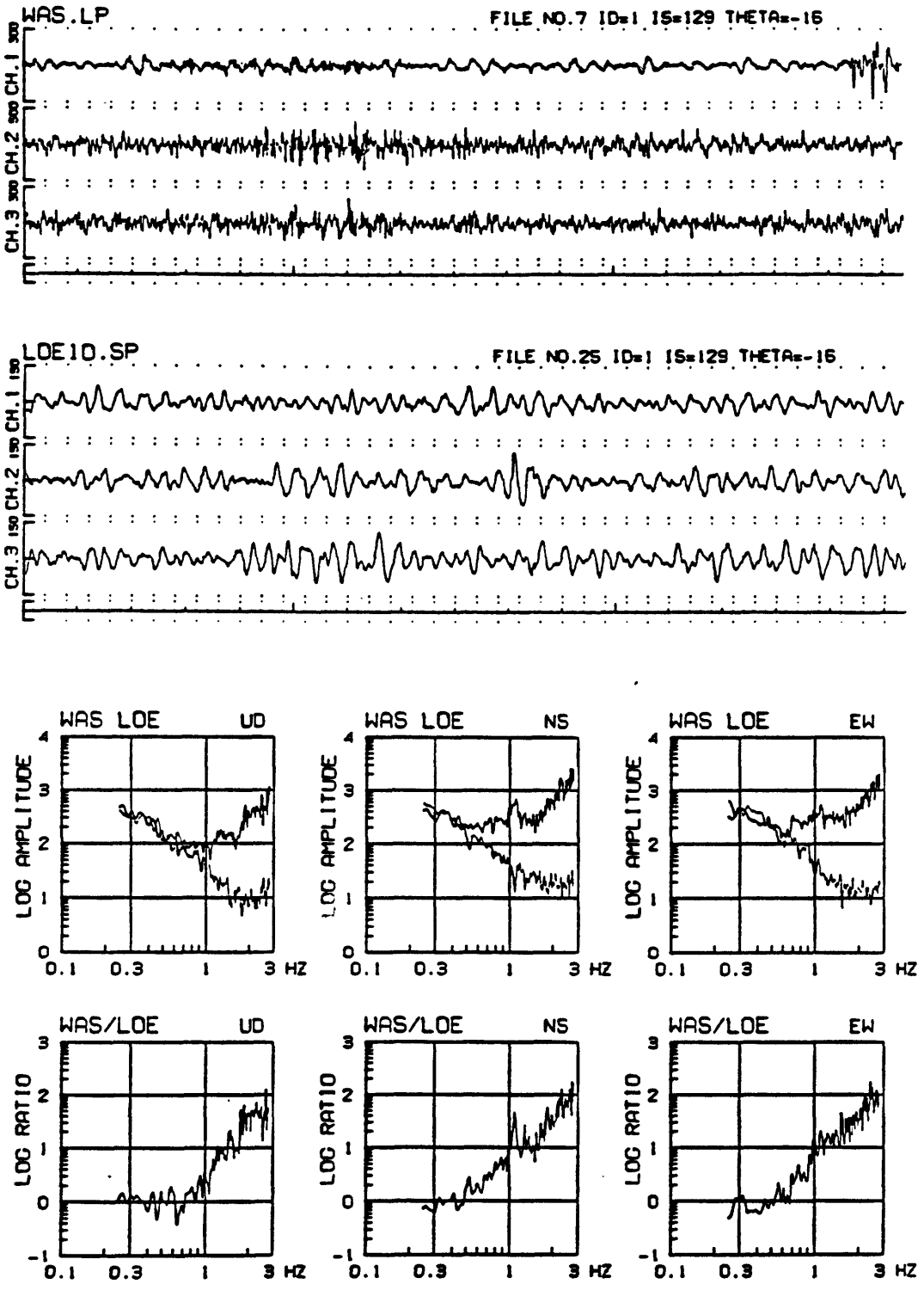

Fig. A.30 Velocity seismograms at **WAS** and **LOE**, amplitude spectra and their ratios (**WAS/LOE**). Seismogram scale is in 10^{-8} m/s and spectra in 10^{-8} m. **WAS** is located on alluvium (Qal).

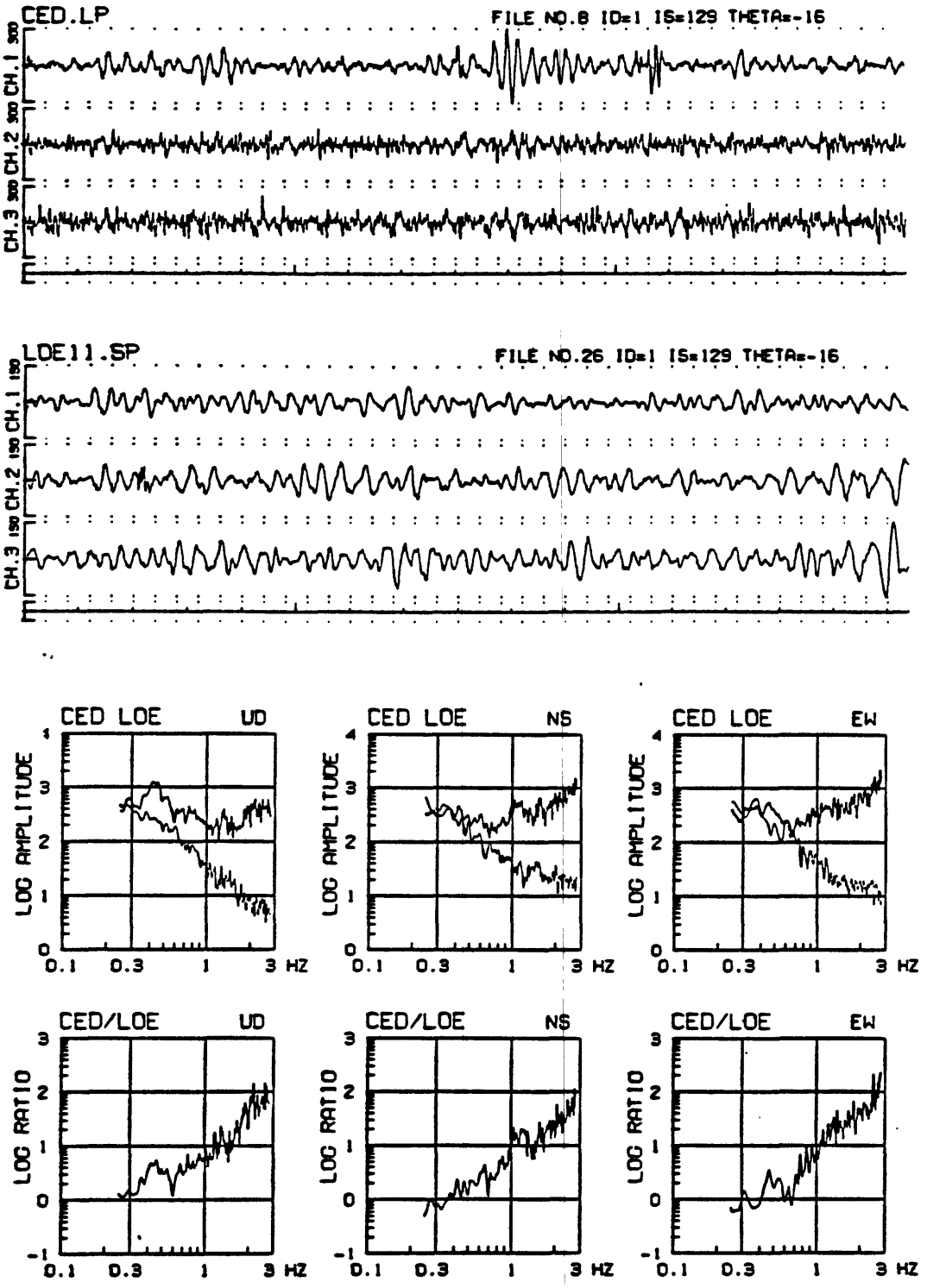

Fig. A.31 Velocity seismograms at **CED** and **LOE**, amplitude spectra and their ratios (**CED/LOE**). Seismogram scale is in 10^{-8} m/s and spectra in 10^{-8} m. **CED** is located on alluvium (Qal).

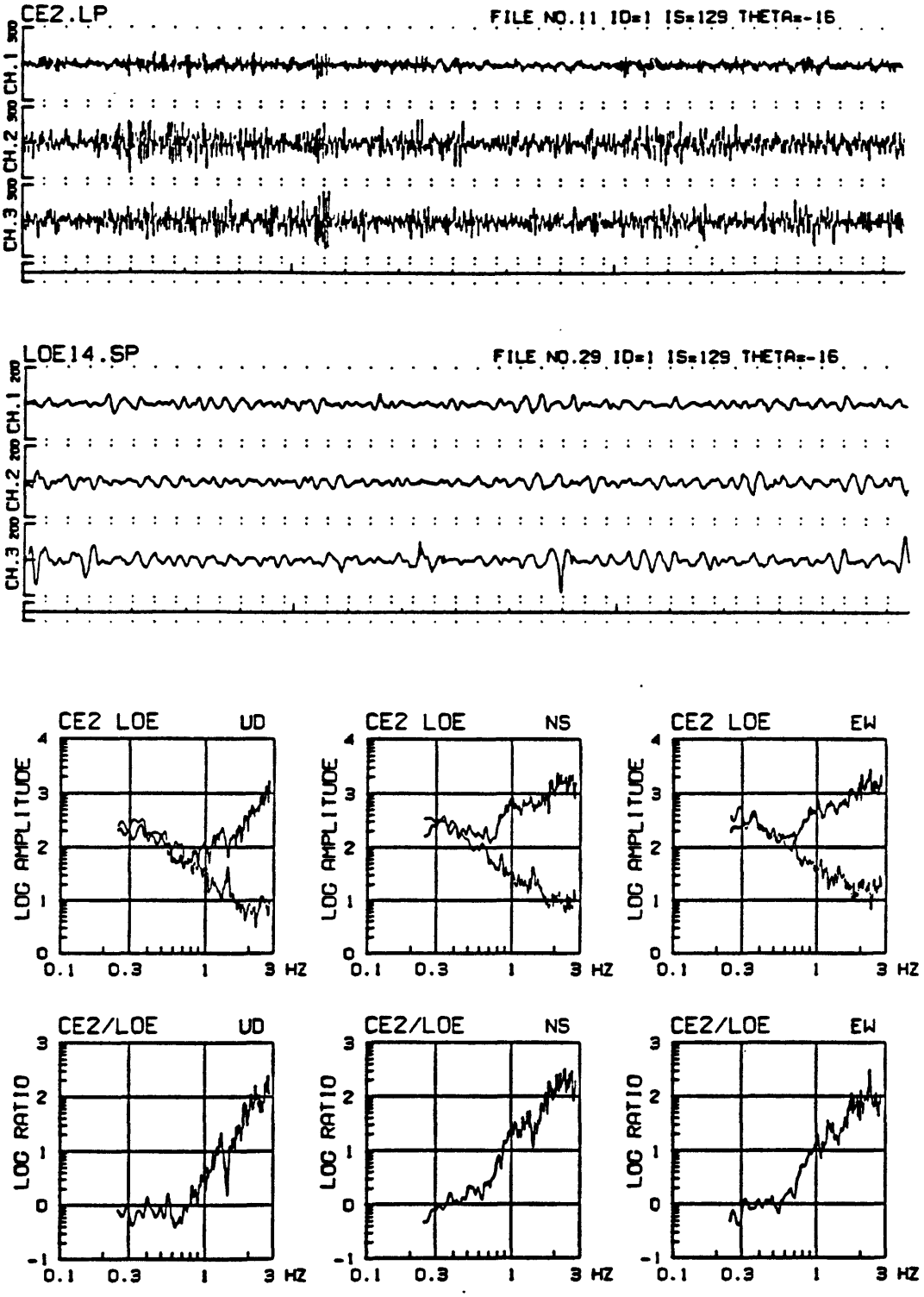

Fig. A.32 Velocity seismograms at **CE2** and **LOE**, amplitude spectra and their ratios (**CE2/LOE**). Seismogram scale is in 10^{-8} m/s and spectra in 10^{-8} m. **CE2** is located on alluvium (Qal).

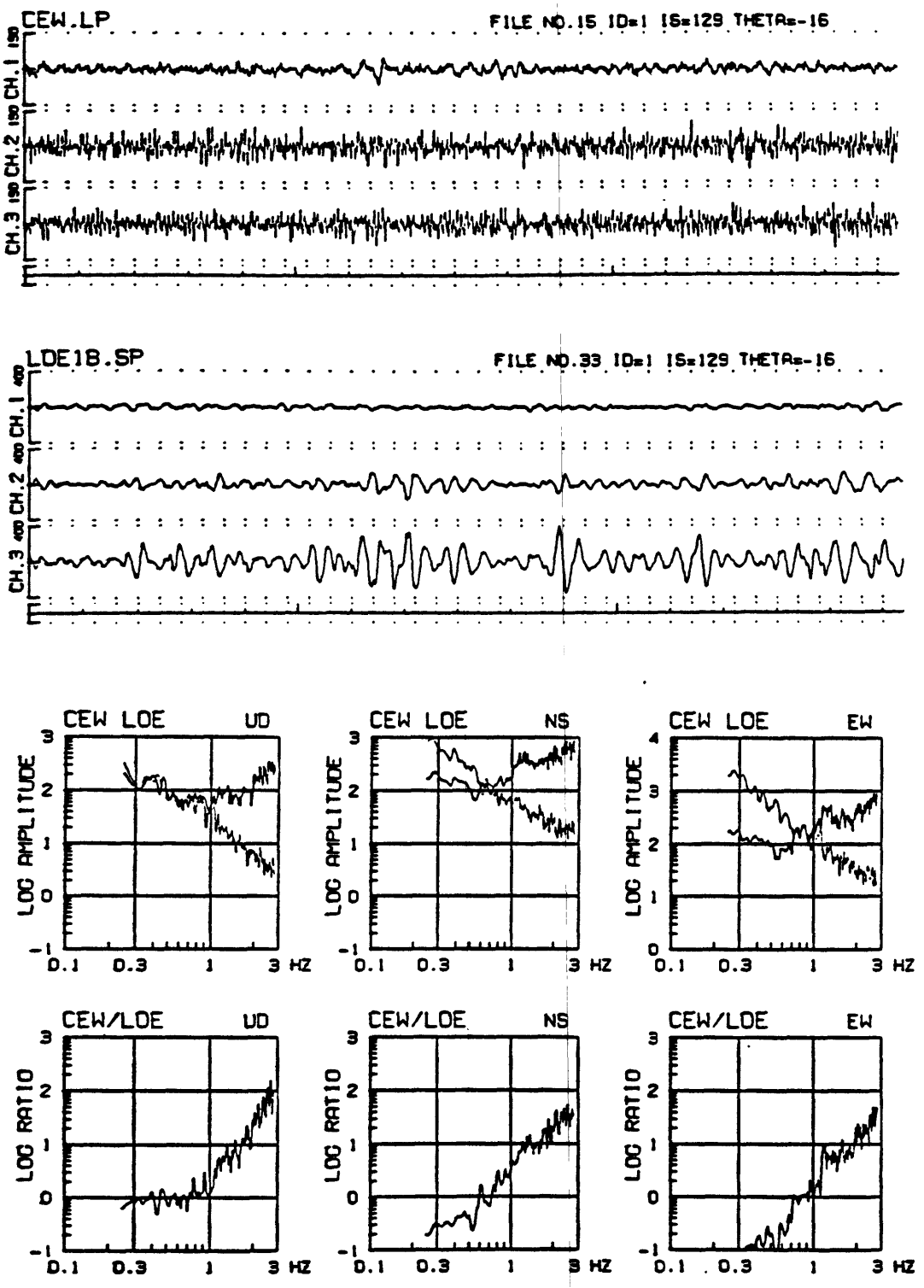

Fig. A.33 Velocity seismograms at **CEW** and **LOE**, amplitude spectra and their ratios (**CEW/LOE**). Seismogram scale is in 10^{-8} m/s and spectra in 10^{-8} m. **CEW** is located on alluvium (Qal).

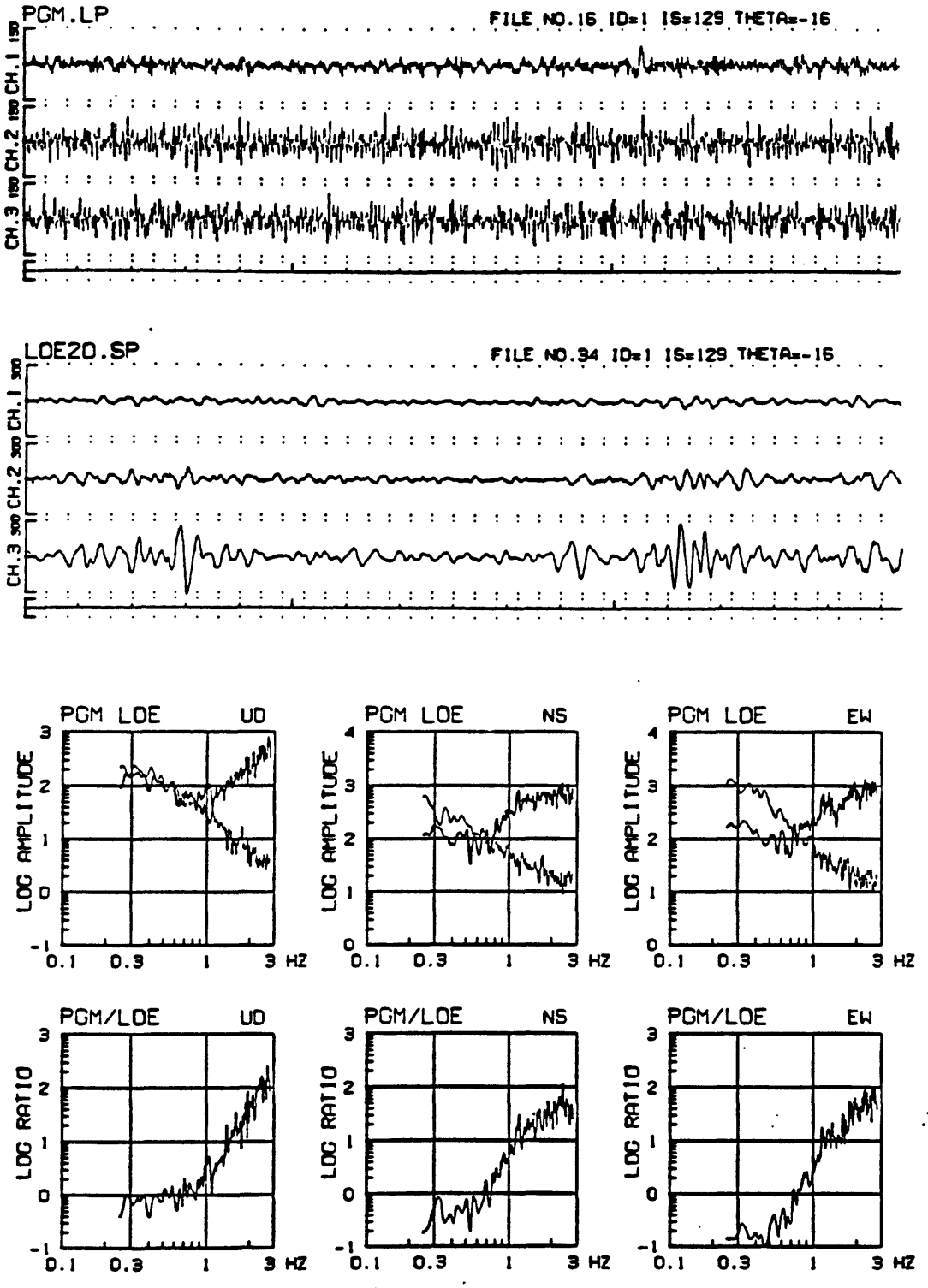

Fig. A.34 Velocity seismograms at **PGM** and **LOE**, amplitude spectra and their ratios (**PGM/LOE**). Seismogram scale is in 10^{-8} m/s and spectra in 10^{-8} m. **PGM** is located on alluvium (Qal).

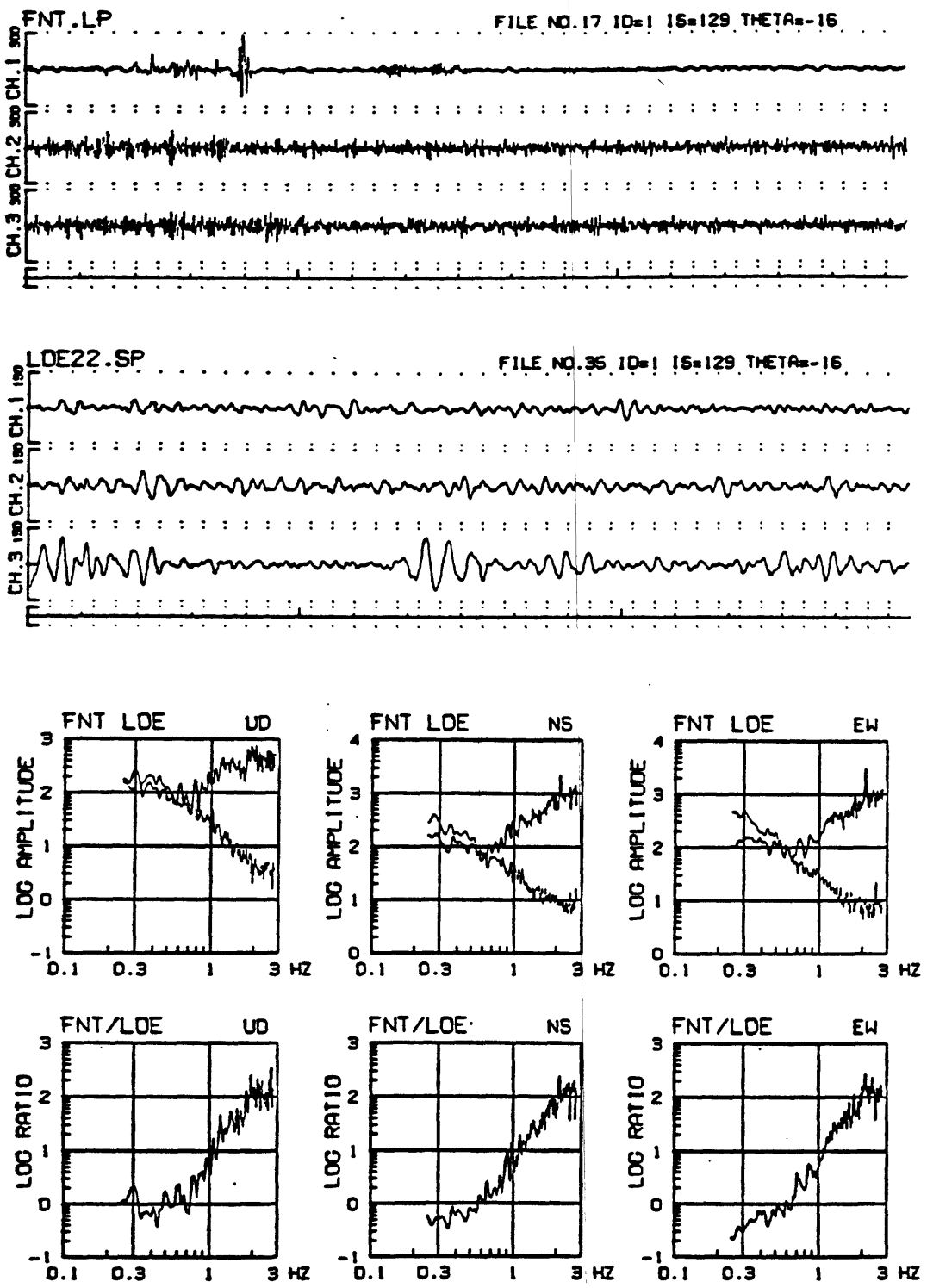

Fig. A.35 Velocity seismograms at **FNT** and **LOE**, amplitude spectra and their ratios (**FNT/LOE**). Seismogram scale is in 10^{-8} m/s and spectra in 10^{-8} m. **FNT** is located on alluvium (Qal).

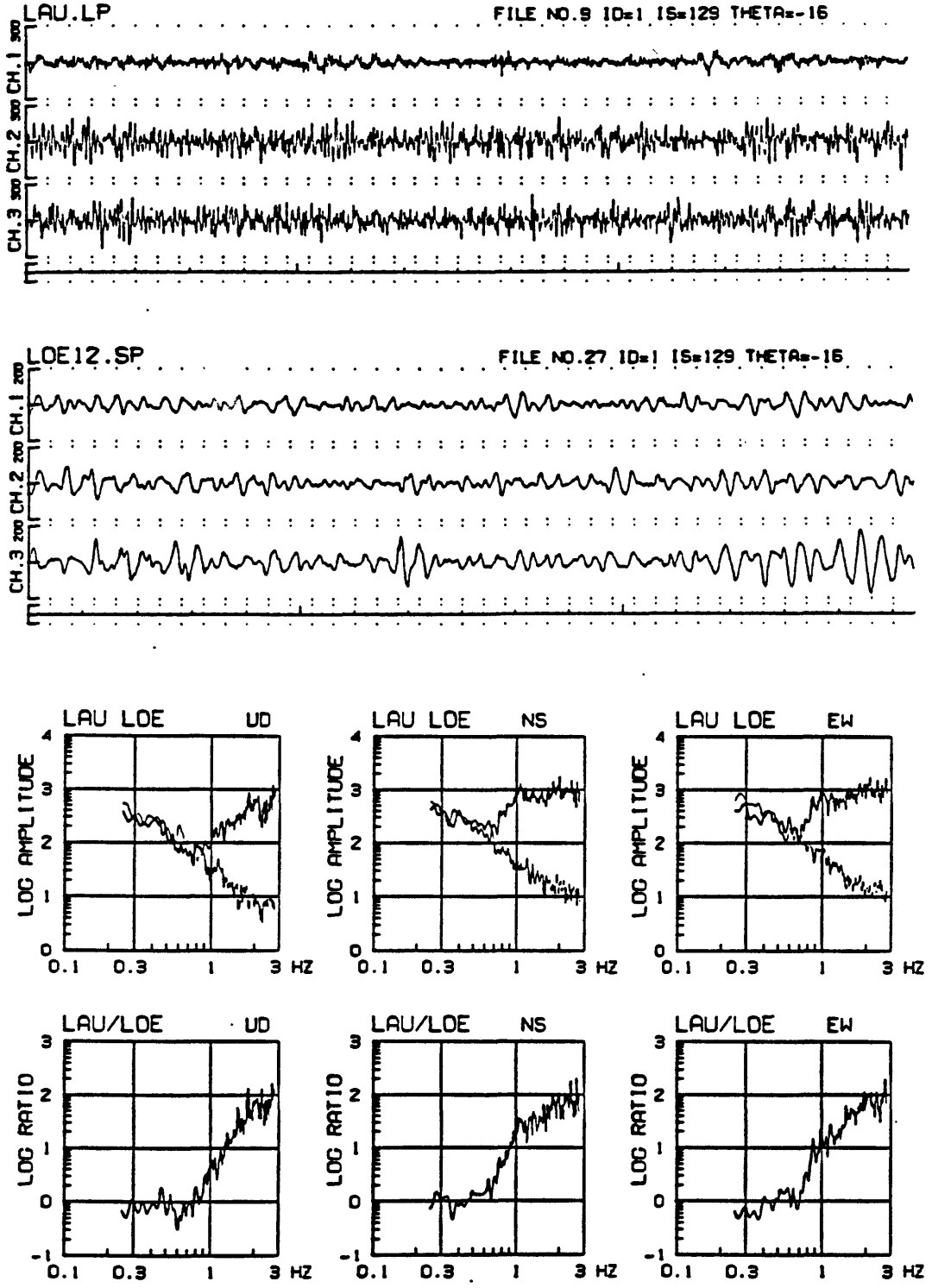

Fig. A.36 Velocity seismograms at **LAU** and **LOE**, amplitude spectra and their ratios (**LAU/LOE**). Seismogram scale is in 10^{-8} m/s and spectra in 10^{-8} m. **LAU** is located on marble (m).

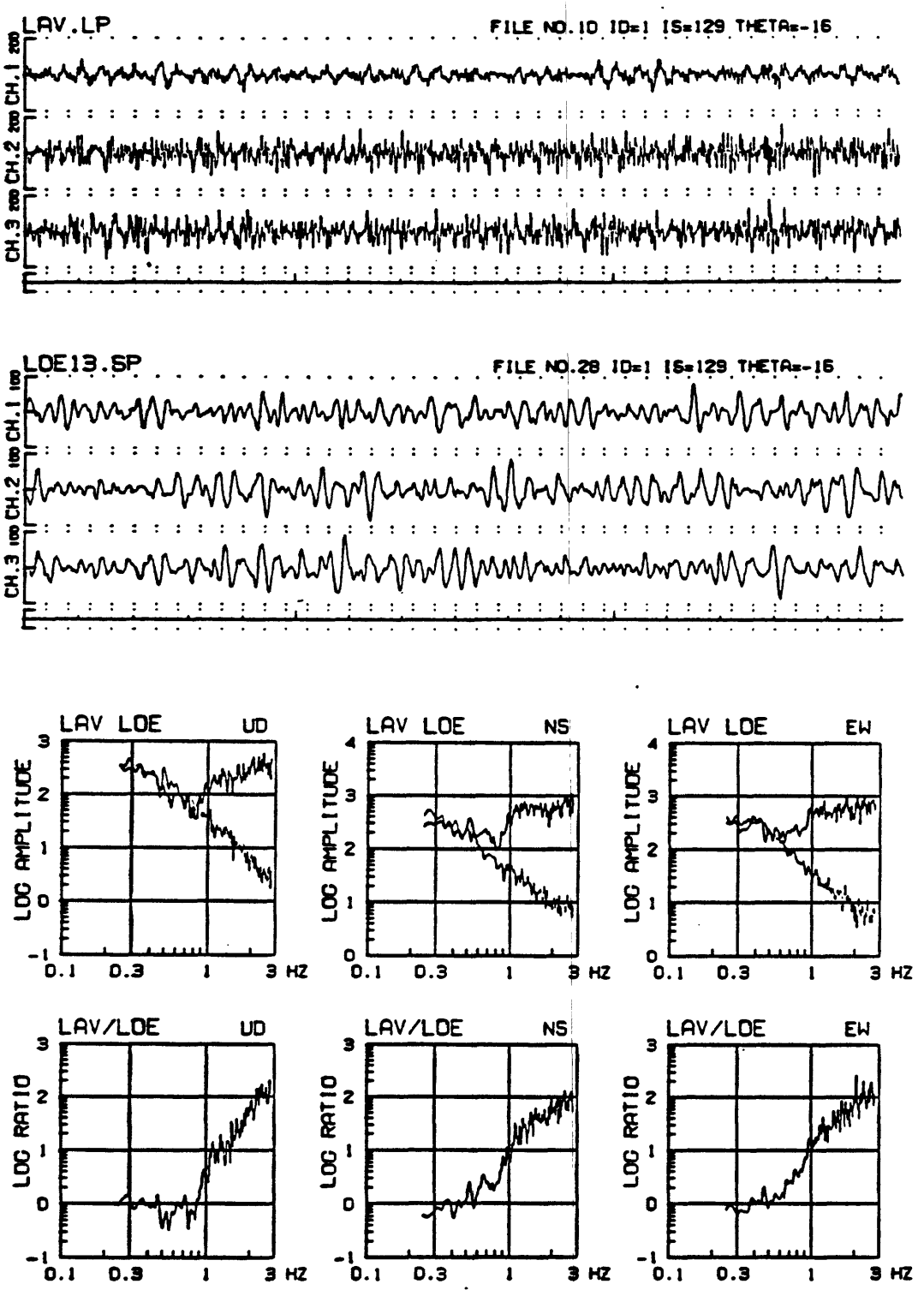

Fig. A.37 Velocity seismograms at **LAV** and **LOE**, amplitude spectra and their ratios (**LAV/LOE**). Seismogram scale is in 10^{-8} m/s and spectra in 10^{-8} m. **LAV** is located on alluvium (Qal).

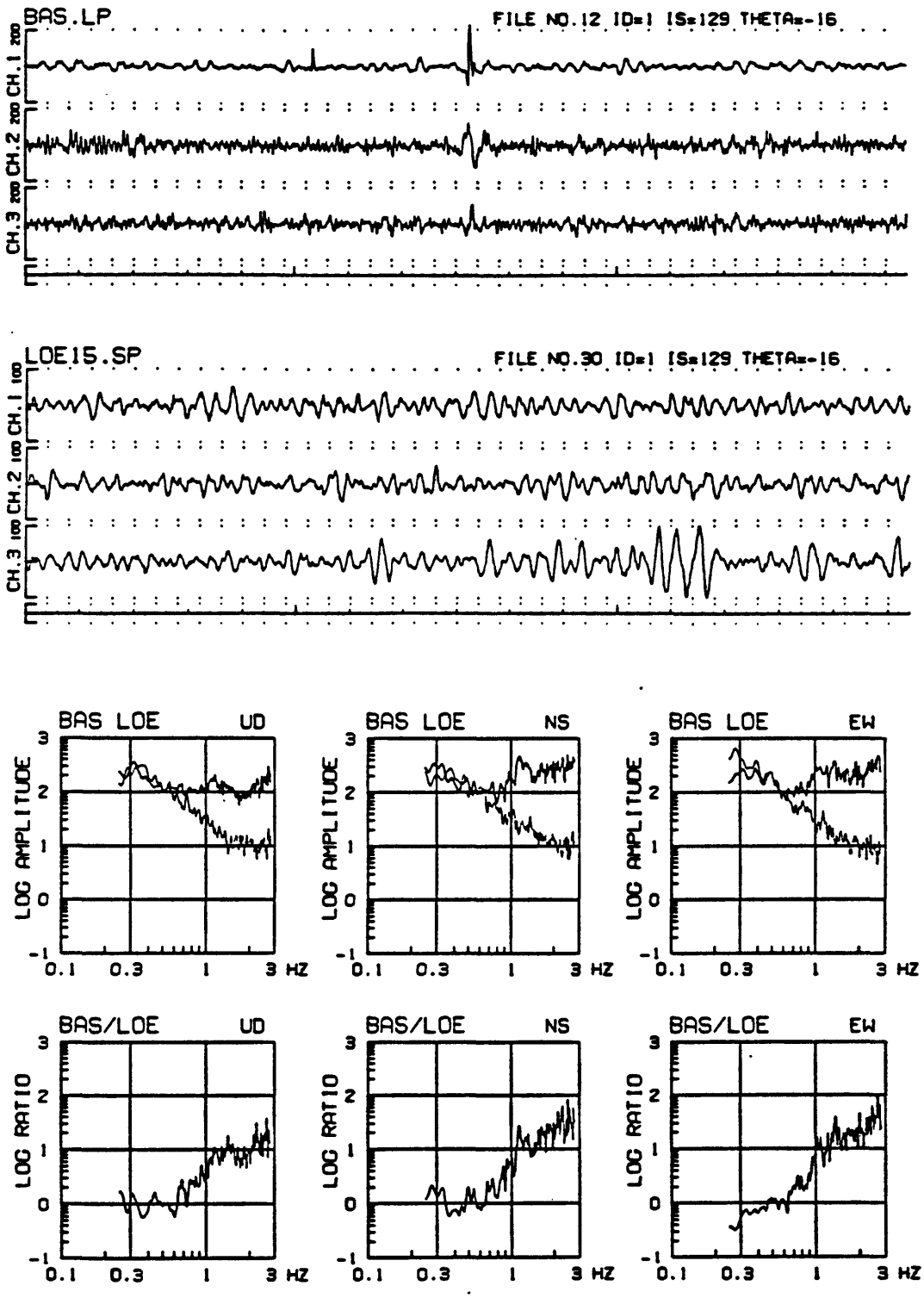

Fig. A.38 Velocity seismograms at **BAS** and **LOE**, amplitude spectra and their ratios (**BAS/LOE**). Seismogram scale is in 10^{-8} m/s and spectra in 10^{-8} m. **BAS** is located on alluvium (Qal).